Electronic Supplementary Material (ESI) for New Journal of Chemistry.

Supplementary Data

Tetrahydroisoquinoline based 5-Nitro-2-furoic acid Derivatives: A Promising New Approach for Anti-Tubercular Agents

Adinarayana Nandikolla,[a] Yogesh Mahadu Khetmalis,[a] Guruvelli Padma Vijaya Sangeetha,[b] Ala Chandu,[c] Swati,[d] Muthyala Murali Krishna Kumar,[b] Vivek Sharma,[d] Sankaranarayanan Murugesan,[c] and Kondapalli Venkata Gowri Chandra Sekhar*[a]

[a]*Department of Chemistry, Birla Institute of Technology and Science, Pilani, Hyderabad Campus, Jawahar Nagar, Kapra Mandal, Hyderabad – 500078, Telangana, India.*

[b]*College of Pharmaceutical Sciences, Andhra University, Visakhapatnam, Andhra Pradesh – 530 003, India*

[c]*Medicinal Chemistry Research Laboratory, Department of Pharmacy, Birla Institute of Technology and Science Pilani, Pilani Campus, Pilani-333031, Rajasthan. India.*

[d]*Department of Biological Sciences, Birla Institute of Technology and Science, Pilani, Hyderabad Campus, Jawahar Nagar, Hyderabad 500 078, Telangana, India.*

*Corresponding author
Tel.: +91 40 66303527; E-mail: kvgc@hyderabad.bits-pilani.ac.in; kvgcs.bits@gmail.com

Contents: **Page**

Experimental section: Chemistry

1. *Materials and methods*

All chemical reagents and solvents are purchased from Aldrich, Alfa Aesar, Finar. The solvents and reagents were of LR grade. All the solvents were dried and distilled before use. Thin-layer chromatography (TLC) was carried out on aluminum-supported silica gel plates (Merck 60 F254) with visualization of components by UV light (254 nm). Column chromatography was carried out on silica gel (Merck 100-200 mesh). ^{1}H NMR and ^{13}C NMR spectra were recorded at 400 MHz and 101 MHz respectively using a Bruker AV 400 spectrometer (Bruker CO., Switzerland) in DMSO-*d6* solution with tetramethylsilane as the internal standard and chemical shift values (δ) were given in ppm. ^{1}H NMR spectra were recorded in r DMSO-*d6*. The following abbreviations are used to designate multiplicities: s = singlet, d = doublet, t = triplet, m = multiplet, br = broad. Melting points were determined on an electro thermal melting point apparatus (Stuart-SMP30) in open capillary tubes and are uncorrected. Elemental analyses were performed by Elementar Analysensysteme GmbH vario MICRO cube CHN Analyzer. Mass spectra (ESI-MS) were recorded on Schimadzu MS/ESI mass spectrometer.

2. General procedure and analytical data

Brief general procedure for the synthesis of key intermediate 5,7-dichloro-1,2,3,4-tetrahydroisoquinoline-6-carboxylic acid (6):

The designed target molecules were synthesized in eight steps (**Scheme-1**) and (**Scheme-2**) as per the literature protocol[1]. Firstly, compound **1** (1 equiv), was treated with sodium cyanoborohydride (1.2 equiv), with 1-chloro-2-aminoethane hydrochloride (1.5 equiv), in methanol at room temperature for overnight and then quenched with aq. NH_4Cl solution, extracted with ethyl acetate and was added 4M HCl in dioxane, stirred for 1 h. solid precipitated was filtered to get compound **2** which was proceeded for next step without further purification. Compound **2** (1 equiv), and $AlCl_3$ (3 equiv), was heated to 185-190 °C, quenched with ice water and basified with aq. NaOH solution, extracted with dichloromethane, distilled the solvent to get compound **3**.

To a solution of compound **3** (1 equiv), in DCM was treated with DIPEA (2 equiv), trityl chloride (1.2 equiv), and maintained for 4 h at room temperature, quenched with aq. NH_4Cl solution, extracted with dichloromethane, distilled the solvent to get compound **4**. Compound **4** (1 equiv), was dissolved in THF, TMEDA (1 equiv), was added and the solution cooled to -78 °C stirred for 1 h. *n*-BuLi

(1.6 M in hexane) (1 equiv), was added slowly and the solution stirred for 1 h at -78 °C. Dry CO_2 gas was purged into the solution and slowly brought to room temperature, maintained for 1 h. Reaction mass was quenched with 1N Aq. HCl solution and THF layer was separated. To this solution, 4M HCl in 1,4 dioxane was added and stirred for 4h at room temperature. Solid precipitated was filtered and washed with Ethyl acetate, suck dried under vacuum to get compound **6** off white solid (15 g, yield 89 %).

Brief procedure for preparation of aromatic acid chlorides 8(a-z):

Different substituted acid chlorides were synthesized by treating the corresponding acids **7(a-z)** (1 equiv), with oxalyl chloride (1.5 equiv), in dichloromethane. DMF catalytic amount was added to the mixture and stirred at rt overnight. The solvent was distilled off to get corresponding acid chloride **8(a-z)** (1 g, yield 80-90 %). Proceeded for the next step without further purification.

General procedure for preparation of 9(a-z):

To a stirred solution of compound **6** (1 equiv), in 1,4 dioxane, aq. K_2CO_3 (1.5 equiv), was added and stirred for 1-2 h. Acid chlorides **8(a-z)** (1.5 equiv), were dissolved in 1,4 dioxane and added to the previous solution and stirred at rt for 16 h. On completion, as indicated by TLC, the reaction mass was diluted with water, and was acidified with con. HCl until pH~ 2-4, at 0-5 °C. Solid precipitated was filtered and, washed with water, dried under vacuum to get the desired compounds **9 a-z.** (0.5-0.6 g, yield 60-70 %).

General procedure for preparation of 10(a-z):

To a stirred solution of **9(a-z)** (1 equiv), in DMF was added HOBt (1.2 equiv), EDC.HCl (1.5 equiv), DIPEA (3 equiv), and stirred for 4- 5 h. To the resultant solution, hydrazine hydrate (2 equiv), was added and stirred for 16 h. The reaction mixture was checked with TLC, (R_f = 0.40-0.50 in 30-50% EtOAc/ Hexane). The crude was then poured into ice cold. The precipitated solid was filtered and washed with water, dried under vacuum to get colorless to off-white solids **10(a-z)** (0.3-0.5 g, yield 48-68 %).

General procedure for preparation of titled compounds NFT-1 to NFT-26:

To a stirred solution of 5-nitrofuran-2-carboxylic acid (1 equiv), in DMF was added HOBt (1.2 equiv), EDC.HCl (1.5 equiv), DIPEA (3 equiv), and stirred for 30 mins. To this resultant solution, **10 a-z** (1 equiv), were added and stirred for 4-5 h. The reaction mixture was checked with TLC. After the completion of the reaction, as indicated by TLC, the crude mixture was poured into ice cold water.

The precipitated solids were filtered, washed with water, and dried under vacuum. The crude compounds were purified by silica gel (100-200 mesh size) column chromatography by eluting in 30-50% EtOAc/ Hexane to get the titled compounds **NFT-1 to NFT-26.**

Experimental section: Biology

Anti-TB MABA assay

The compounds were screened for antitubercular activity on MtbH37Rv (ATCC 27294) using Microplate Alamar Blue Assay (MABA) [1]. In brief, growth on Lowenstein-Jensen (LJ) medium was suspended in sterile Middlebrook 7H9 broth supplemented with 0.2%glycerol and 10% OADC (oleate-albumin-dextrose-catalase) enrichment and a 1:20 dilution used as the inoculum for MABA. The 96 wells plate received 100 µl of the Middlebrook7H9 broth and serial dilution of compounds was made directly on the plate. The final drug concentrations tested were 0.8 to 100 µg/ml. Plates were covered and sealed with parafilm and incubated at 37 ºC for five days. After this, 25µl of freshly prepared 1:1 mixture of Alamar Blue reagent and 10% tween80 added to the plate and incubated for 24 hrs. DMSO was added as a co-solvent to facilitate poorly soluble compounds. A blue colour in the well was interpreted as no bacterial growth, and pink colour was scored as growth. The MIC was defined as lowest drug concentration, which prevented the colour change from blue to pink.

Drug-inhibitor combination studies

The x/y quotient calculation method was used with slight modification to evaluate the combined drug (plus inhibitor) action. For this procedure, all the drugs were used at sub-lethal concentrations. The combined drug-inhibitor activity [2]. was assessed by calculating x/y quotients as follows. The y value was the MIC obtained with the combination of drug-inhibitor by using the MABA method, whereas the x value was the lowest MIC obtained at the same time with the drug or the inhibitor used alone. For combinations, an x/y value of 1 indicated that there was no interaction between the two drugs, a quotient of <0.5 indicated enhanced drug action, whereas an x/y quotient of >2 indicated the presence of antagonism between the drug and the inhibitor. The drugs or inhibitors were added at final concentrations

12.5, 6.12, 3.2, 1.6, 0.8, 0.4, 0.2, 0.1. 0.05 and 0.025 µg/mL in 1:1 ratio. MIC of the drug-inhibitor combination is compared with the MIC of drug.

Cytotoxicity Studies

Cell culture

Human cancer cells– HEK293T (purchased from NCCS Pune) were grown in complete medium, DMEM (Invitrogen) containing 10% fetal bovine serum (FBS) supplemented with 1 % penicillin/streptomycin solution (Gibco).

Cell proliferation assay – IC50 experiments

Cell proliferation assays were done as described previously using the WST-1 reagent (Cat# 05015944001, Roche) [3, 4]. Briefly, cells were seeded at a concentration of 7,000 cells/well in 96-well plates and treated with the compounds at different concentrations 5-50 µM and 7-2000 µM for 48 hours and cell proliferation was quantified at OD of 450 nm. The half- maximal inhibitory concentration (IC 50) values were calculated using GraphPad Prism version 5 at different concentrations for each drug.

Experimental section: Computational

4. Computation studies

Materials and methods

Molecular docking:

Computational sources: Xenon W3565 processor, Ubuntu 18.04

Software and version: Schrodinger software, version 2019-1 [5,] (Glide module for docking).

Retrieval of the protein: RCSB protein data bank [6]

(PDB-4OHU, https://www.rcsb.org/structure/4BAE).

Docking method: Extra precession mode.

Results analysis: XP visualizer (Schrodinger)

Computational sources: Tyrone workstation (NVIDIA RTX 2040), Ubuntu 18.04

Software and version: Desmond software, D.E Shaw research group (Academic license, Version 2020-1; [7]

Docking workflow: To perform docking studies, ChemDraw 16.0 was used to sketch the ligand. Then, the Ligprep module of the software (Version 2019-1, Schrodinger) (Schrodinger, n.d.) was used to minimize the energy with Optimized Potentials for Liquid Simulations (OPLS3e) force field. The minimization process enables the allocation of bond orders, addition of hydrogens to ligands and the conversion of 2D into 3D structures to improve docking. Further, docking studies were conducted using the output file (Best conformations of the ligands). [8]

In Schrodinger, the protein preparation wizard (version 2019-1, Schrodinger; is the primary application for preparing proteins and minimizing their energy content. It adds hydrogen atoms to proteins and assigns charges to them. [9] The Het states were generated using Epik at pH 7.0 ± 2.0. Using workspace analysis, the protein was refined, modified and the heteroatoms in the water were removed. The crucial water molecules stayed the same, but all other molecules apart from the water were removed except the co-crystal ligand. The OPLS3 force field was then used to minimize the protein. An active site grid was generated by considering co-crystal ligands, which are included in the active site of the selected protein target (PDB-4BAE). Root mean square deviation (RMSD) was calculated using the overlay view of the X-ray native pose of co-crystal ligand and its docked pose in XP mode to validate the protein.

Molecular dynamics workflow: Simulation of Molecular Dynamics (MD) helps visualize the action of Protein-Ligand complexes (PLC) at the target's binding site region under physiological conditions. MD was performed using Desmond module of Schrödinger developed by D.E Shaw research group (Academic license, Version 2020-1; [7,] through the system's builder panel; the orthorhombic simulation box was prepared with the Simple Point-Charge (SPC) explicit water model in such a way that the minimum distance between the protein surface and the solvent surface is 10 Å. Complexes docked with receptors were solvated with the orthorhombic TIP3P water model. [10] Neutralization of the solvated system was accomplished by using counterions and limiting the salt concentration in the physiological system to 0.15 M. The receptor-ligand complex system was designated with the OPLS AA force field. [11]

Two seconds of relaxation time was used for the Reversible reference system Propagator Algorithms (RESPA) integrator [12,] Nose-Hoover chain thermostat [13] and Martyna-Tobias-Klein barostat. The final production of MD simulations was performed using the equilibrated system. This MD simulation was set to run for 100 ns with 310 K temperatures at 1.0 bar pressure, with the NPT (Isothermal-Isobaric ensemble, constant temperature, constant pressure, constant number of particles) ensemble at default settings [14] for relaxation before simulation. The MD simulation was performed with MD simulation tool, with the simulation time set to 100 ns. Furthermore, the .out file was used to view the trajectories and create a movie. The out.cms file was imported and the movie was exported at higher resolution (1280x1024) with better quality. The trajectories were written with 1000 frames during MD simulation. The protein backbone frames were aligned to the backbone of the initial frame to better understand the complex's stability during MD simulation. Finally, after loading the .out file and selected the Root Mean Square Deviation (RMSD) and Root Mean Square Fluctuation (RMSF) in the analysis type to oblique, the simulation interaction diagram and the results were analyzed. [15,16]

***In silico* ADMET studies:**

The ADMET result of the most active compounds **NFT-12**, **NFT-19** and **NFT-20**, were compared with the co-crystal ligand. A compound is considered to have a high Caco-2 permeability if it has log Papp value > 0.90 cm/s. The titled compounds **NFT-12**, **NFT-19** and **NFT-20** values were a bit lower than the ideal one indicating poor caco-2 permeability. The Intestine is normally the primary site for absorption of a drug from an orally administered solution. A molecule with an Intestinal Absorption of less than 30% is considered to be poorly absorbed. **NFT-12** is 91.366% absorbed in the intestine which shows it has greater absorption than the co-crystal (89.884%), but **NFT-19** and **NFT-20** has comparable percentage absorption as that of reference ligand. The P-glycoprotein functions as a biological barrier by extruding toxins out of the cells. The prediction is in the positive direction in the case of titled compounds, thus they likely to be a substrate for P-glycoprotein and P-glycoprotein inhibitors (I & II). A compound is considered to have a relatively low skin permeability if it has a log Kp > -2.5. It means that active compounds could be of interest for developing transdermal drug delivery. The compounds showed an excellent high skin permeability (log Kp > -2.5) than the reference molecule.

Distribution:

Volume of distribution at steady state (VDss) is the theoretical volume required by a drug to be uniformly distributed in blood. The recommended values for good distribution in blood was > 0.45, all the active compounds were fall out of this threshold, implies poor volume of distribution. The Fraction Unbound parameter predicts the fraction that will be unbound in plasma, results were depicted in **Table 1**. The knowledge of the ability of a drug to cross into the brain is an important parameter that may help to reduce side effects and toxicities. A log BBB (for Blood-Brain Barrier) > -0.3 for a given drug is considered to easily cross the BBB while molecules with log BBB > -1 are poorly distributed to the brain, being predicted that promising compounds have a good BBB permeability. Another measurement is the blood-brain permeability-surface area product or CNS Permeability where compounds with a log PS > -2 will be able to enter the Central Nervous System (CNS), while those with log PS < -3 will be unable to penetrate the CNS. For the current study, active compounds were predicted to penetrate the CNS.

Metabolism

Cytochrome P450 is an important detoxification enzyme in the body. Many drugs are deactivated by the cytochrome P450 isoforms while some can be activated by it. As can be seen from **Table 1**, both the biologically active compounds and co-crystal are predicted as being P450 inhibitors for some isoform.

Excretion

Drug clearance occurs as a combination of hepatic clearance and renal clearance (excretion via the kidneys) which is related to bioavailability. The predicted total clearance of the **NFT-12**, **NFT-19**, **NFT-20** and co-crystal are given in log (ml/min/kg). Organic cation transporter 2 (OCT2) is a renal uptake transporter that plays an important role in disposition and renal clearance of drugs. In this case, it is predicted that neither of the compounds will behave as OCT2 substrates.

Toxicity

AMES Toxicity is a widely employed methodology considered to check the mutagenic potential of a given drug using bacteria, thus indicating that when the results is positive, the studied compound will be mutagenic and could behave as a carcinogen. The predictions are negative for **NFT-12** and co-crystal but positive for **NFT-19** and **NFT-20** under study. The maximum recommended tolerated dose

(MRTD) provides an estimate of the toxic dose threshold of chemicals in humans. A low value for significantly potent compounds and high value for co-crystal are found in the results in **Table 1**. Also, the predictions indicate that both the active compounds and co-crystal are unlikely to be hERG I inhibitors, but for the case of hERG II, all three potent compounds along with co-crystal are not hERG II inhibitors. The lethal dosage values (LD_{50}) are a standard measurement of acute toxicity and is defined as the amount of a compound that causes the death of 50% of a group of test animals and are measured through the oral rat acute toxicity (ORAT) and oral rat chronic toxicity (ORCT) indices where the predicted values are given in mol/kg. Hepatoxicity is associated with disrupted normal function of the liver and Skin Sensitization of the predicted values for active compounds and co-crystal are positive. In minnow toxicity co-crystal is showing low acute toxicity than the significantly active compounds.

Table 1. *In silico* ADMET prediction of biologically active compounds and the reference compound using pkCSM webserver

ADMET	Descriptors	NFT-12	NFT-19	NFT-20	Cocrystal ligand
Absorption	Caco2 permeability (log Papp in cm/s)	-0.25	0.51	0.49	1.49
	Intestinal absorption (% Absorbed)	91.37	86.47	88.31	89.88
	Skin Permeability (log Kp)	-2.74	-2.74	-2.74	-2.70
	P-glycoprotein substrate	Yes	Yes	Yes	Yes
	P-glycoprotein I inhibitor	Yes	Yes	Yes	No
	P-glycoprotein II inhibitor	Yes	Yes	Yes	No
Distribution	VDss (human) (log L/kg)	-0.90	-0.63	-0.64	0.70
	Fraction unbound (human)	0.01	0.02	0.02	0.00
	BBB permeability (log BB)	-1.87	-1.54	-1.56	0.88
	CNS permeability (log PS)	-2.21	-2.07	-2.03	-1.59
Metabolism	CYP2D6 substrate	No	No	No	No
	CYP3A4 substrate	Yes	Yes	Yes	Yes
	CYP1A2 inhibitor	Yes	Yes	Yes	Yes
	CYP2C19 inhibitor	Yes	Yes	Yes	Yes
	CYP2C9 inhibitor	Yes	Yes	Yes	Yes
	CYP2D6 inhibitor	No	No	No	No

	CYP3A4 inhibitor	Yes	Yes	Yes	Yes
Excretion	Total Clearance (log ml/min/kg)	-0.29	-0.46	-0.32	-0.06
	Renal OCT2 substrate	No	No	No	No
Toxicity	AMES toxicity	No	Yes	Yes	No
	Max. tolerated dose (log mg/kg/day)	0.15	0.09	0.09	0.81
	hERG I inhibitor	No	No	No	No
	hERG II inhibitor	Yes	Yes	Yes	No
	Oral Rat Acute Toxicity (LD50) (mol/kg)	2.86	2.83	2.83	2.27
	Oral Rat Chronic Toxicity (log mg/kg)	1.57	1.80	1.78	1.75
	Hepatotoxicity	No	No	No	No
	Skin Sensitization	No	No	No	No
	Minnow toxicity (log mM)	1.29	0.43	0.57	-1.95

5. IR spectras of final compounds (NFT-1 to NFT-26):

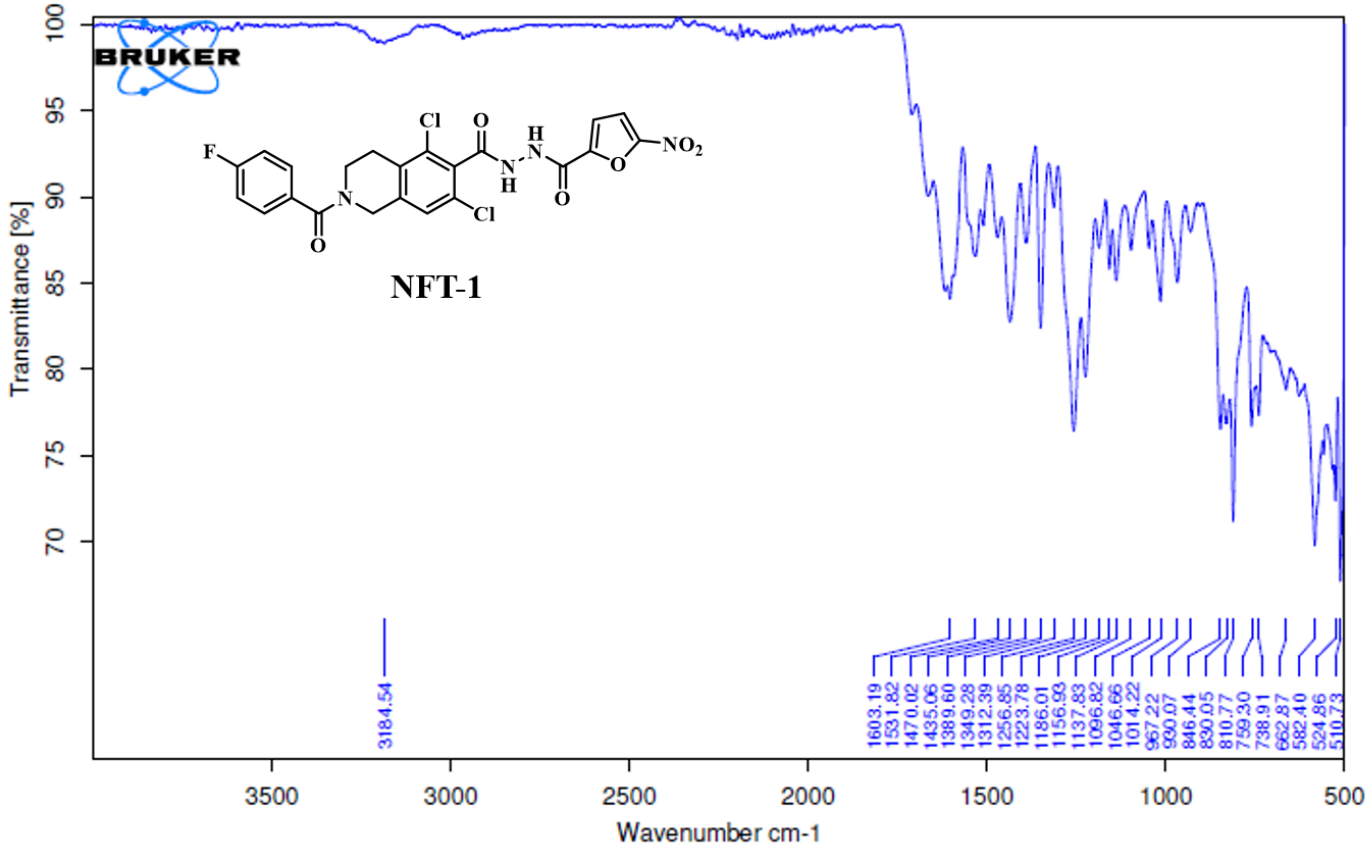

IR spectrum of compound NFT-1

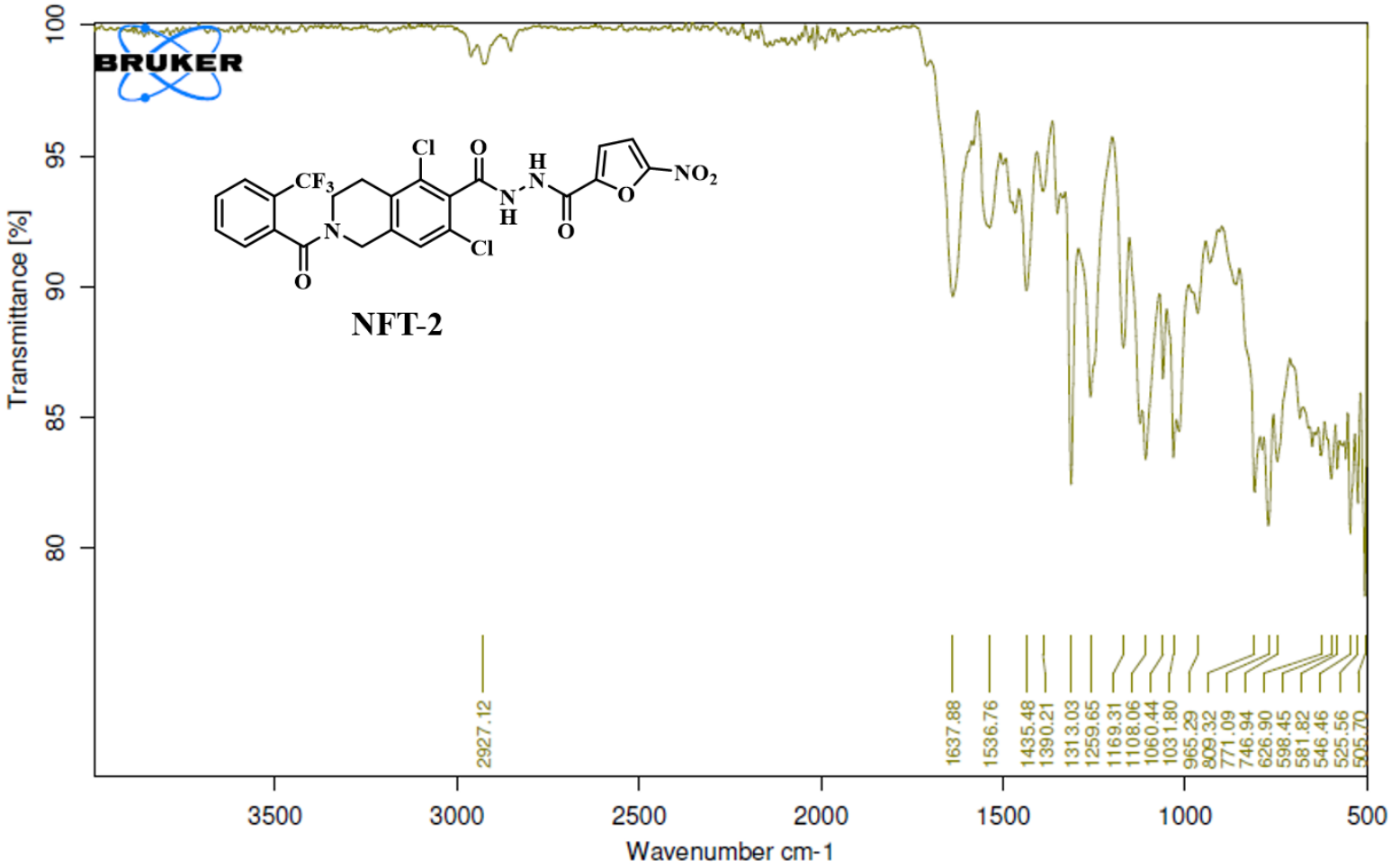

IR spectrum of compound NFT-2

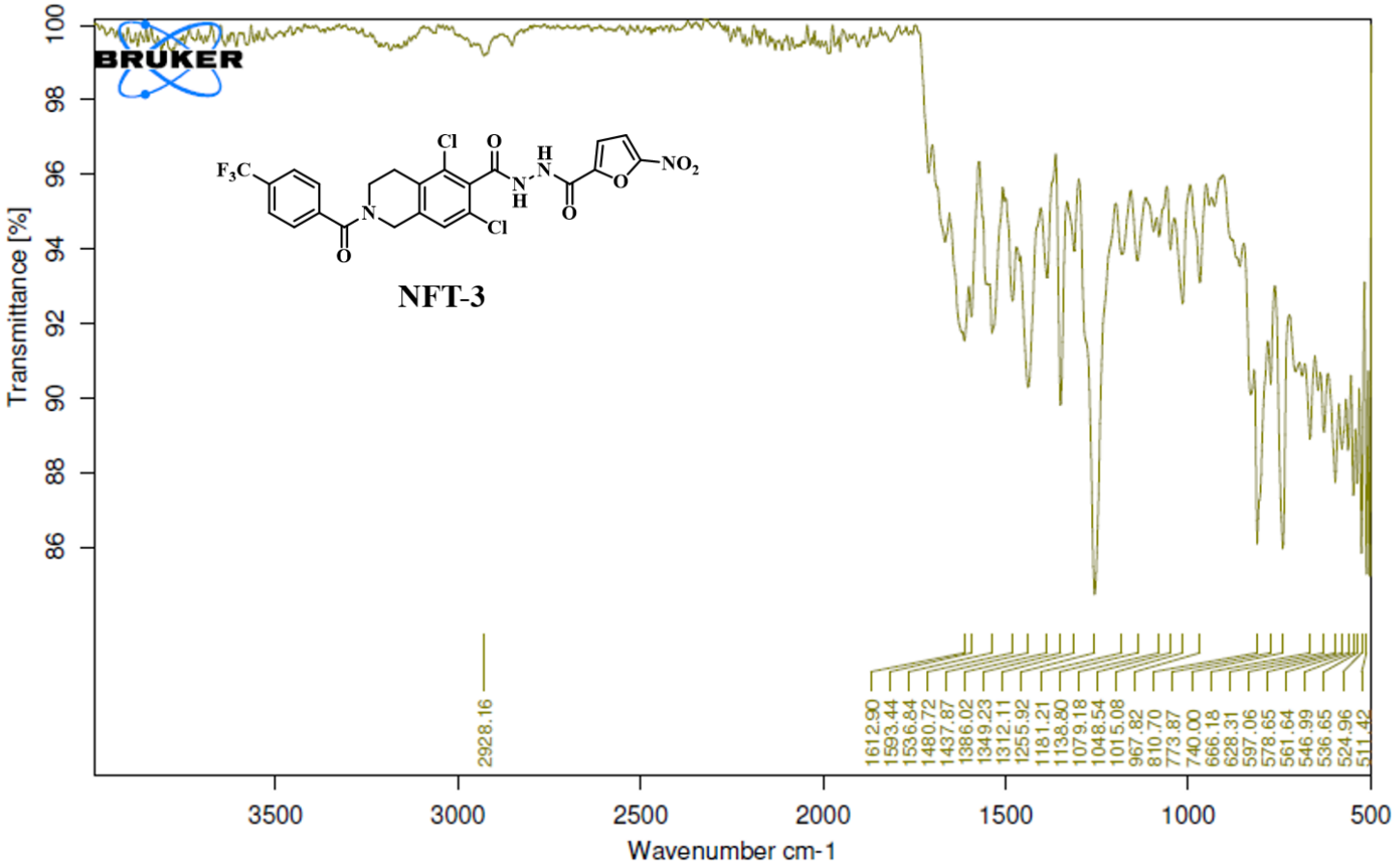

IR spectrum of compound NFT-3

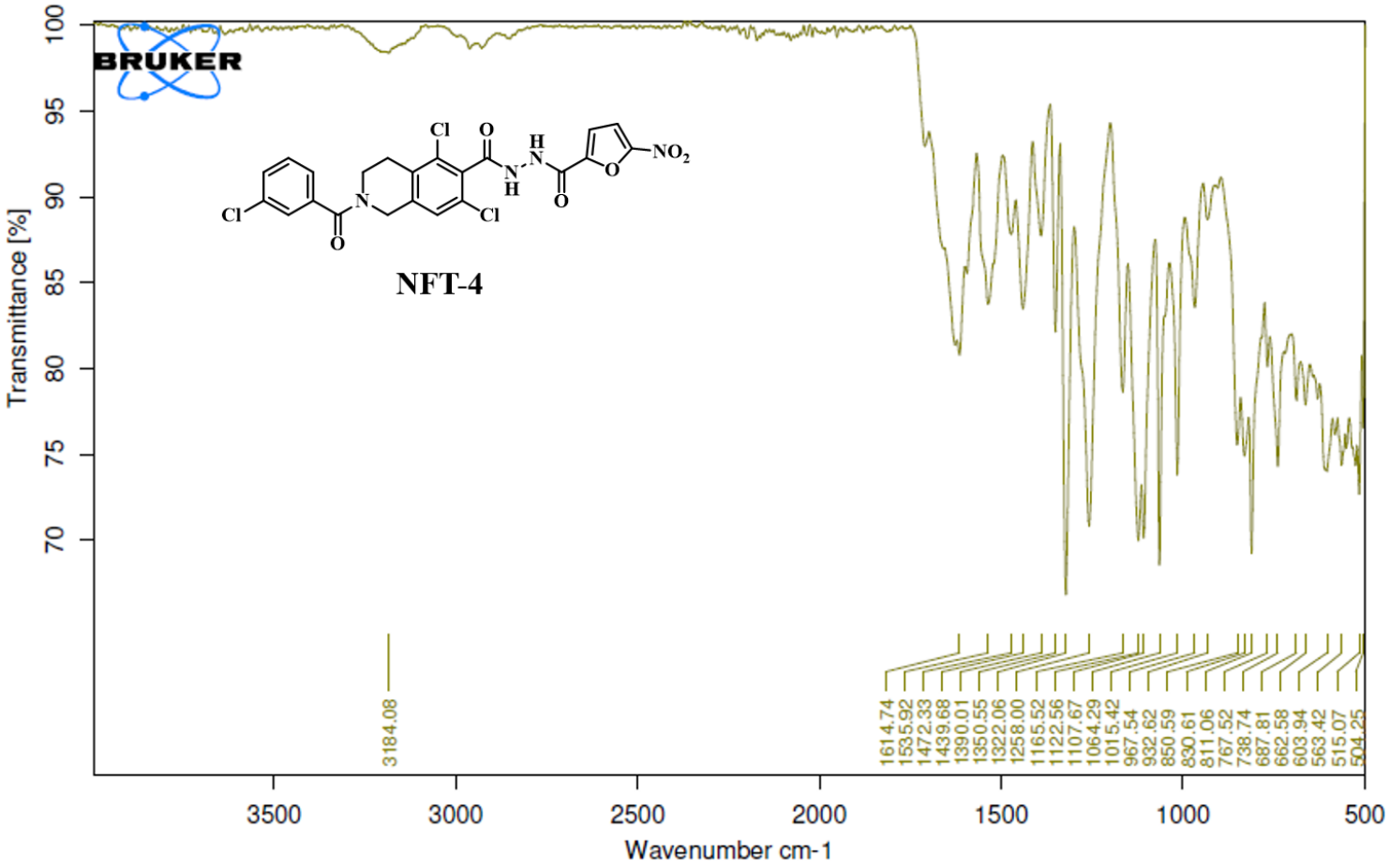

IR spectrum of compound NFT-4

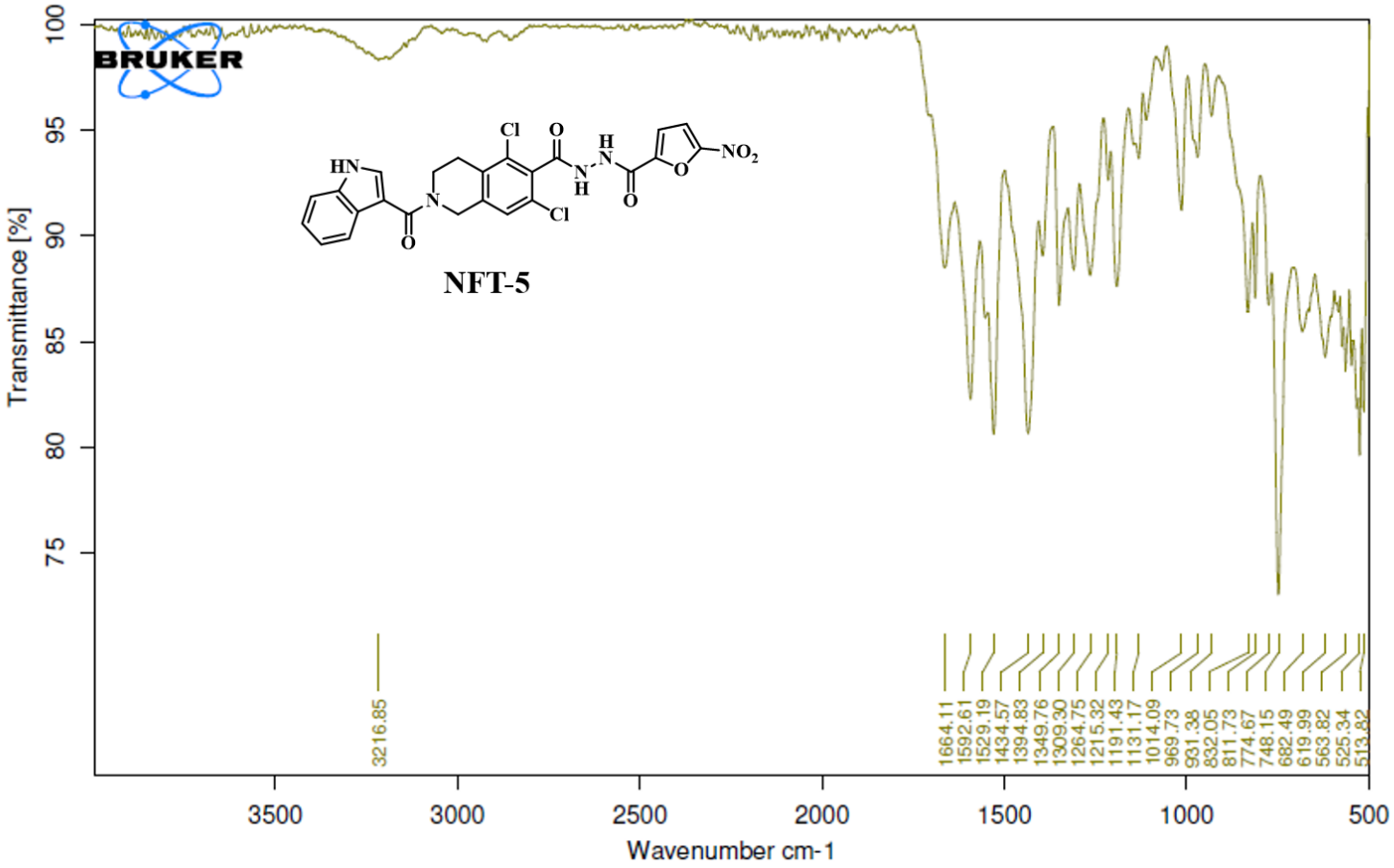

IR spectrum of compound NFT-5

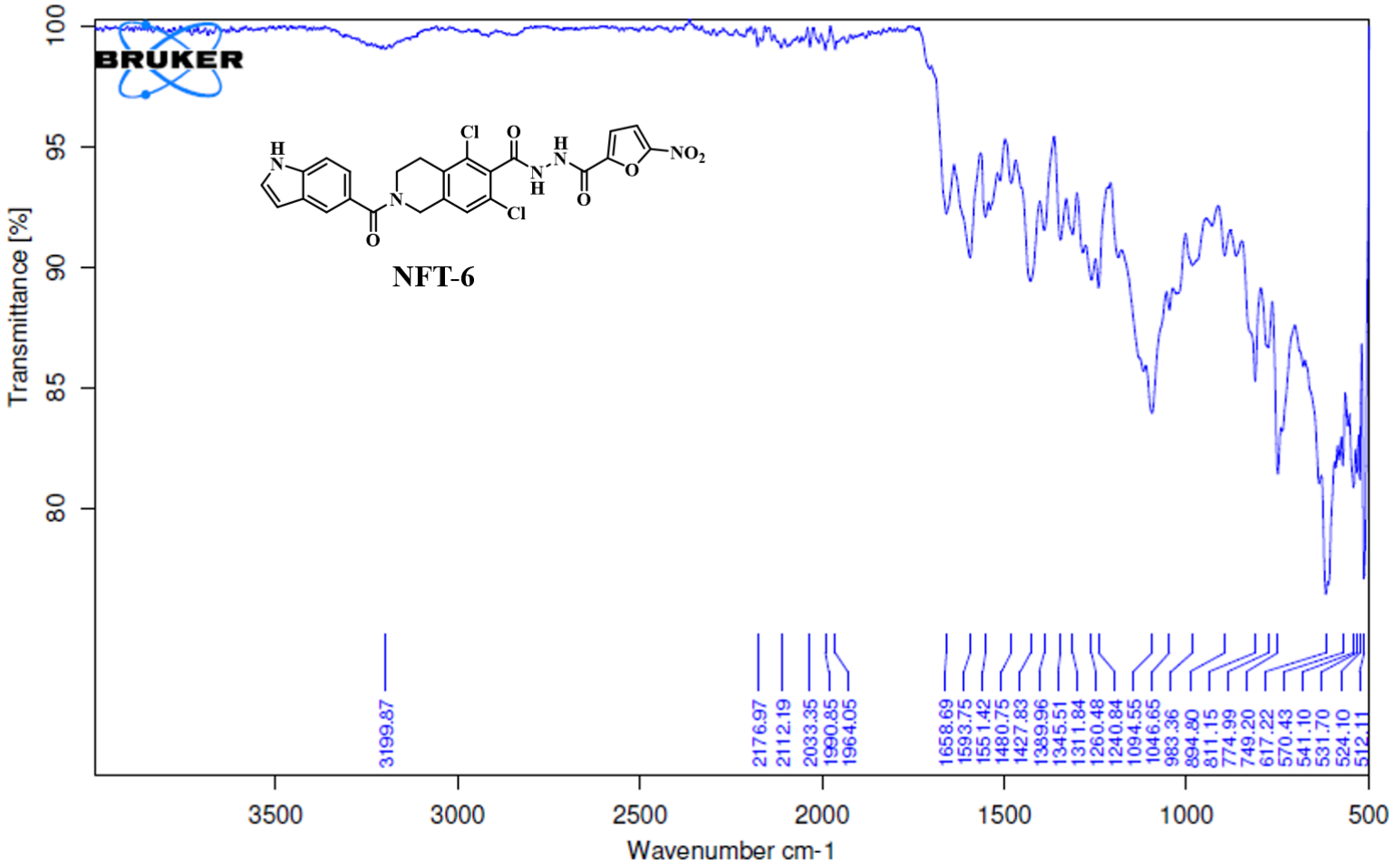

IR spectrum of compound NFT-6

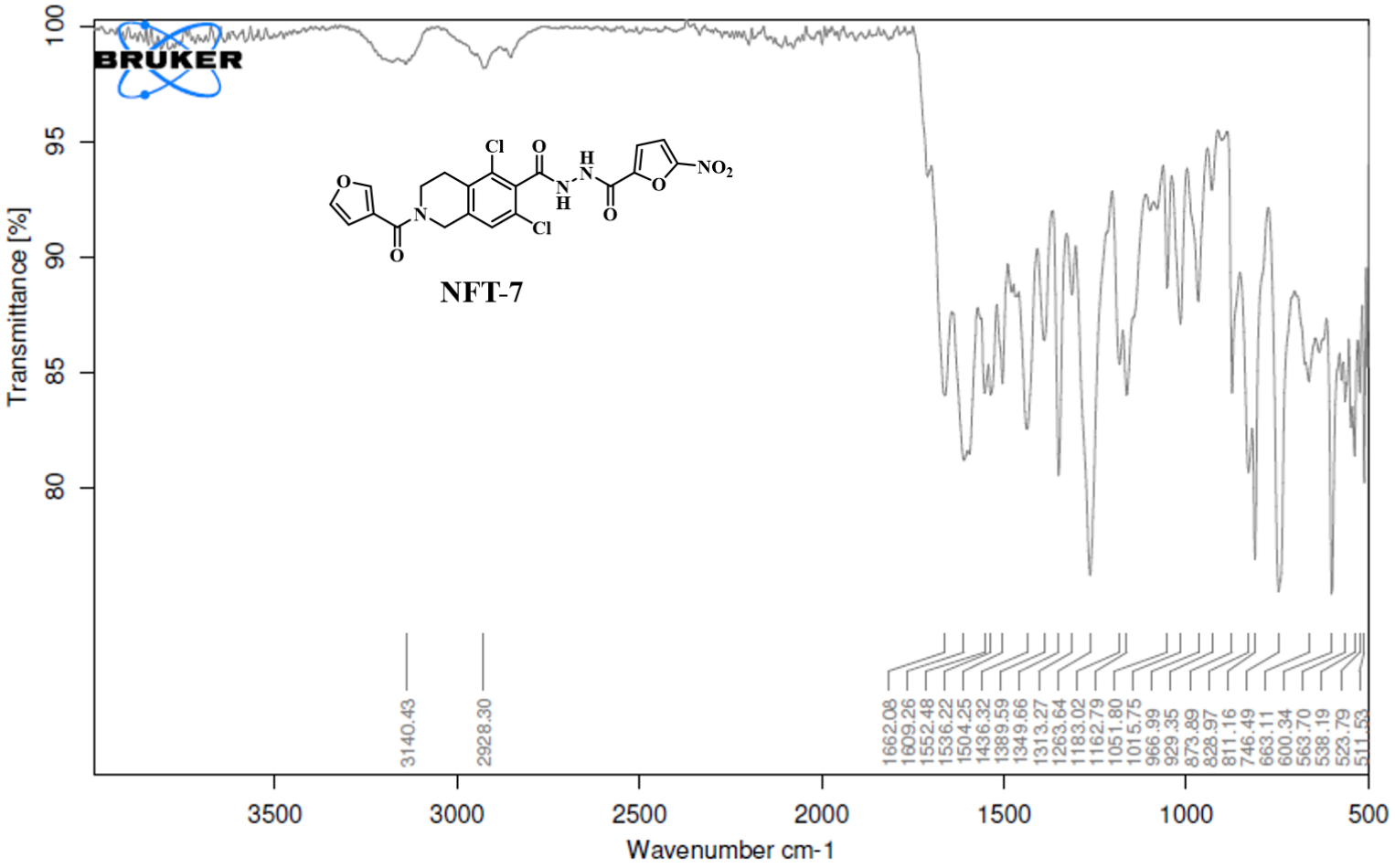

IR spectrum of compound NFT-7

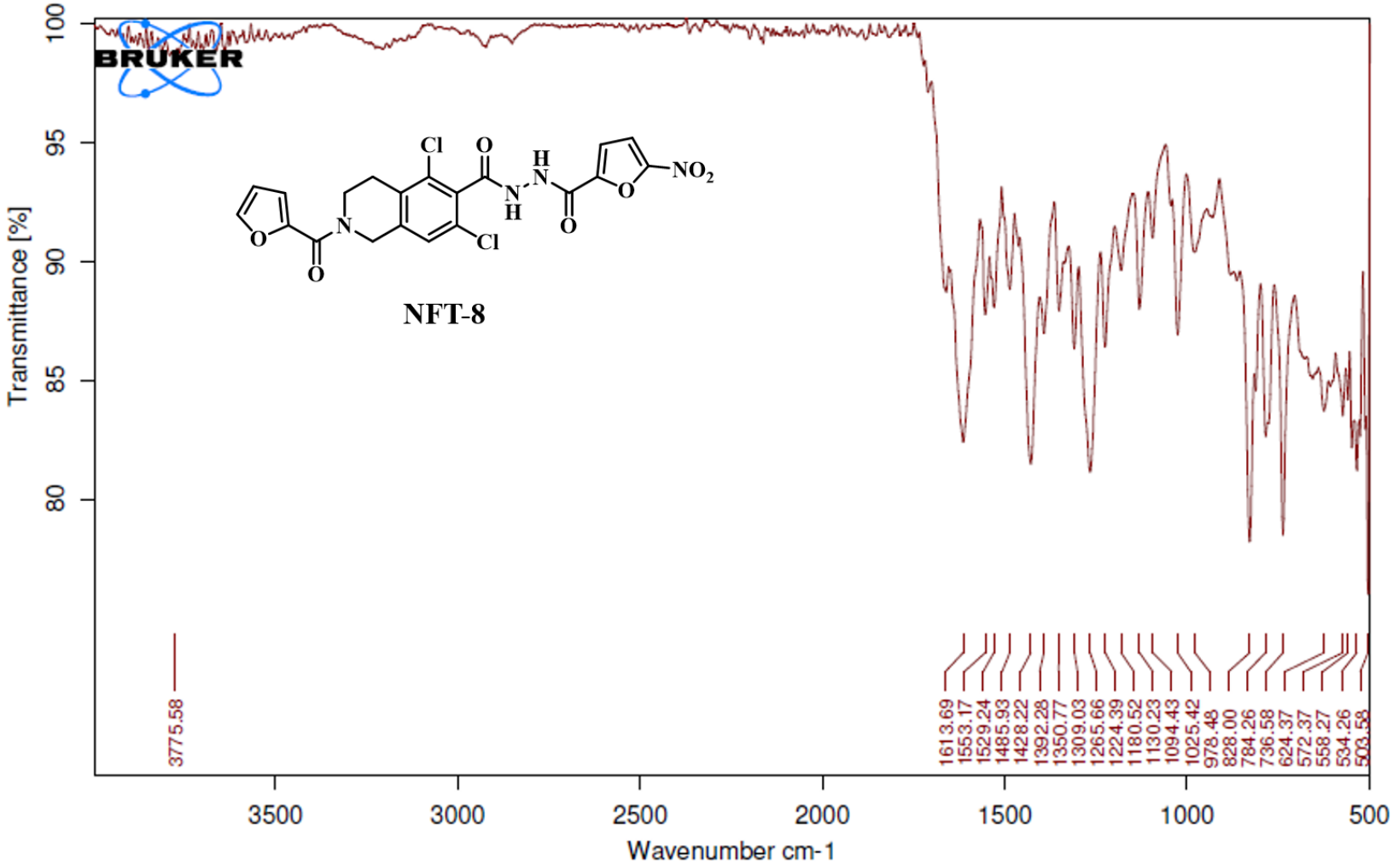

IR spectrum of compound NFT-8

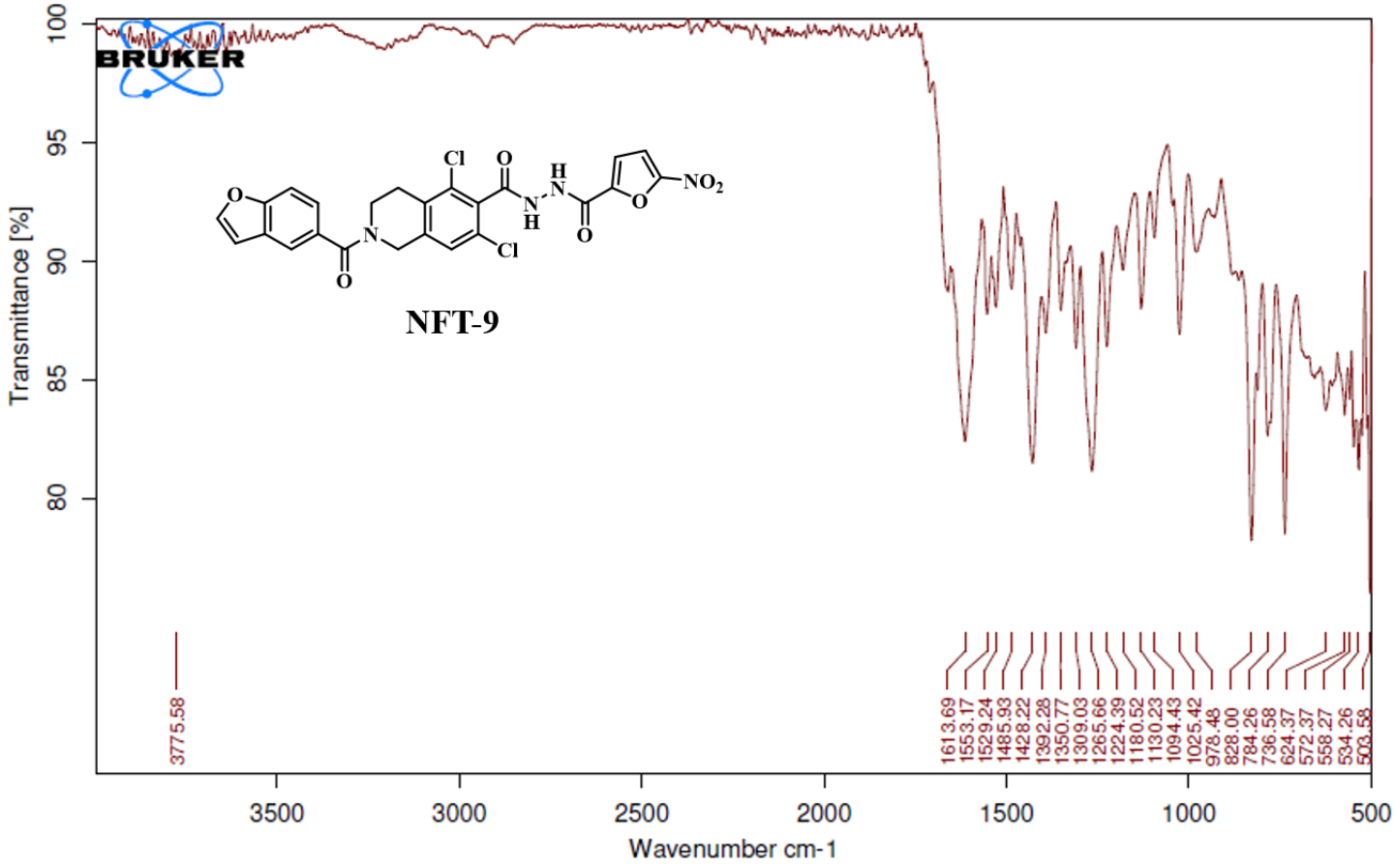

IR spectrum of compound NFT-9

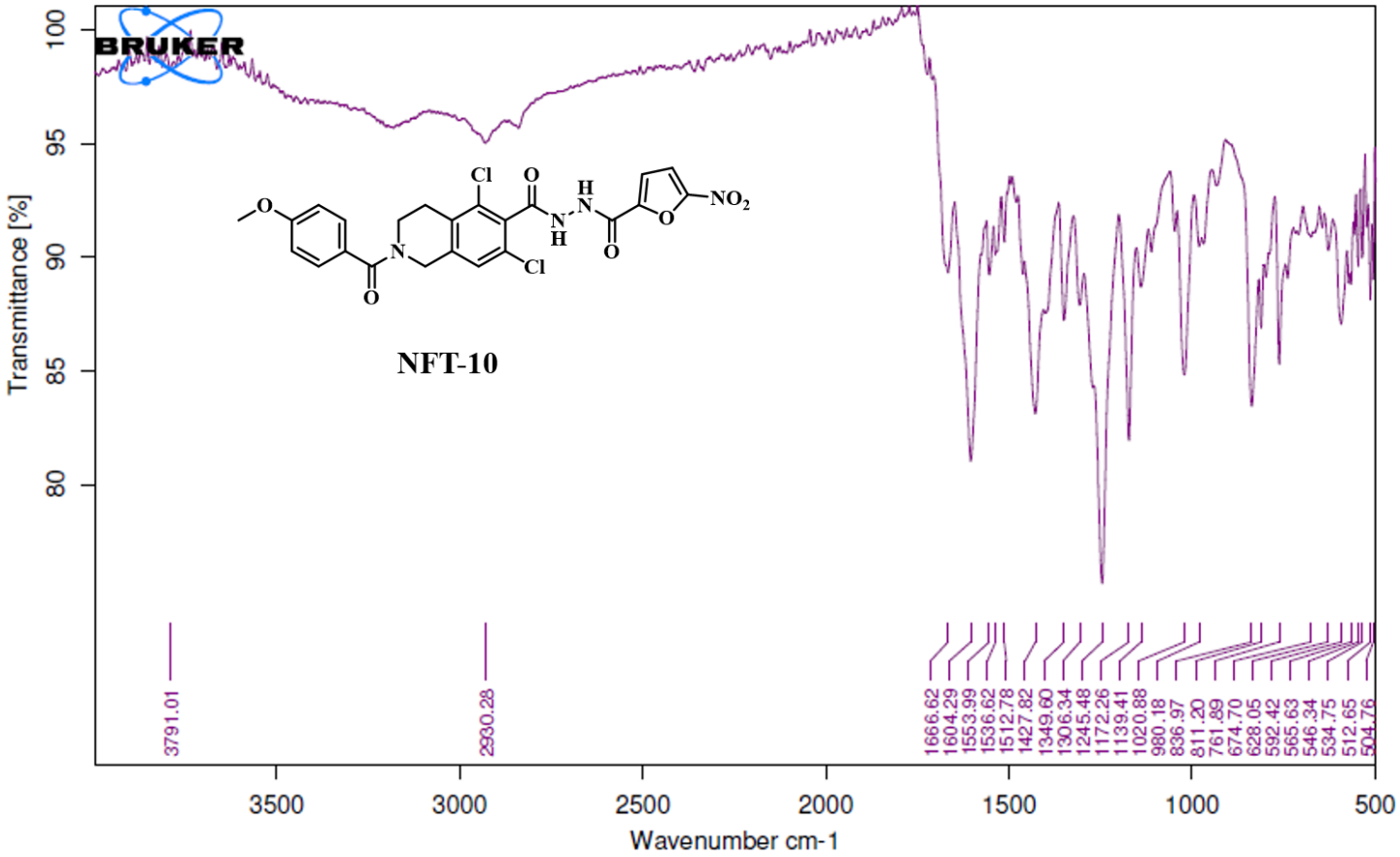

IR spectrum of compound NFT-10

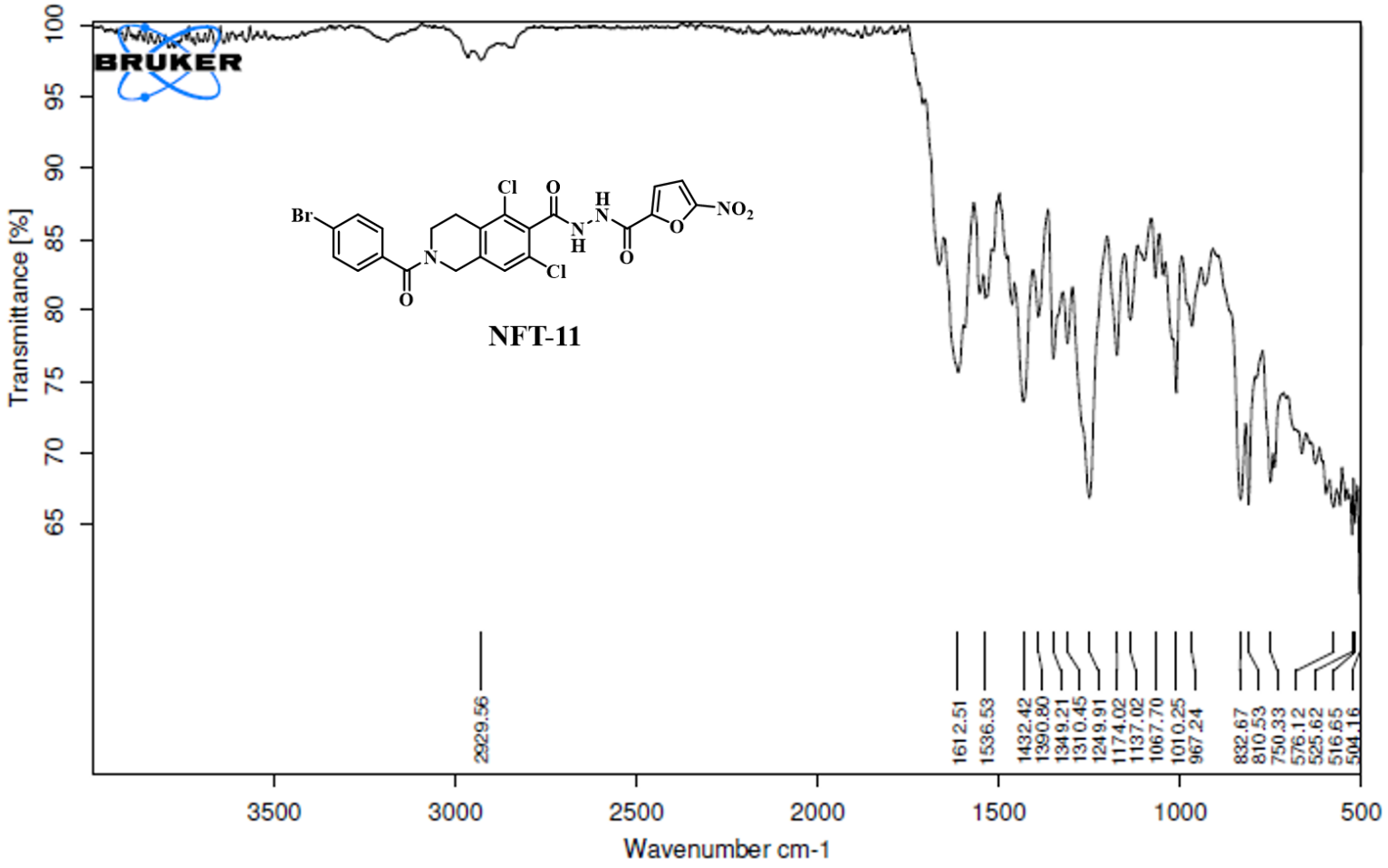

IR spectrum of compound NFT-11

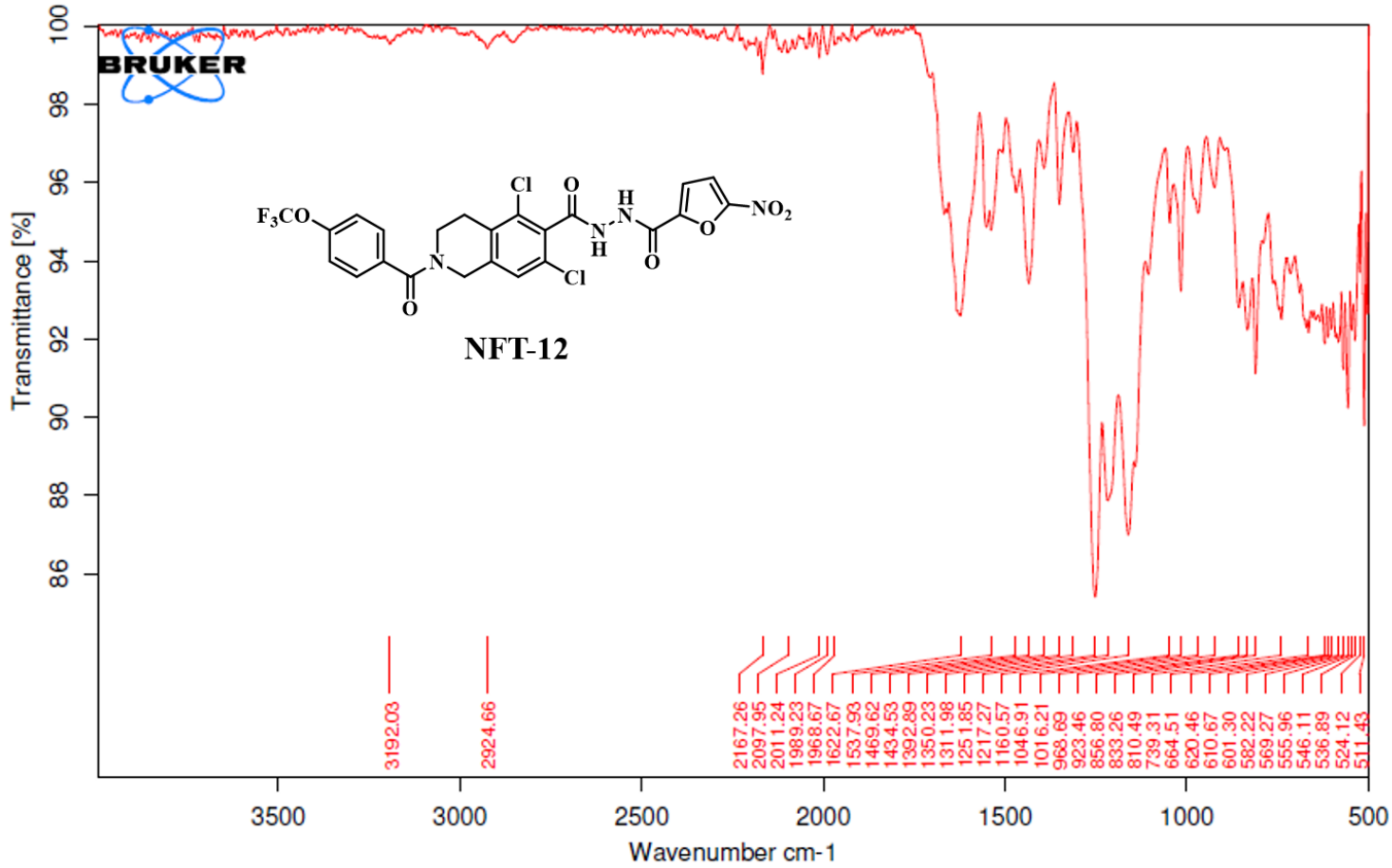

IR spectrum of compound NFT-12

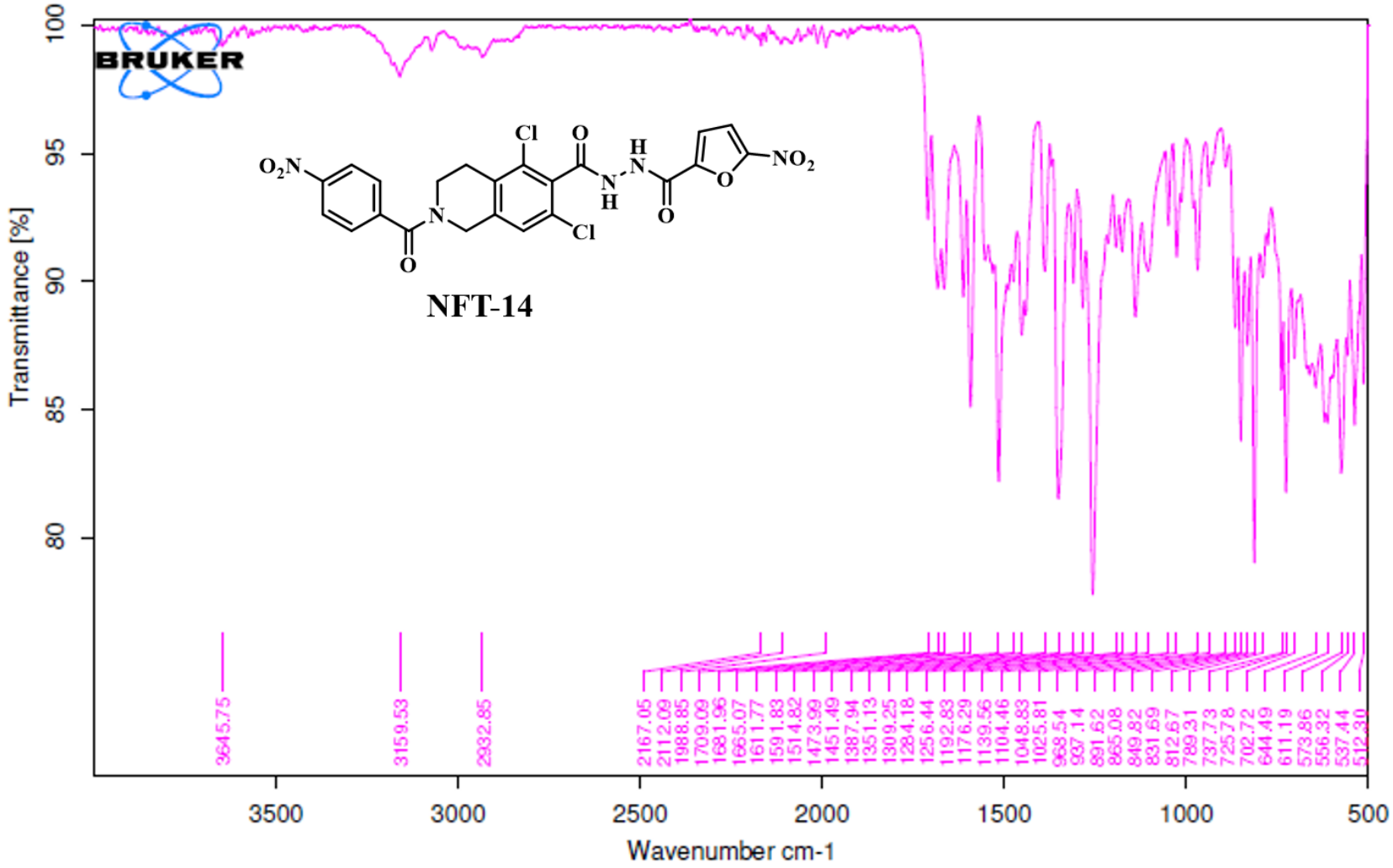

IR spectrum of compound NFT-14

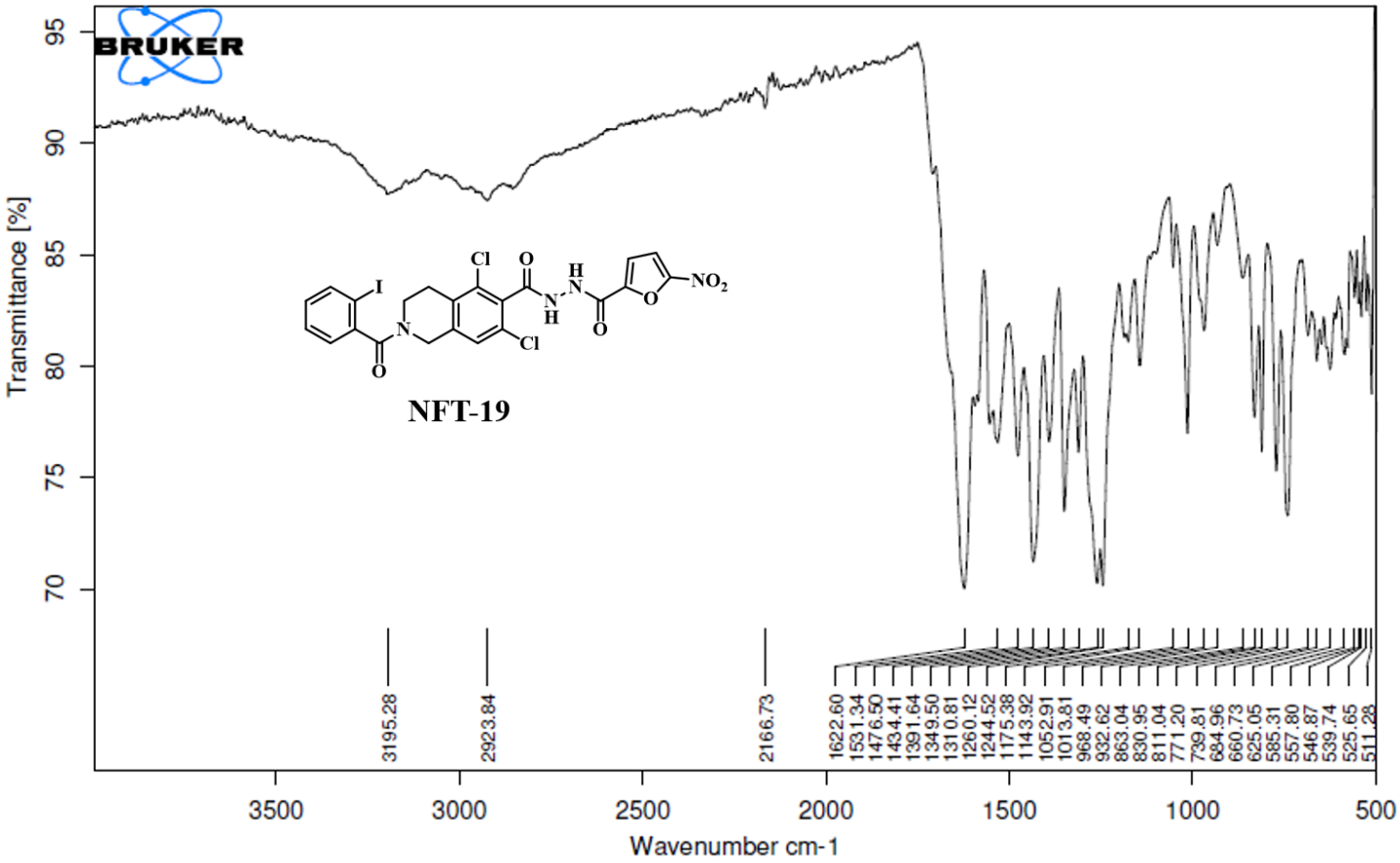

IR spectrum of compound NFT-19

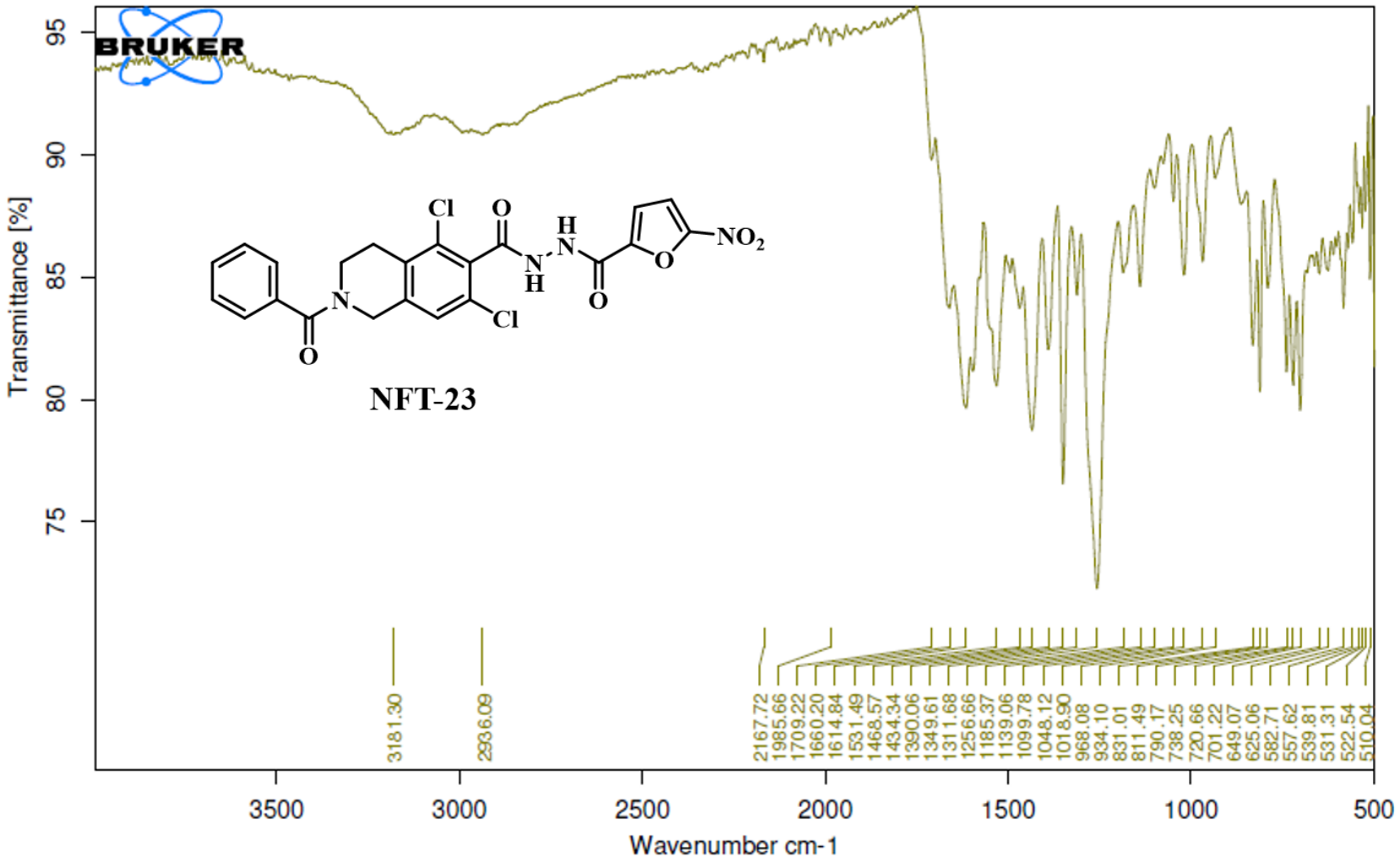

IR spectrum of compound NFT-23

6. *[1]H NMR spectras of final compounds (NFT-1 to NFT-26):*

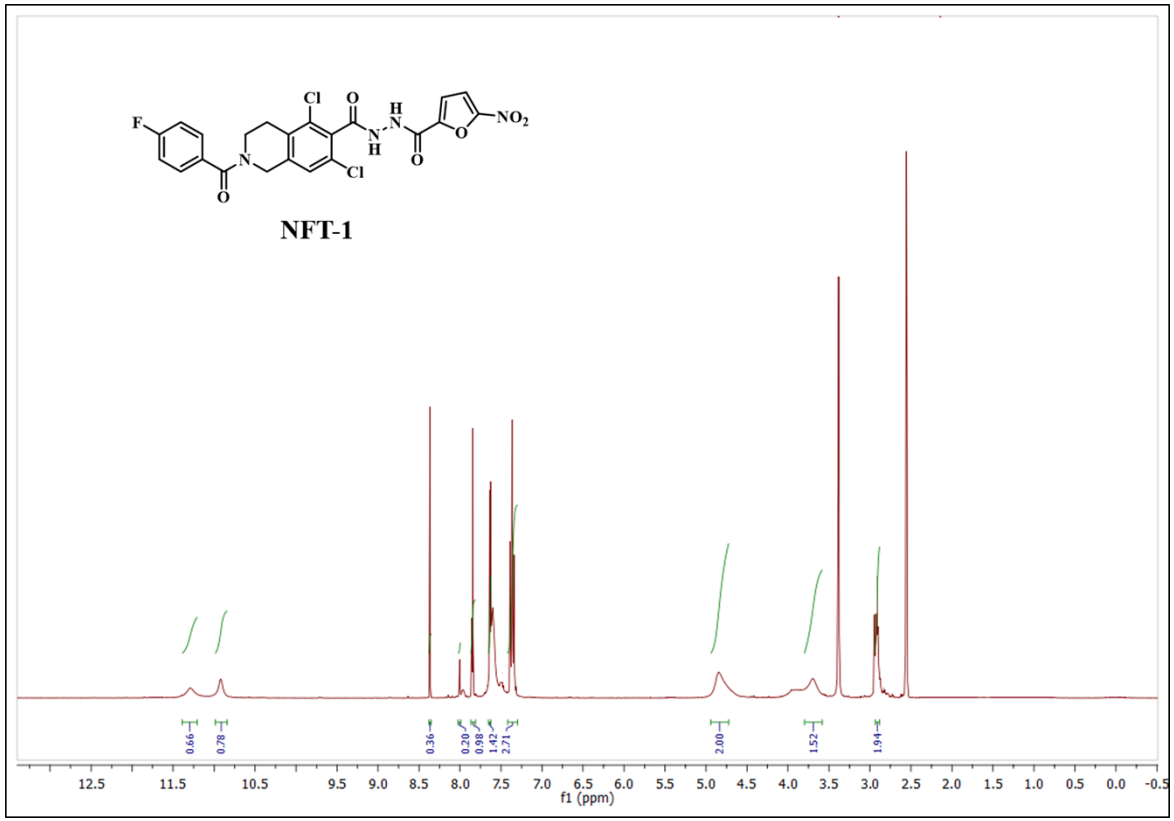

[1]H NMR (400 MHz, DMSO-d_6) spectrum of compound NFT-1

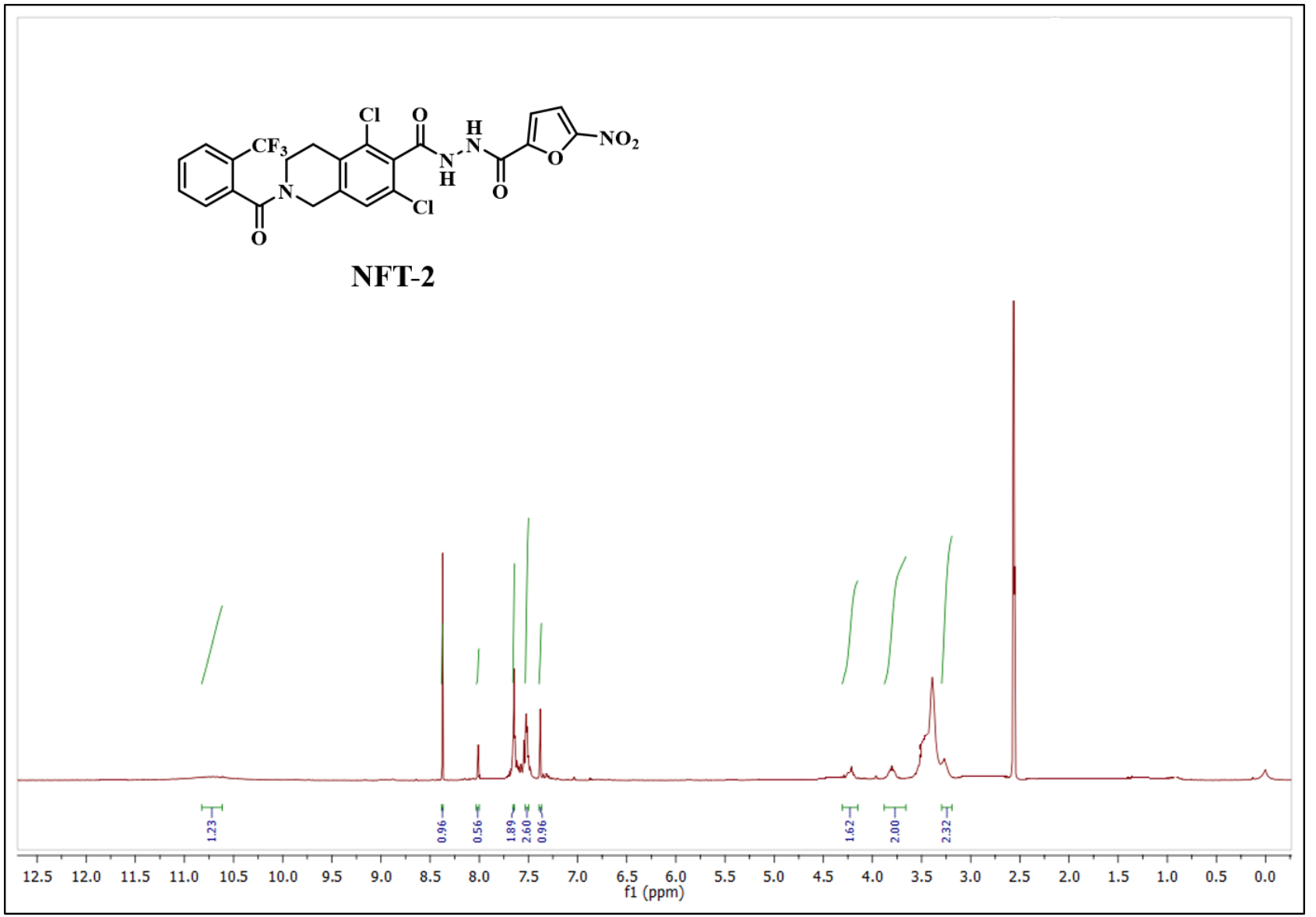

^{1}H NMR (400 MHz, DMSO-d_6) spectrum of compound NFT-2

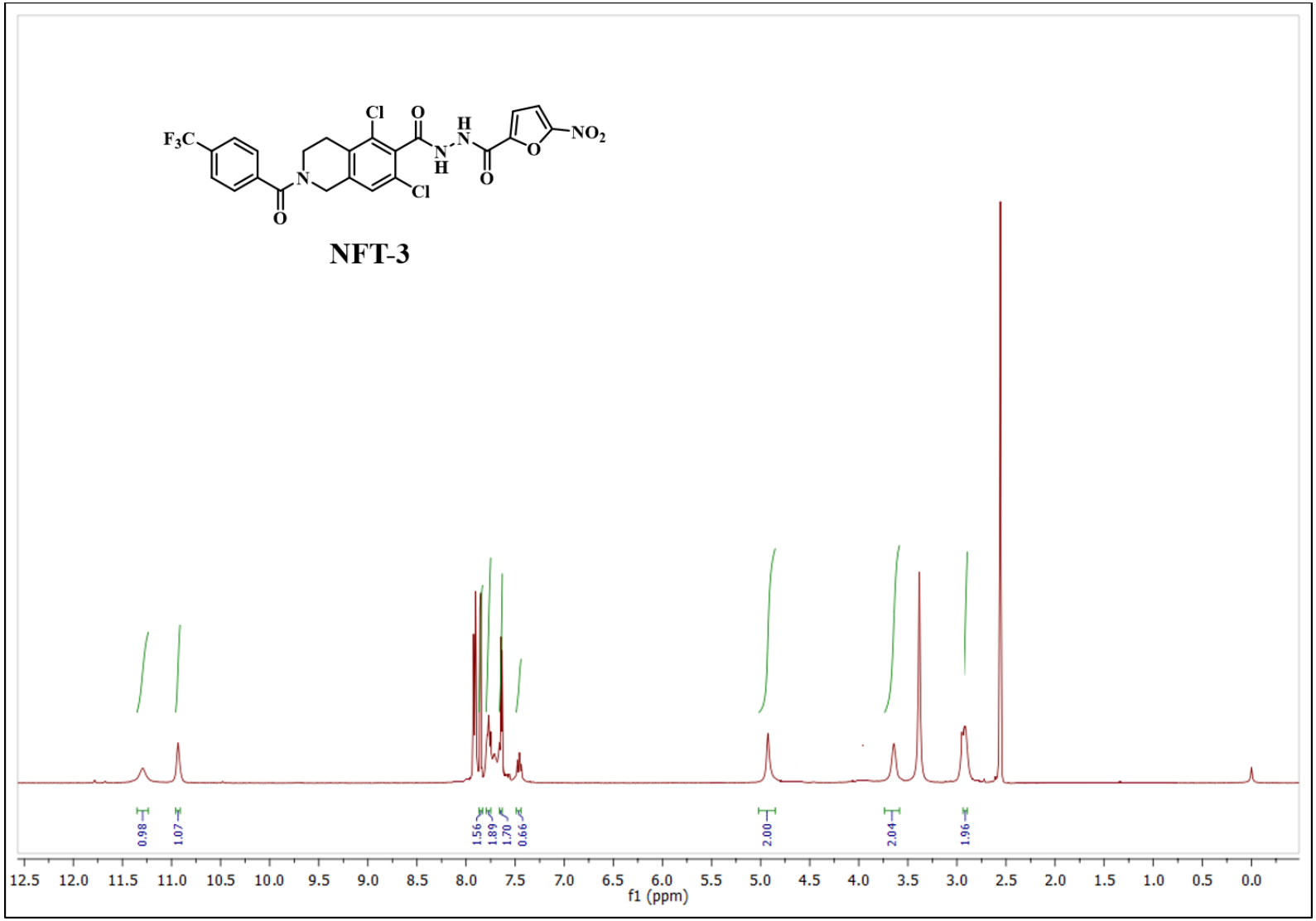

^{1}H NMR (400 MHz, DMSO-d_6) spectrum of compound NFT-3

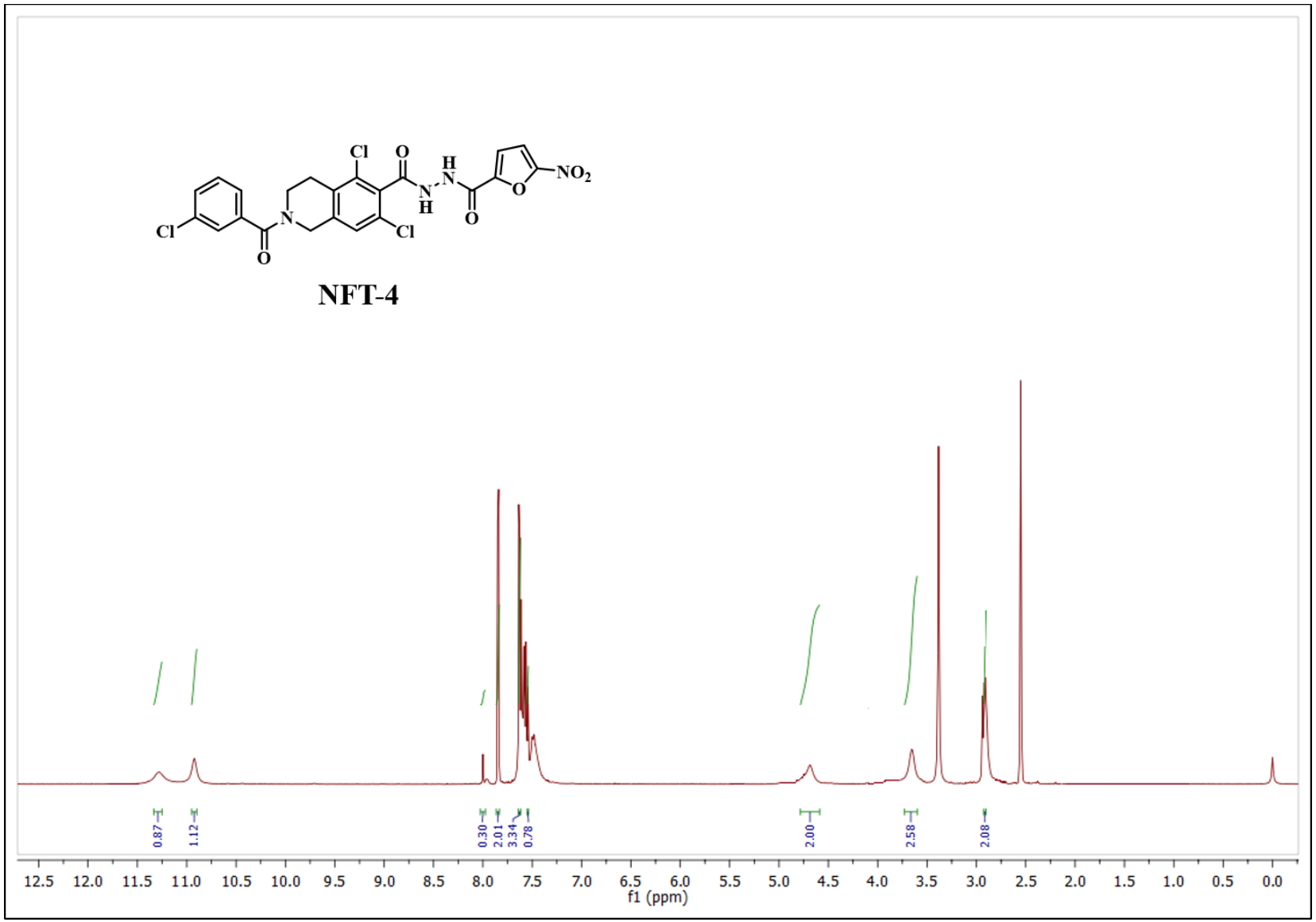

^{1}H NMR (400 MHz, DMSO-d_6) spectrum of compound NFT-4

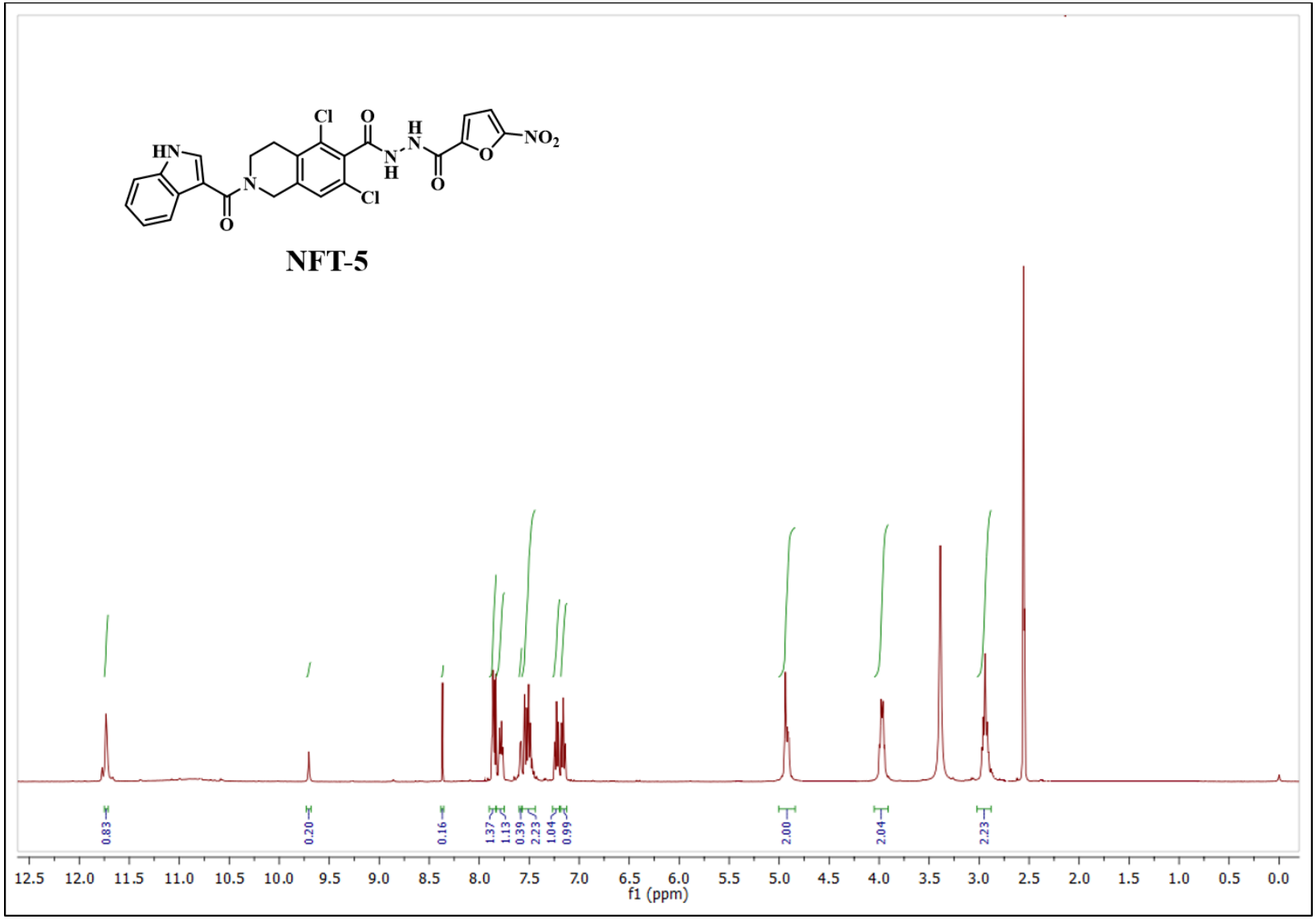

^{1}H NMR (400 MHz, DMSO-d_6) spectrum of compound NFT-5

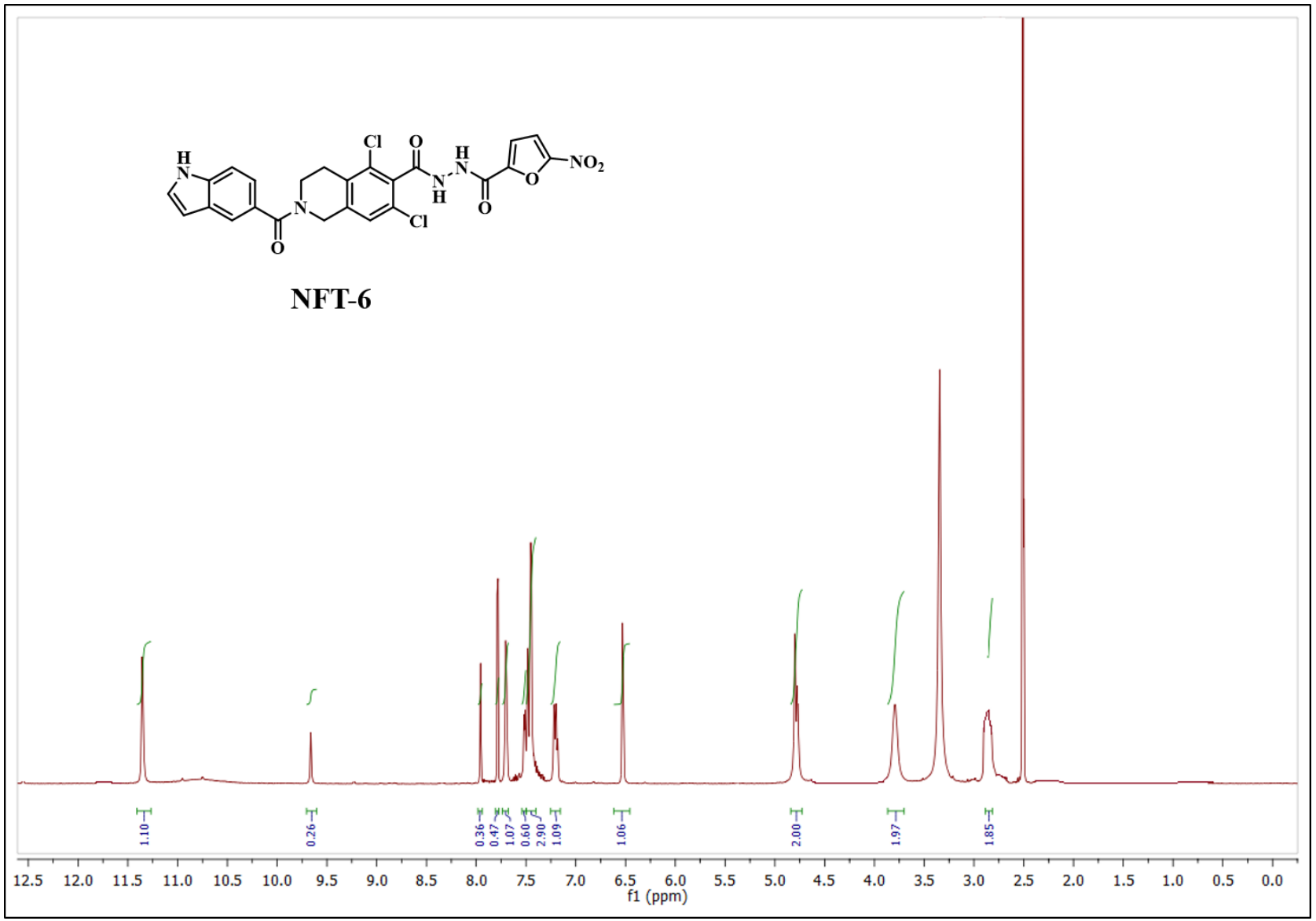

^{1}H NMR (400 MHz, DMSO-d_6) spectrum of compound NFT-6

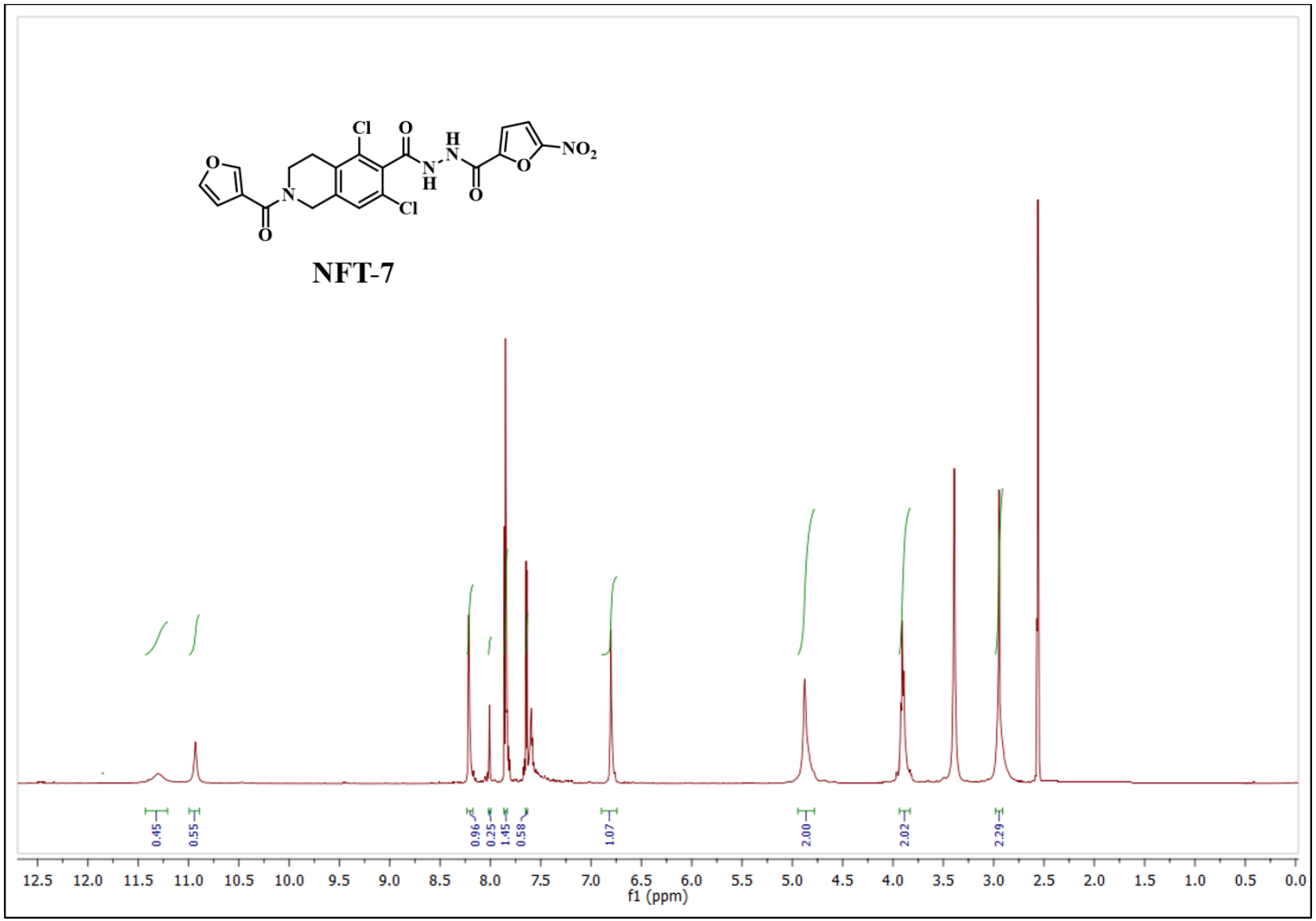

^{1}H NMR (400 MHz, DMSO-d_6) spectrum of compound NFT-7

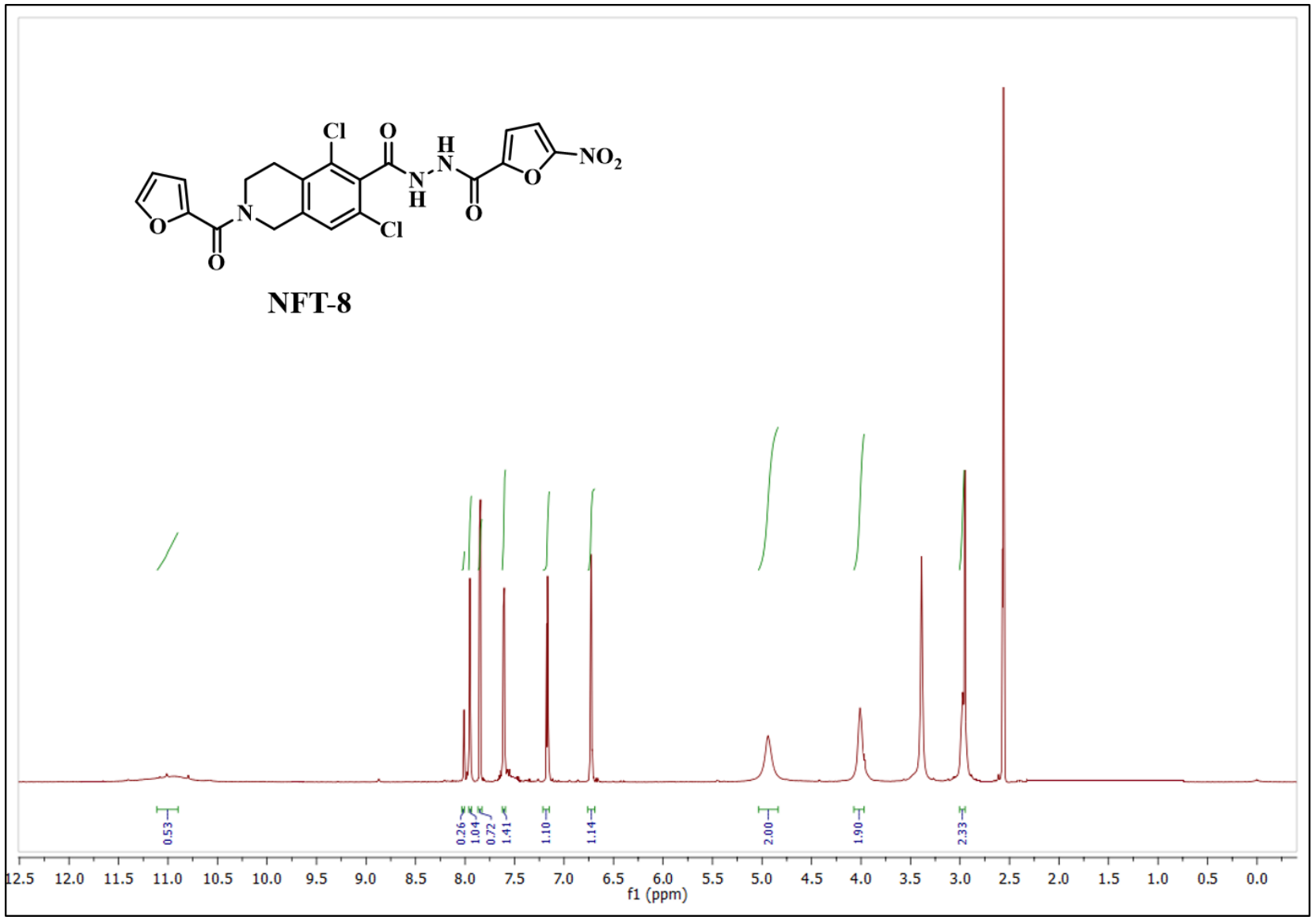

^{1}H NMR (400 MHz, DMSO-d_6) spectrum of compound NFT-8

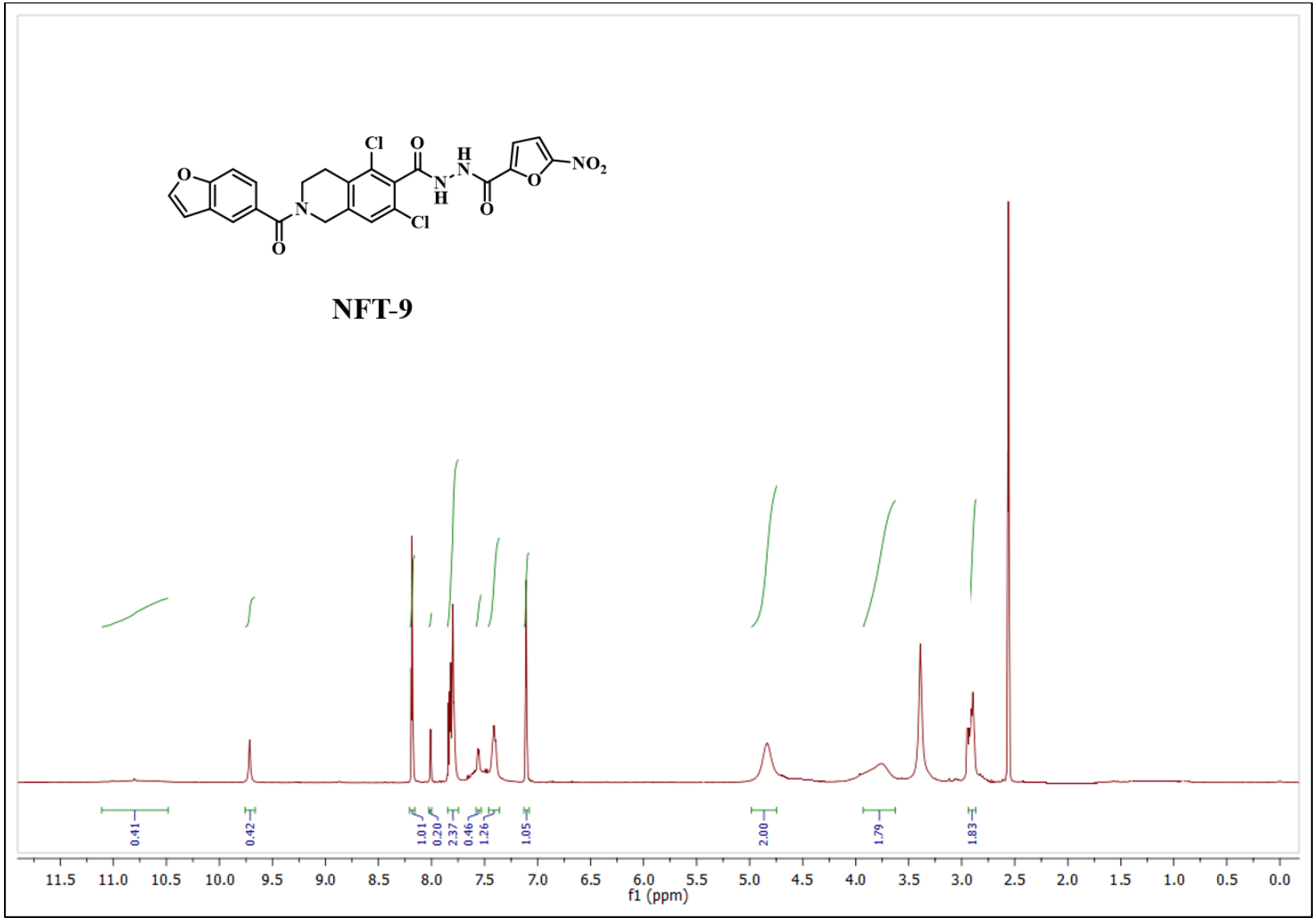

^{1}H NMR (400 MHz, DMSO-d_6) spectrum of compound NFT-9

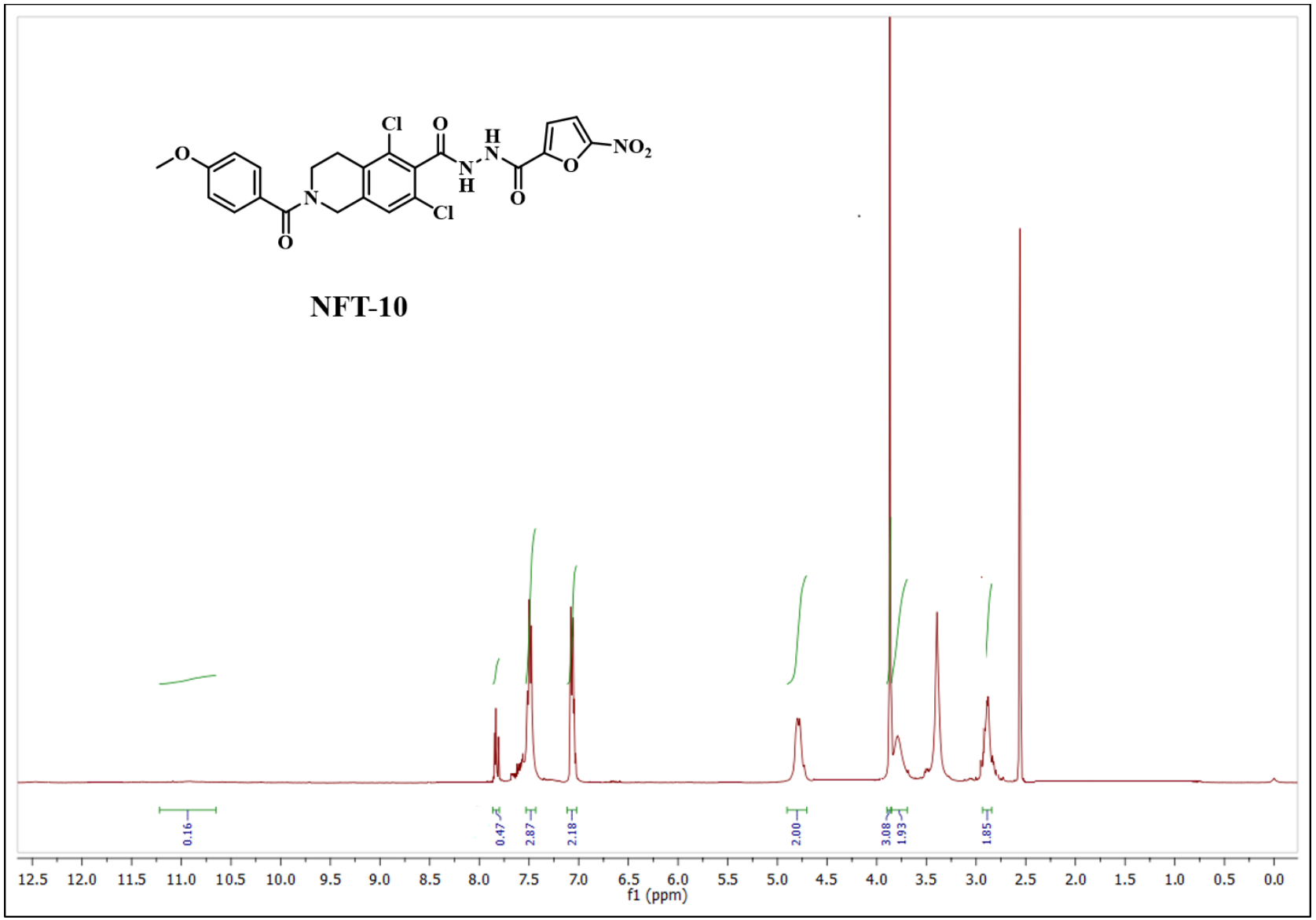

^{1}H NMR (400 MHz, DMSO-d_6) spectrum of compound NFT-10

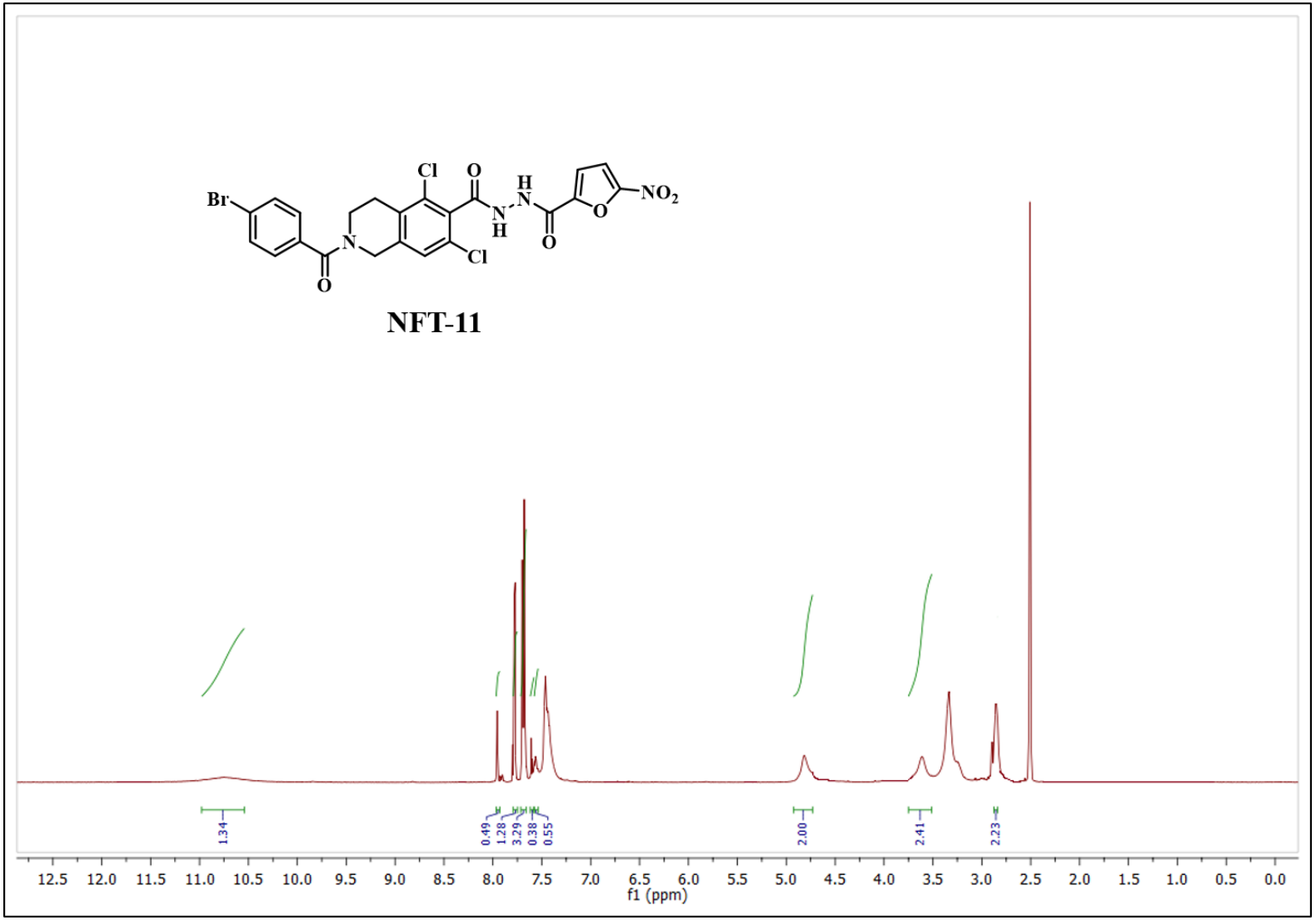

^{1}H NMR (400 MHz, DMSO-d_6) spectrum of compound NFT-11

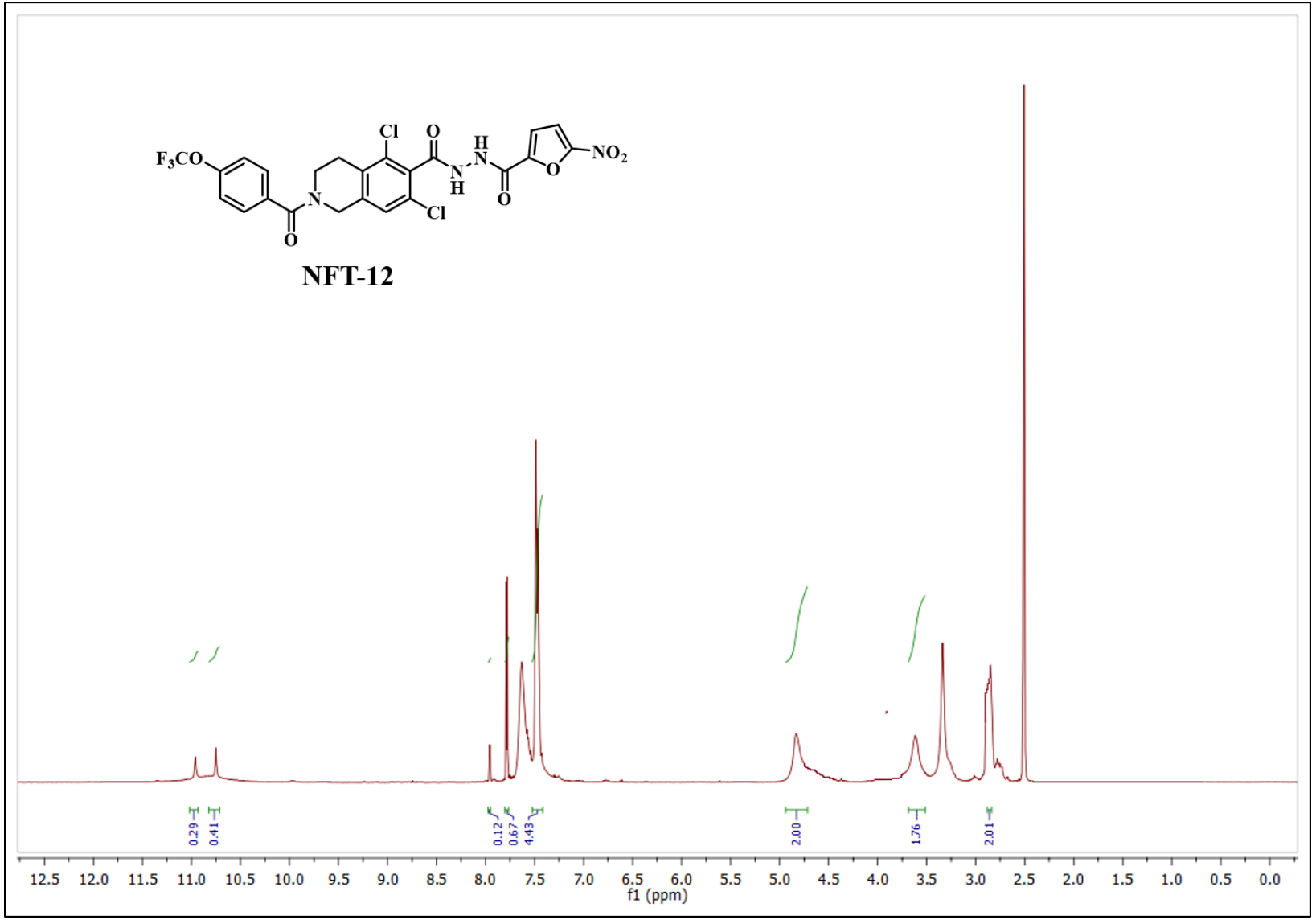

^{1}H NMR (400 MHz, DMSO-d_6) spectrum of compound NFT NFT-12

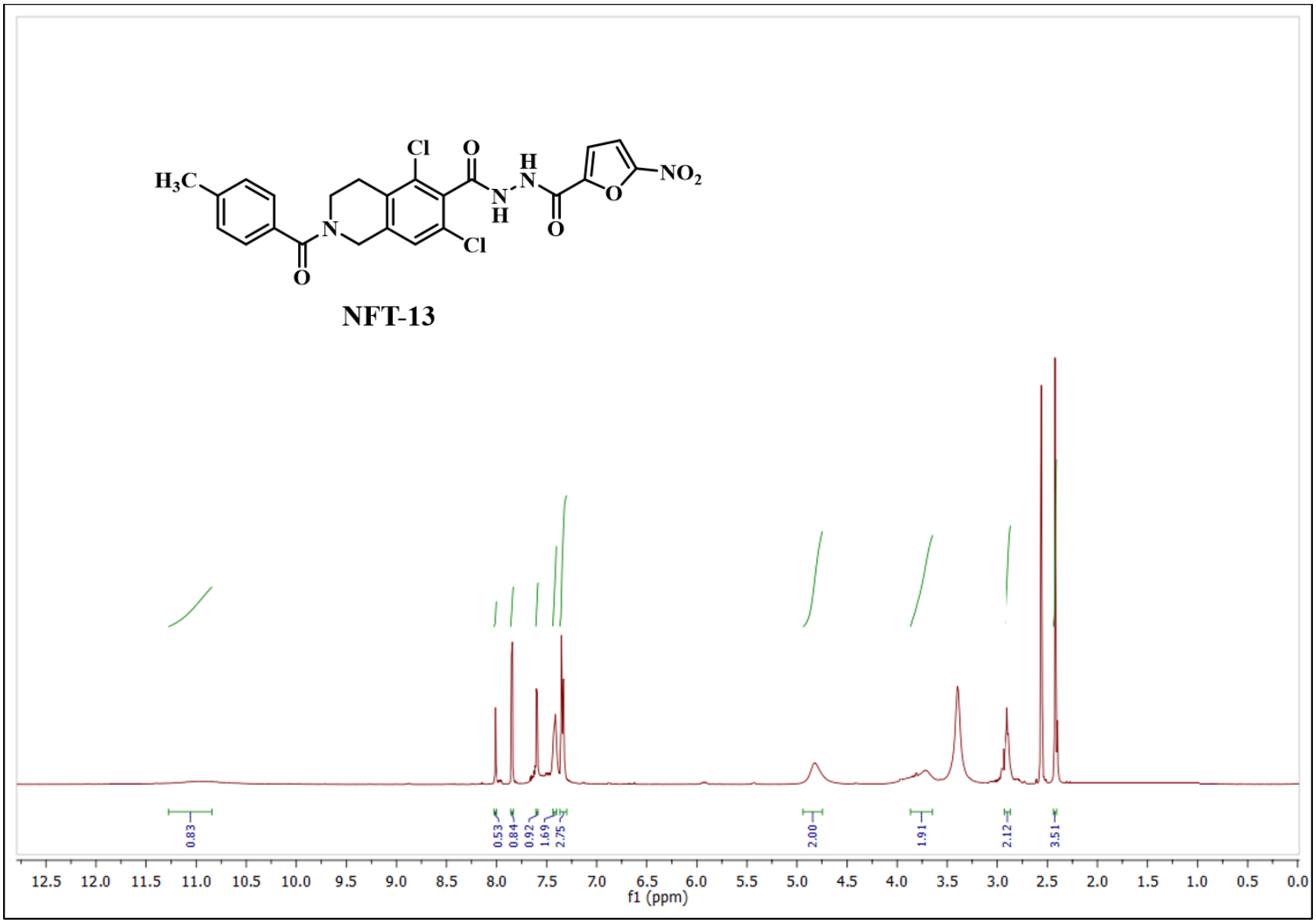

^{1}H NMR (400 MHz, DMSO-d_6) spectrum of compound NFT-13

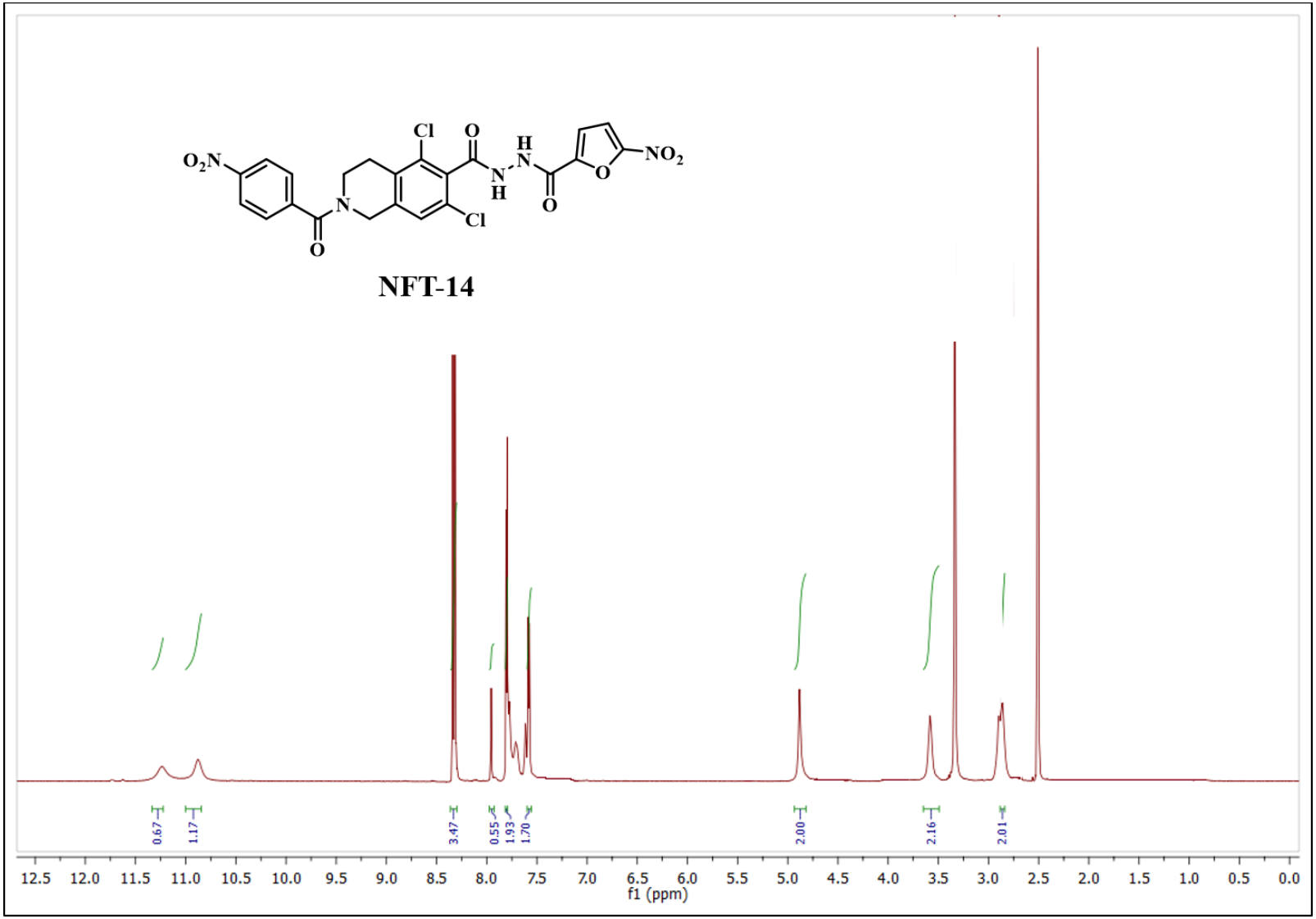

^{1}H NMR (400 MHz, DMSO-d_6) spectrum of compound NFT-14

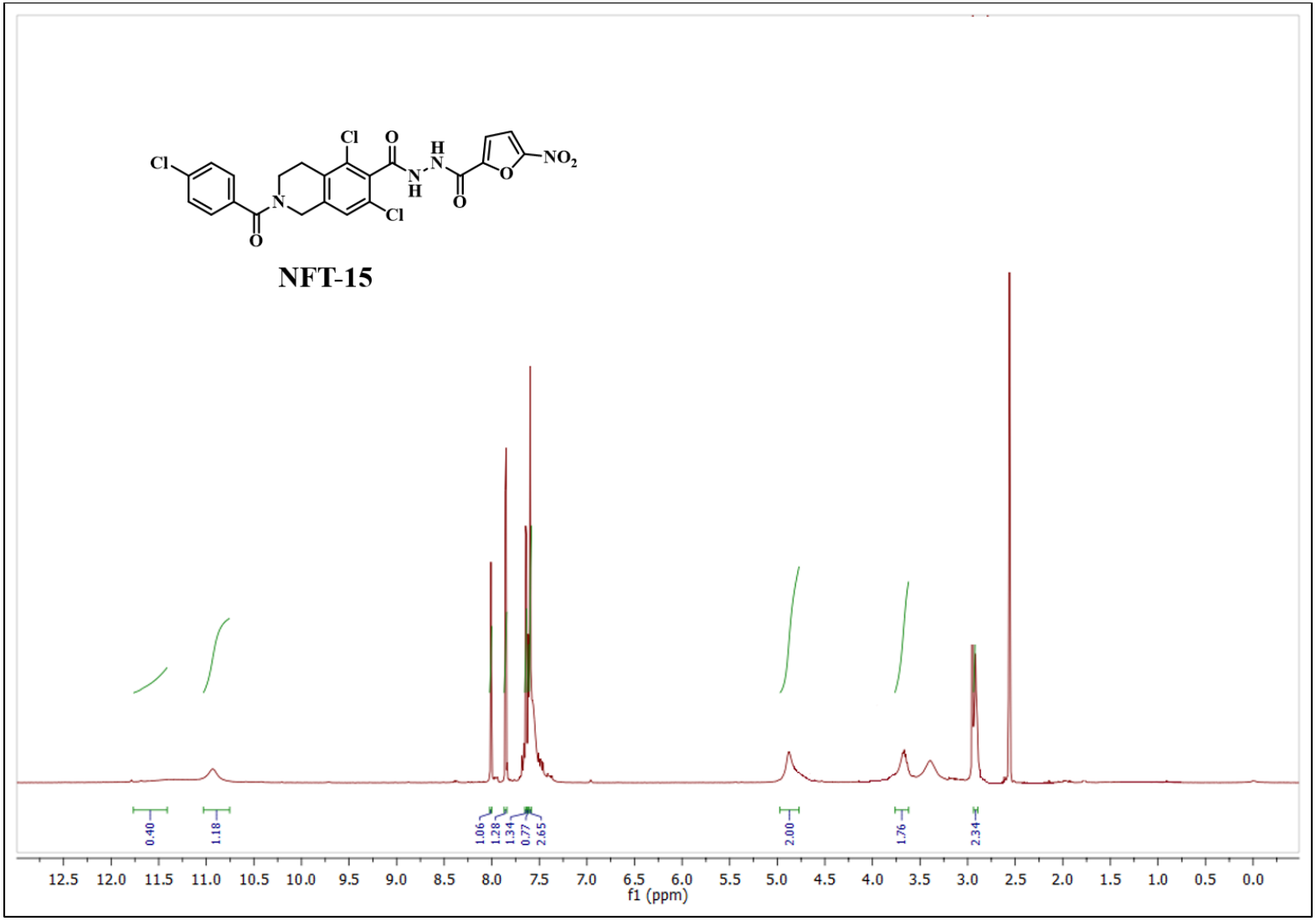

^{1}H NMR (400 MHz, DMSO-d_6) spectrum of compound NFT-15

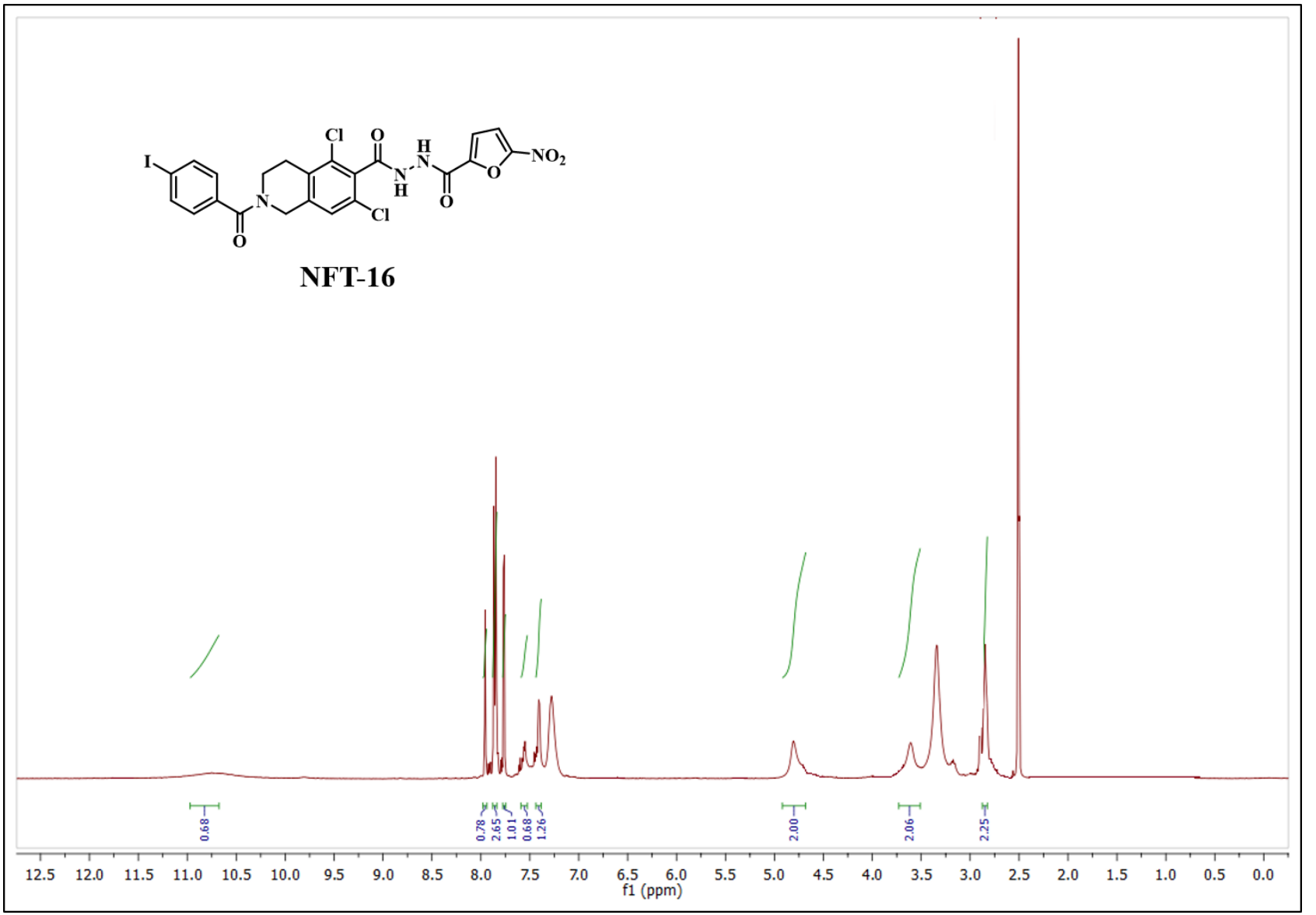

^{1}H NMR (400 MHz, DMSO-d_6) spectrum of compound NFT-16

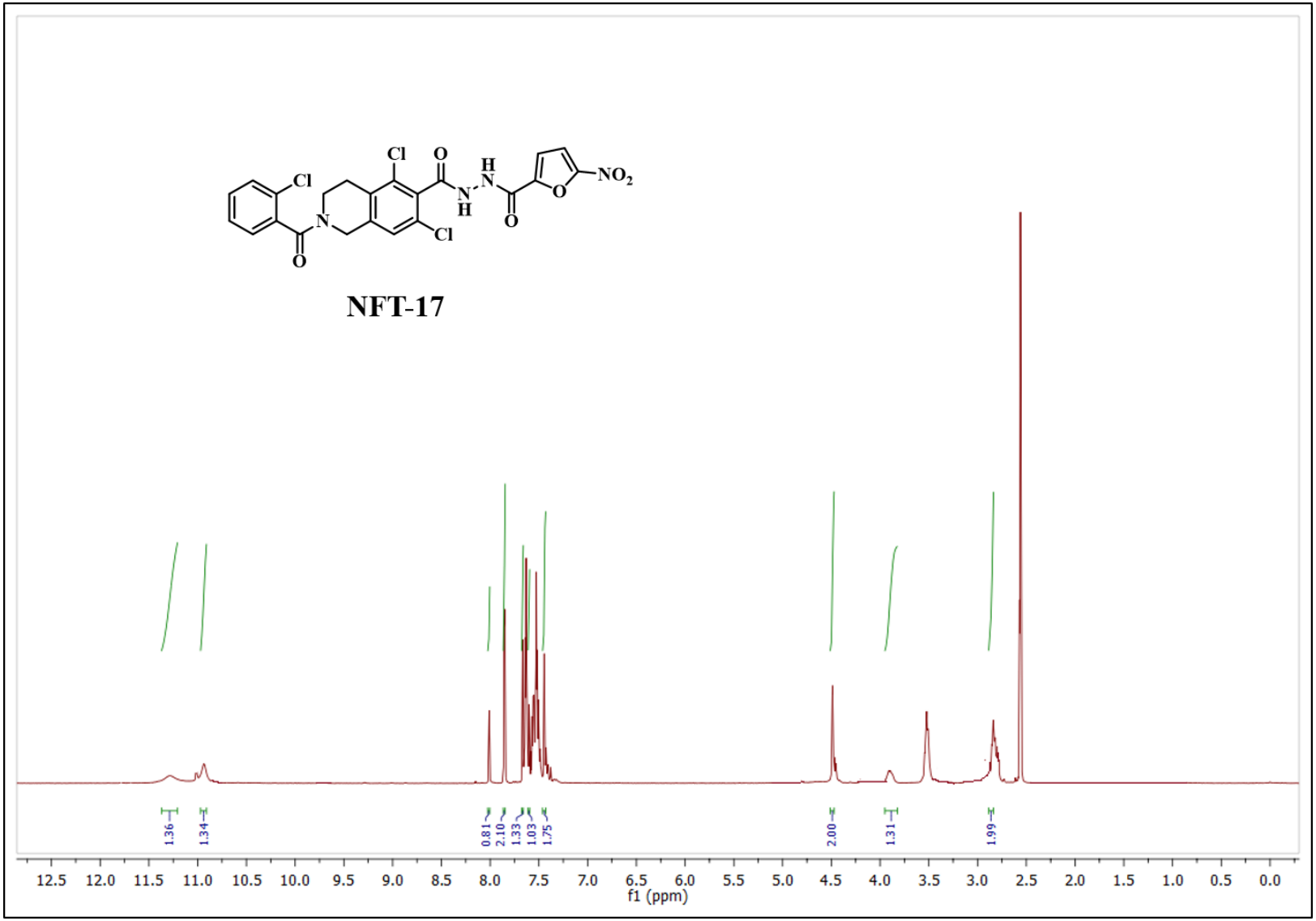

^{1}H NMR (400 MHz, DMSO-d_6) spectrum of compound NFT-17

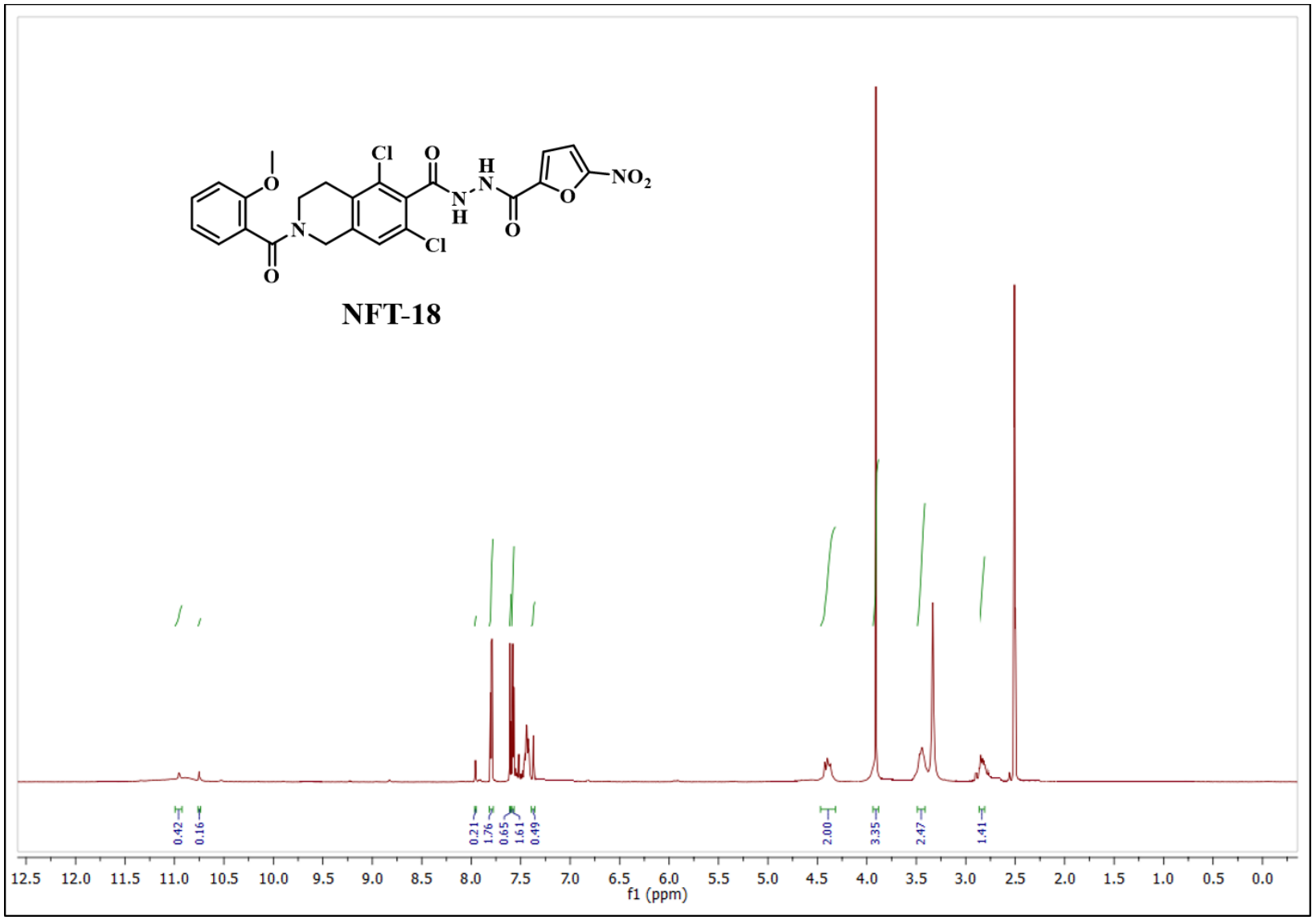

^{1}H NMR (400 MHz, DMSO-d_6) spectrum of compound NFT-18

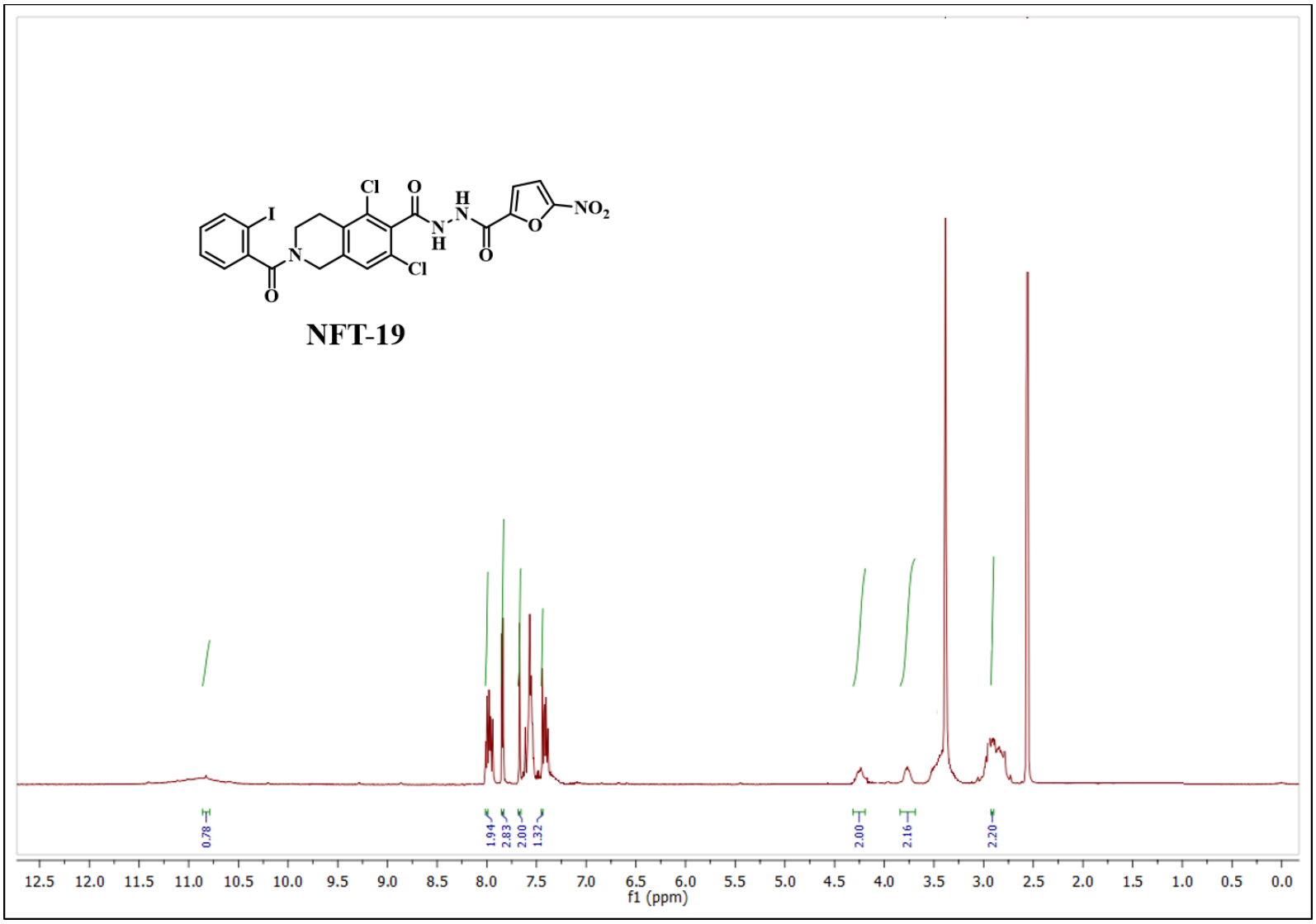

^{1}H NMR (400 MHz, DMSO-d_6) spectrum of compound NFT-19

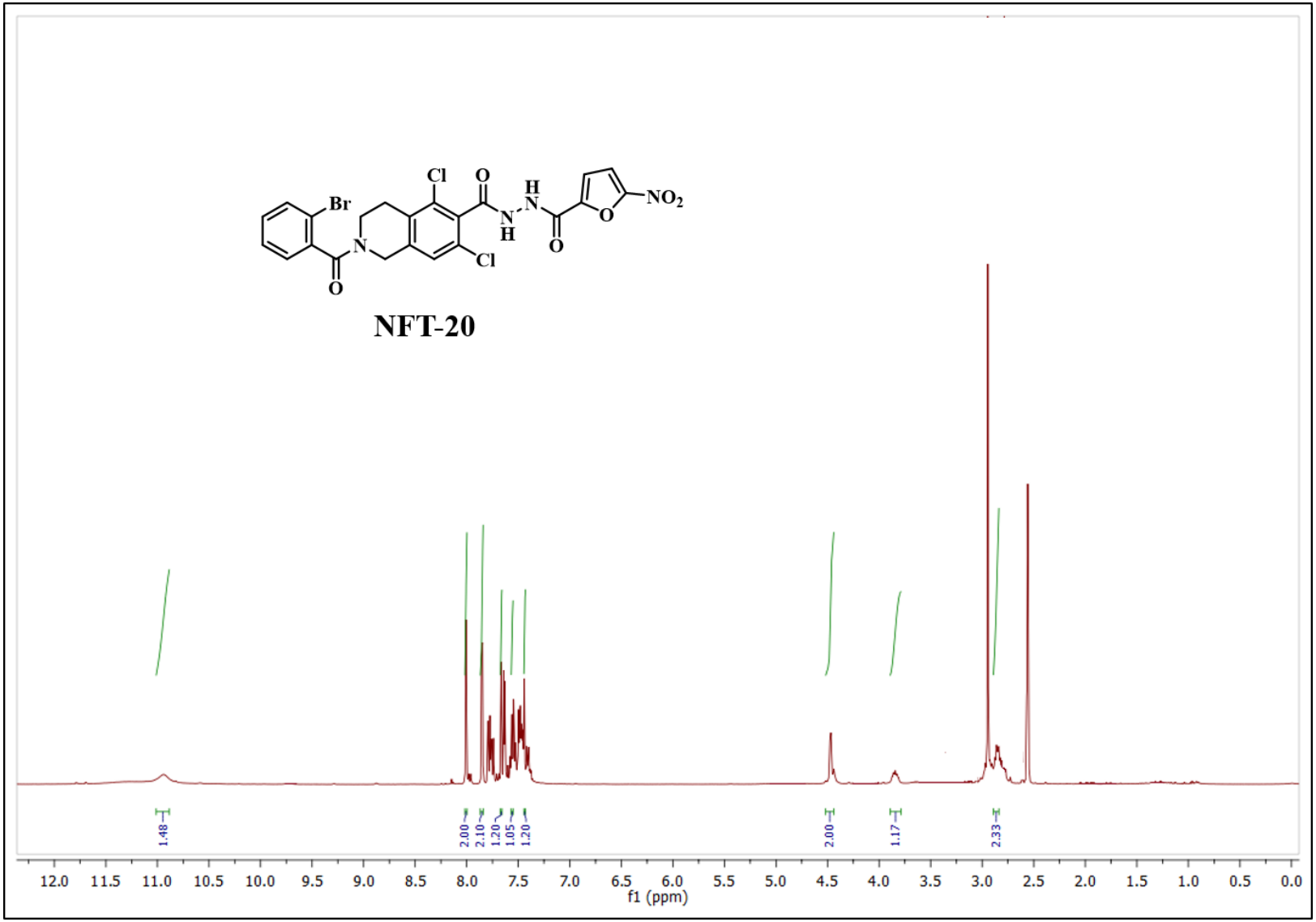

^{1}H NMR (400 MHz, DMSO-d_6) spectrum of compound NFT-20

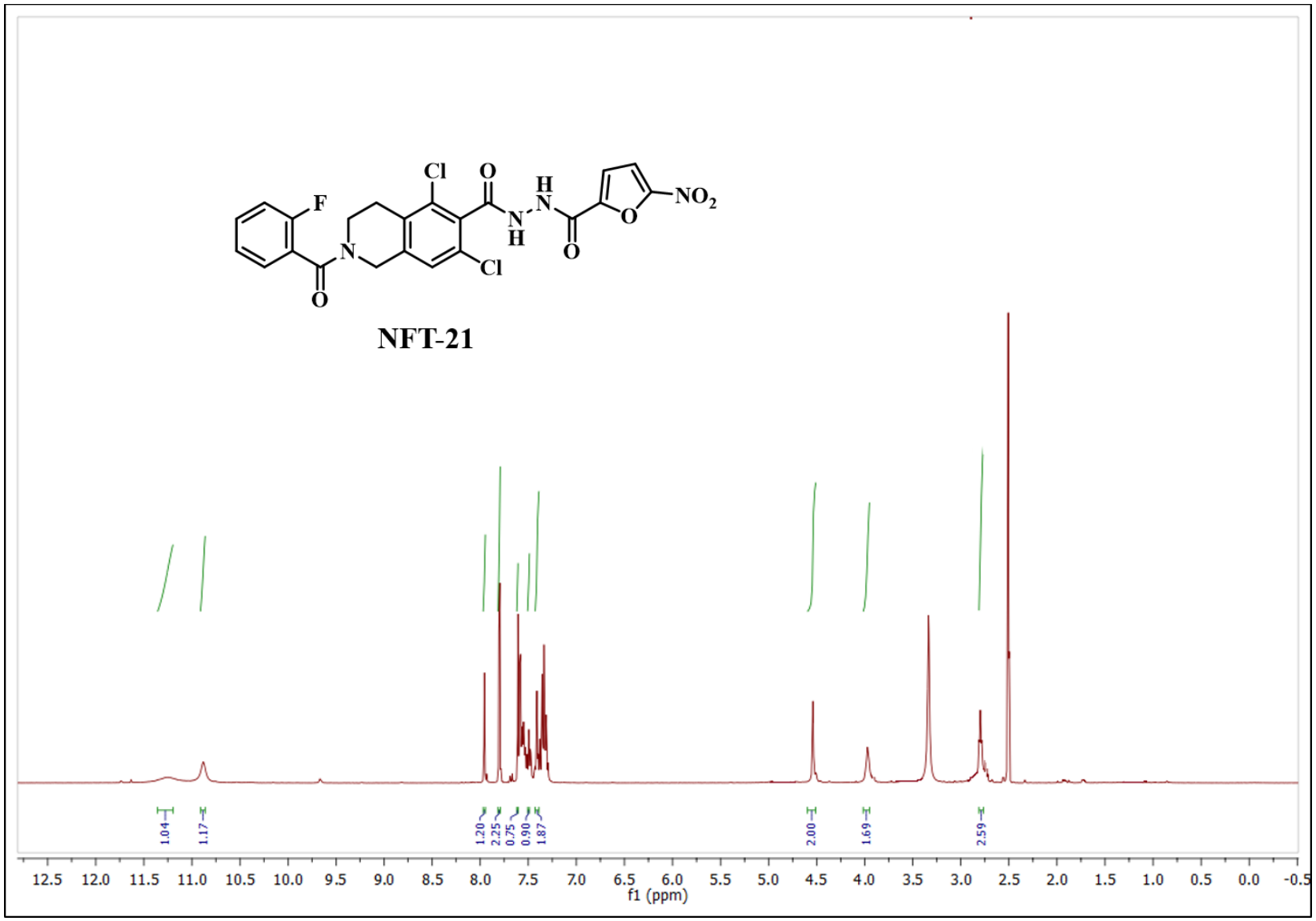

^{1}H NMR (400 MHz, DMSO-d_6) spectrum of compound NFT-21

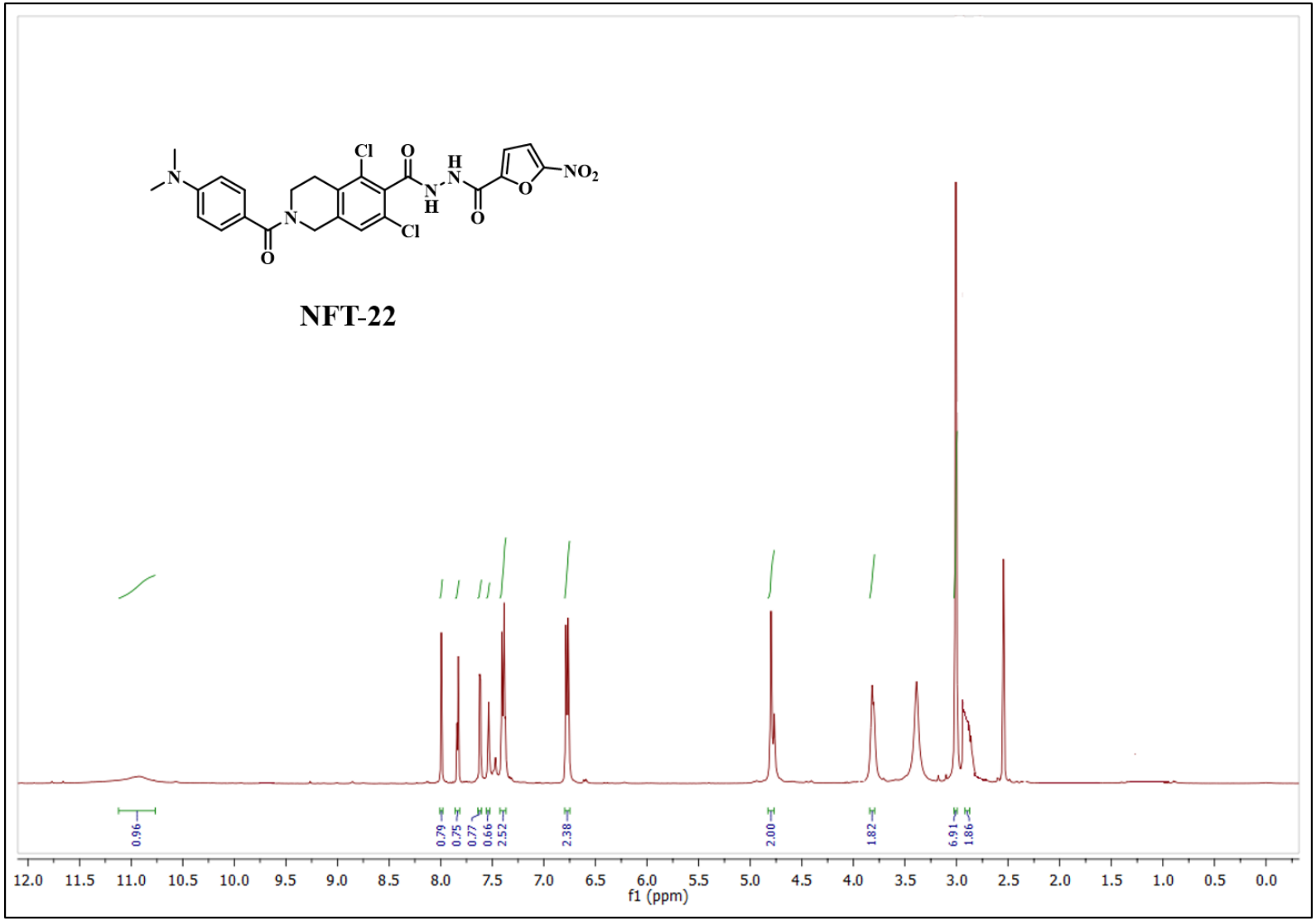

^{1}H NMR (400 MHz, DMSO-d_6) spectrum of compound NFT-22

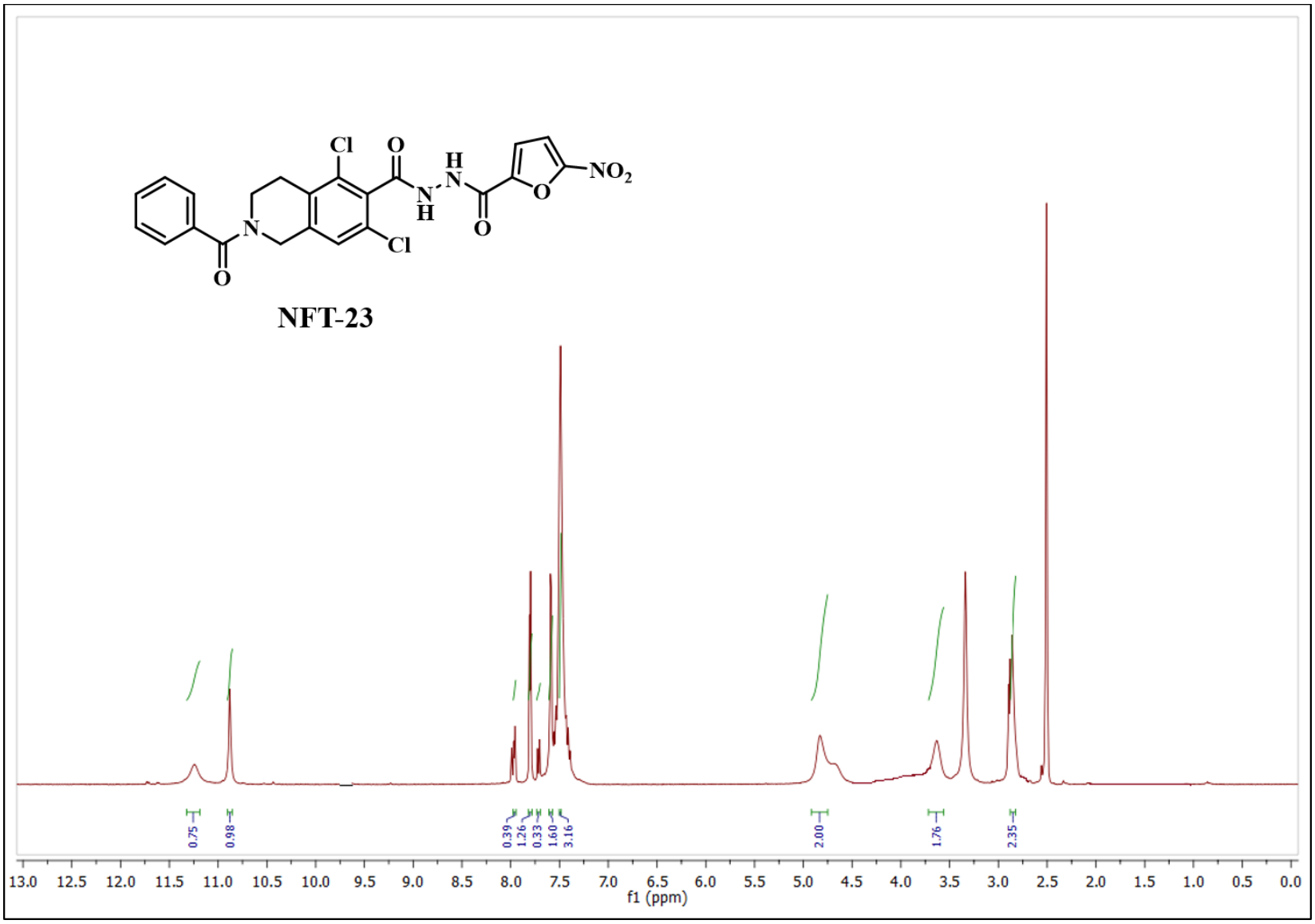

^{1}H NMR (400 MHz, DMSO-d_6) spectrum of compound NFT-23

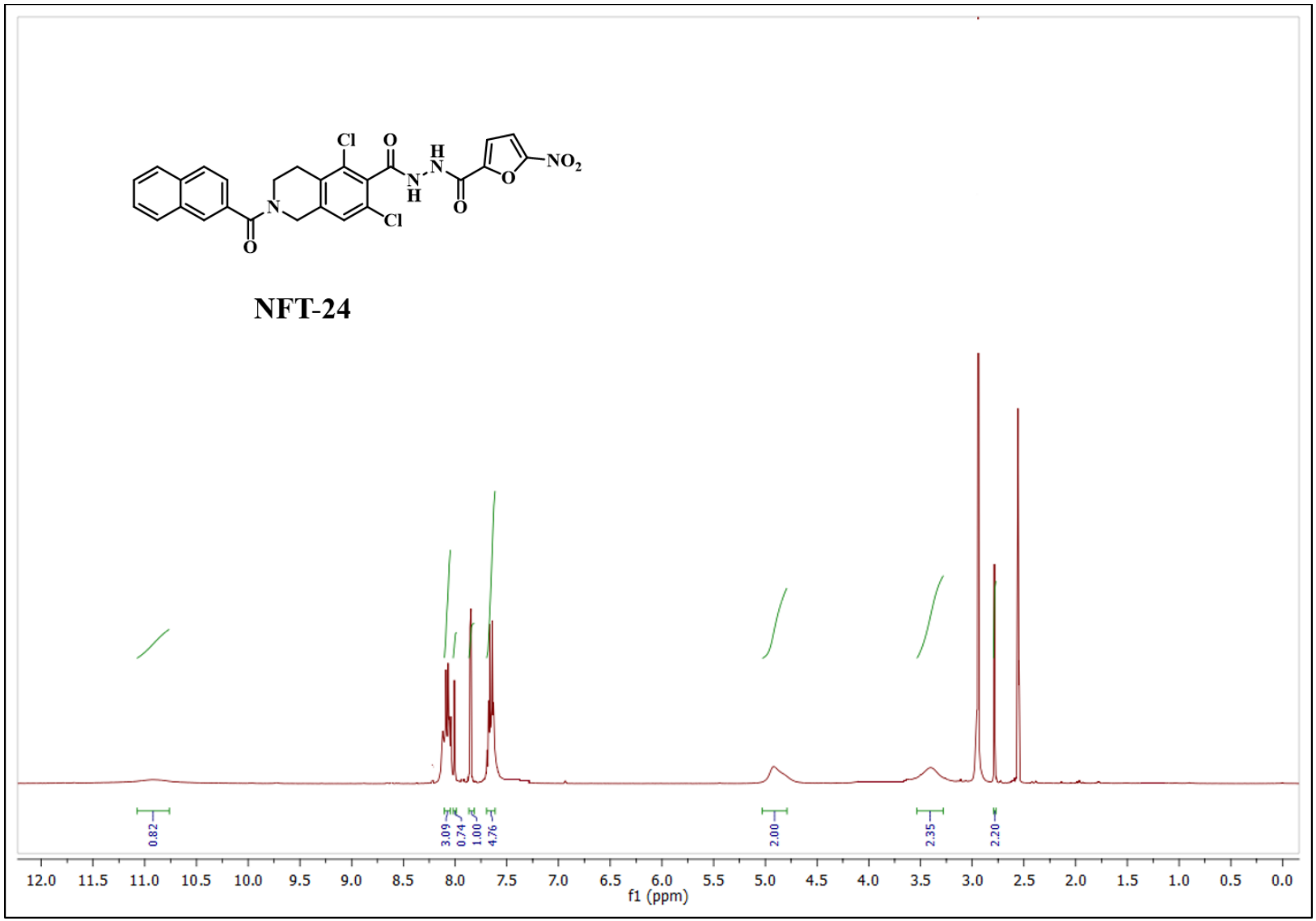

^{1}H NMR (400 MHz, DMSO-d_6) spectrum of compound NFT-24

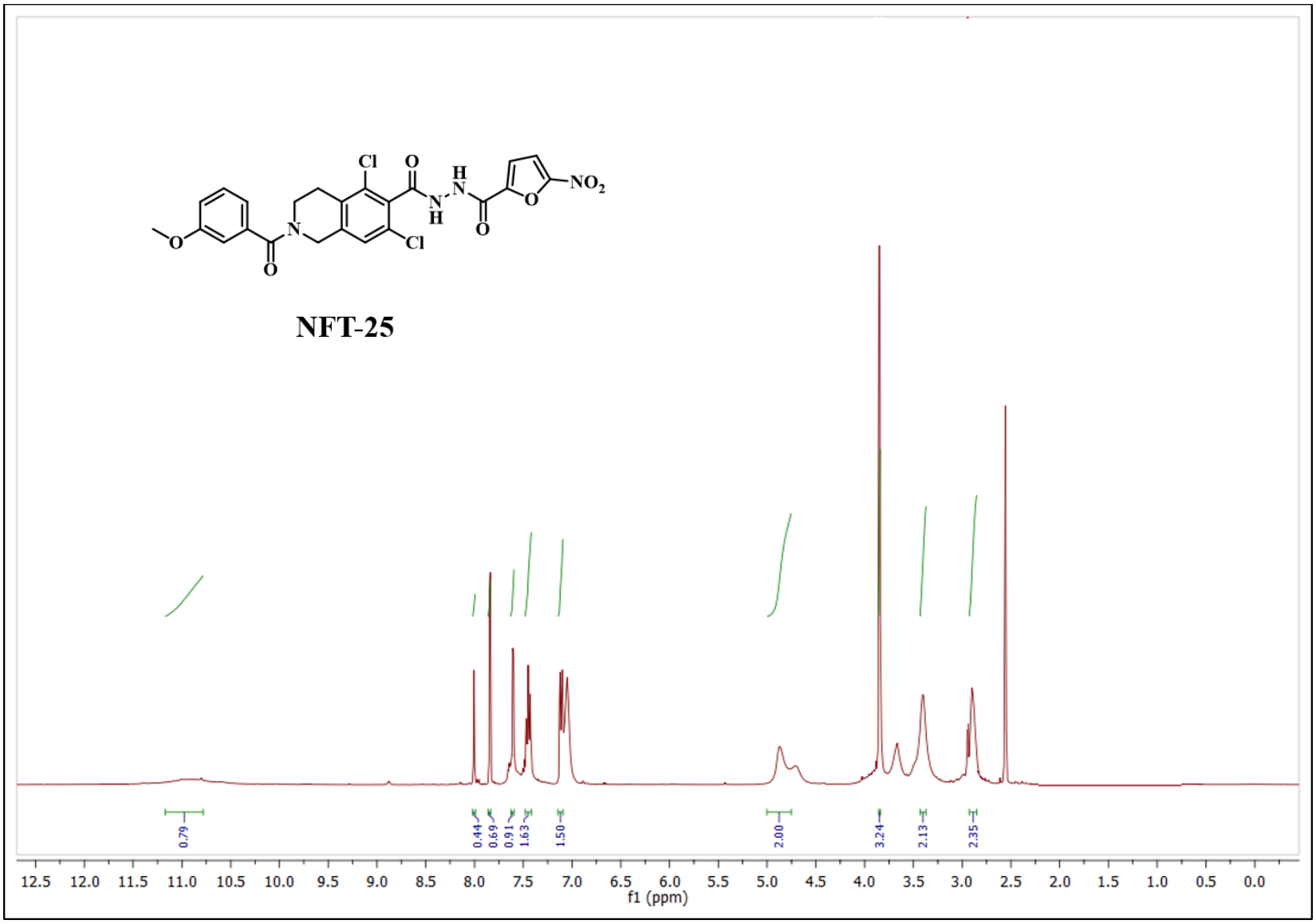

^{1}H NMR (400 MHz, DMSO-d_6) spectrum of compound NFT-25

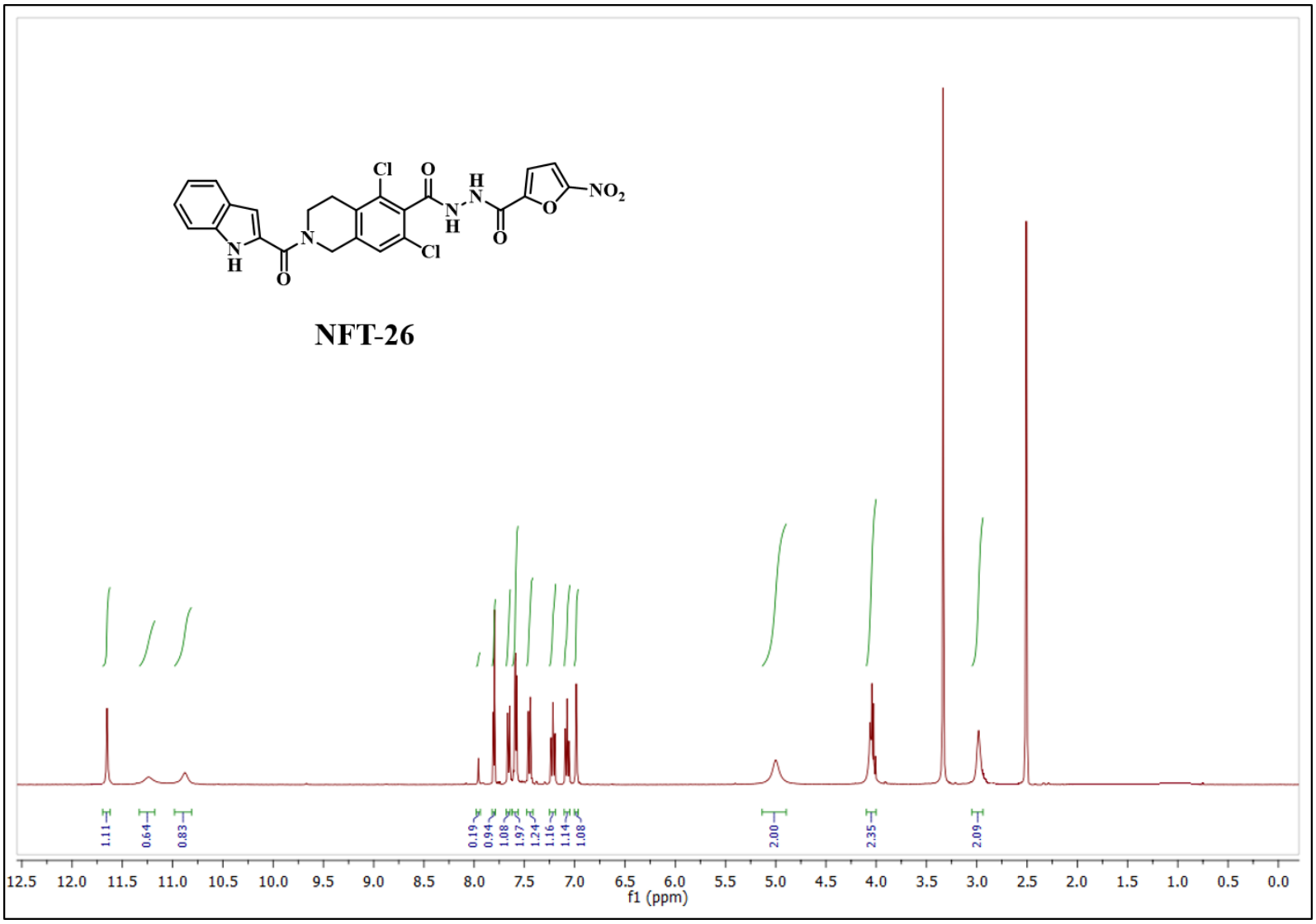

^{1}H NMR (400 MHz, DMSO-d_6) spectrum of compound NFT-26

7. *[13]C NMR spectras of final compounds (NFT-1 to NFT-26):*

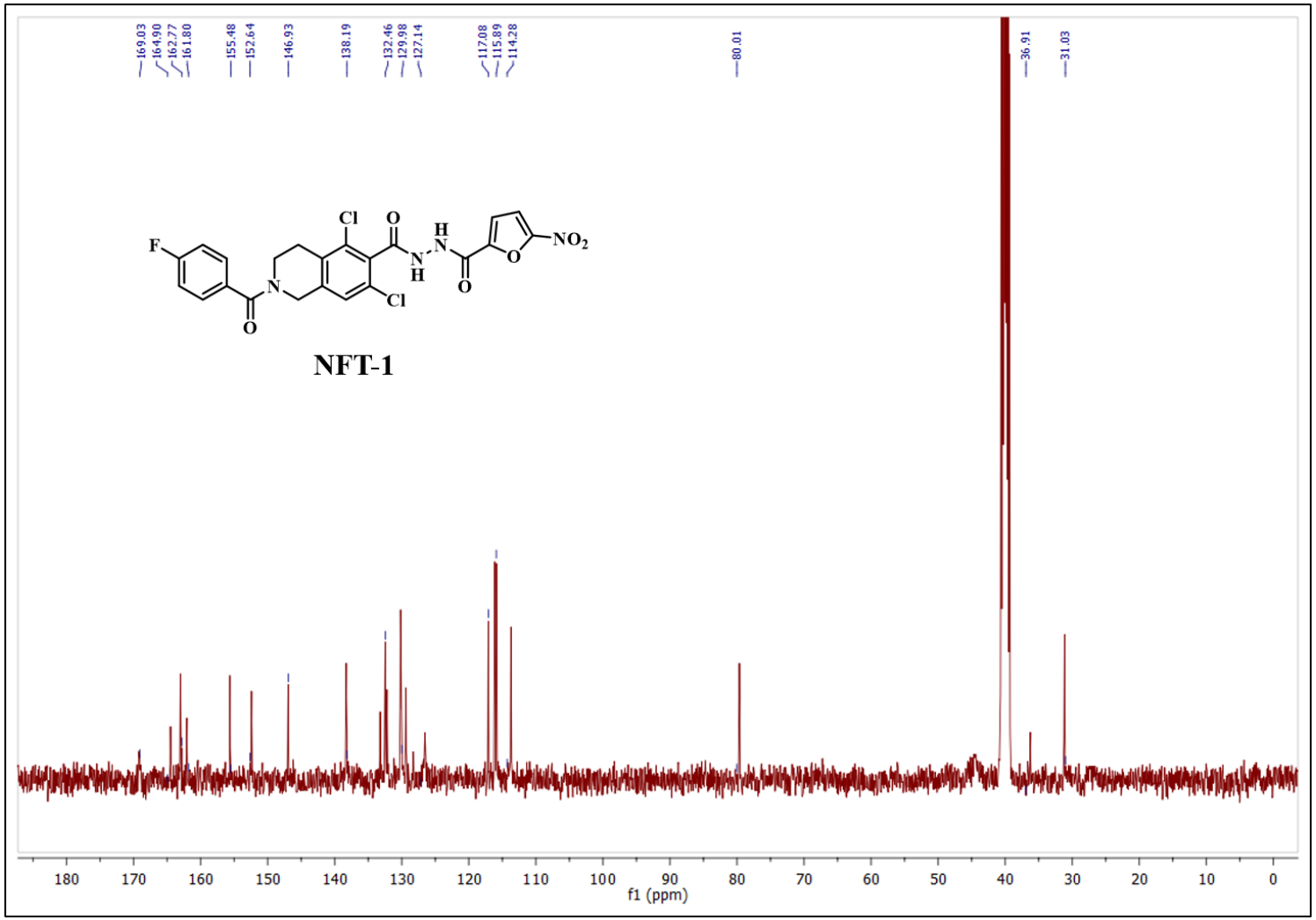

[13]C NMR (101 MHz, DMSO-d_6) spectrum of compound NFT-1

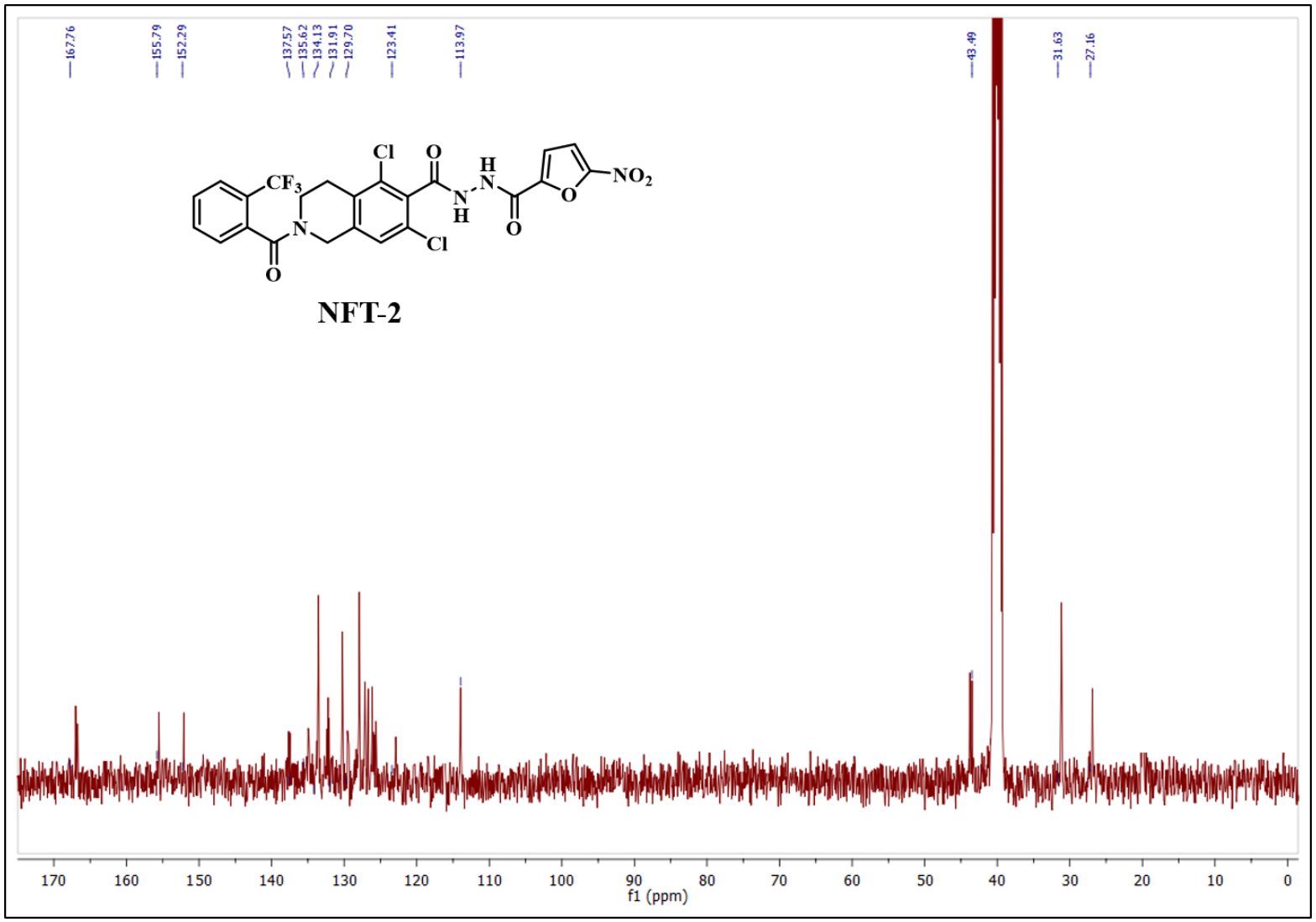

^{13}C NMR (101 MHz, DMSO-d_6) spectrum of compound NFT-2

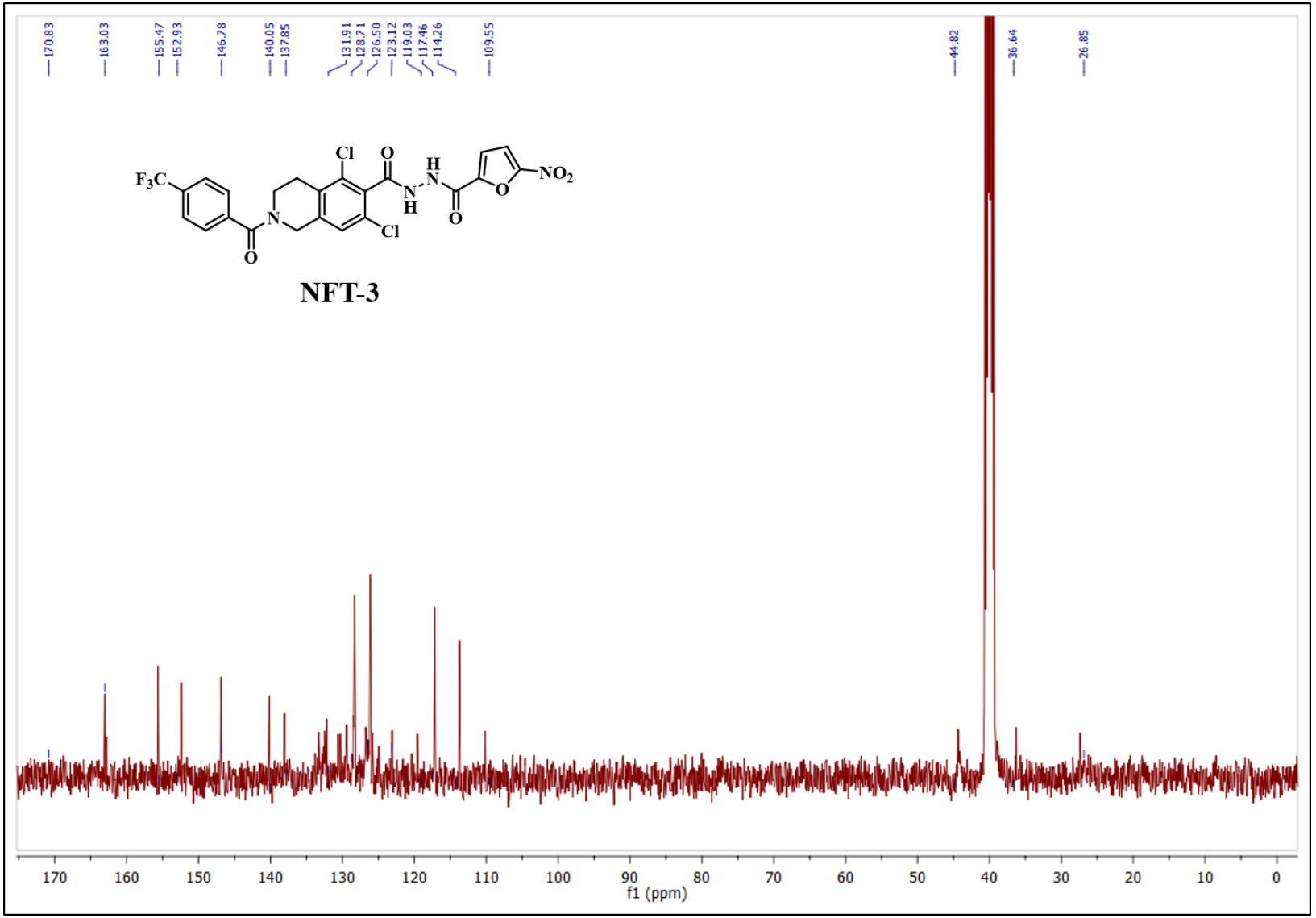

^{13}C NMR (101 MHz, DMSO-d_6) spectrum of compound NFT-3

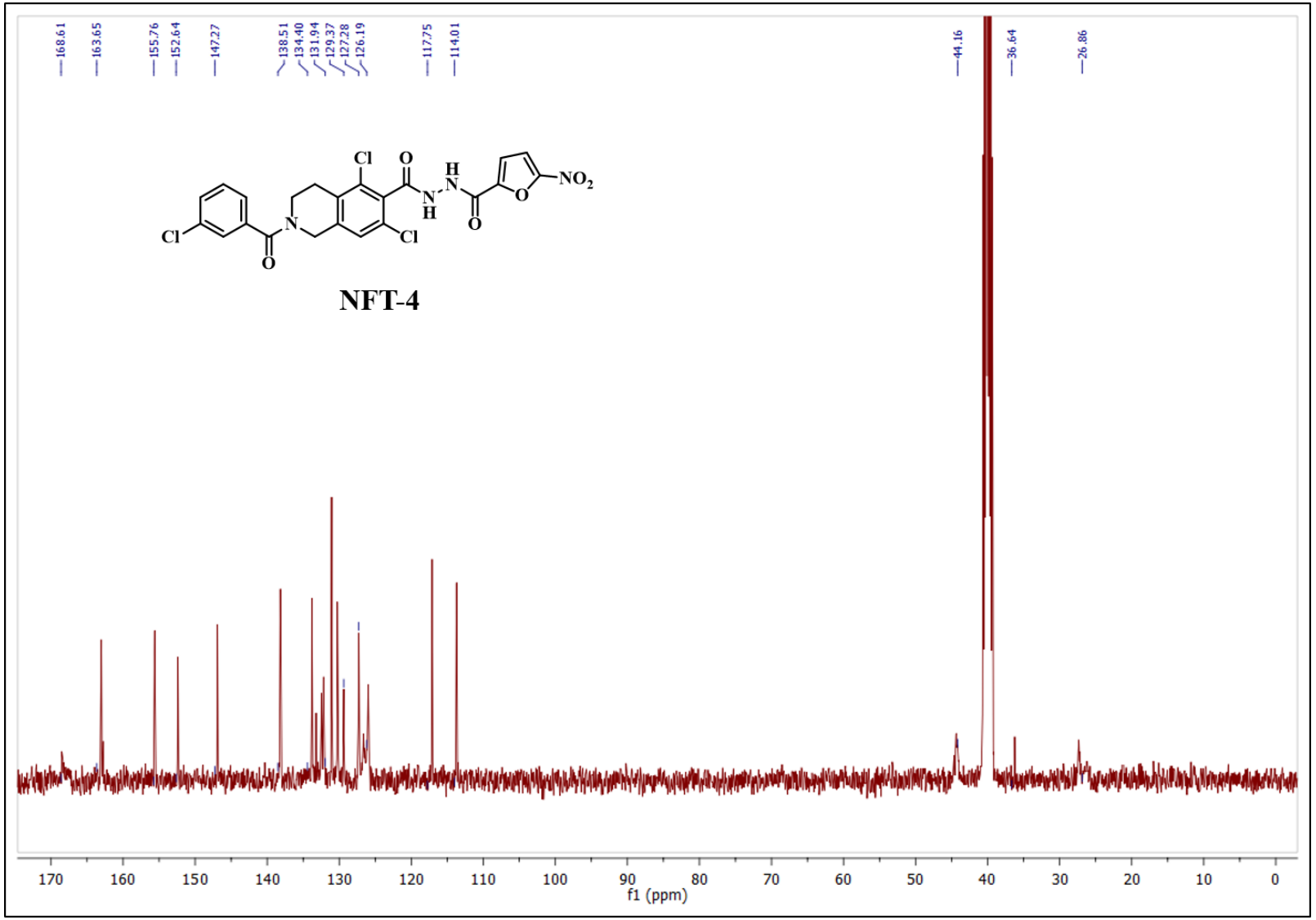

^{13}C NMR (101 MHz, DMSO-d_6) spectrum of compound NFT-4

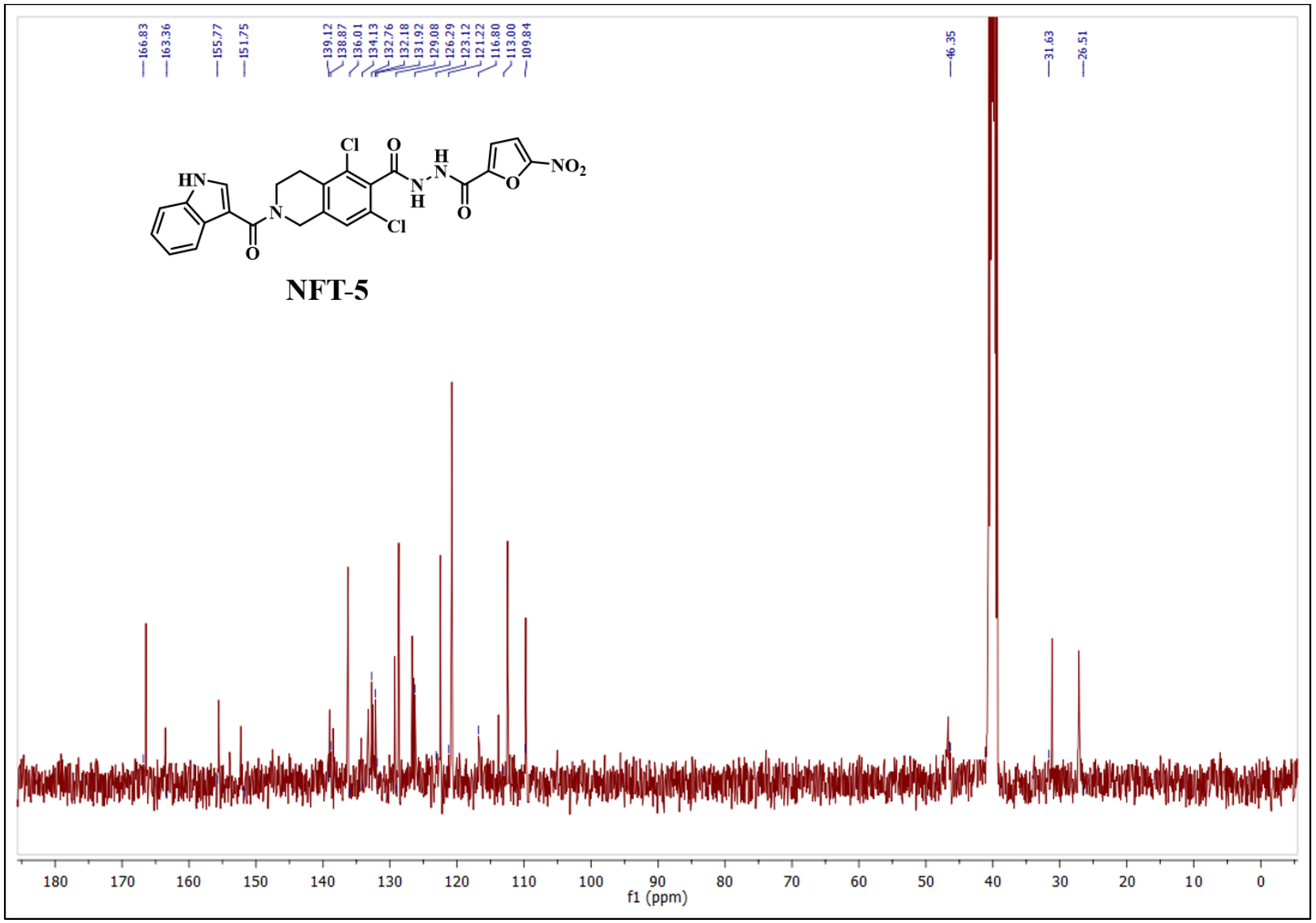

^{13}C NMR (101 MHz, DMSO-d_6) spectrum of compound NFT-5

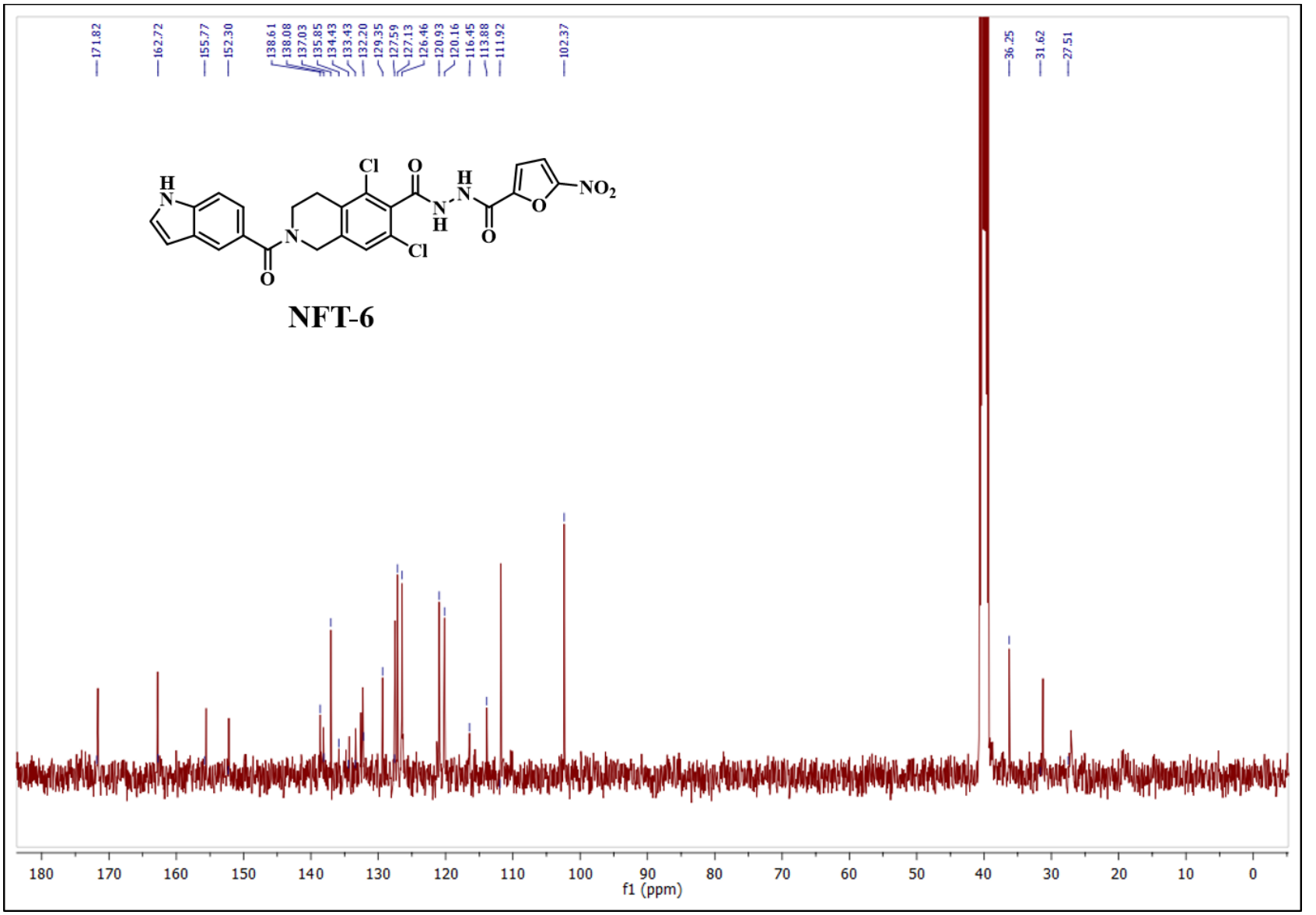

^{13}C NMR (101 MHz, DMSO-d_6) spectrum of compound NFT-6

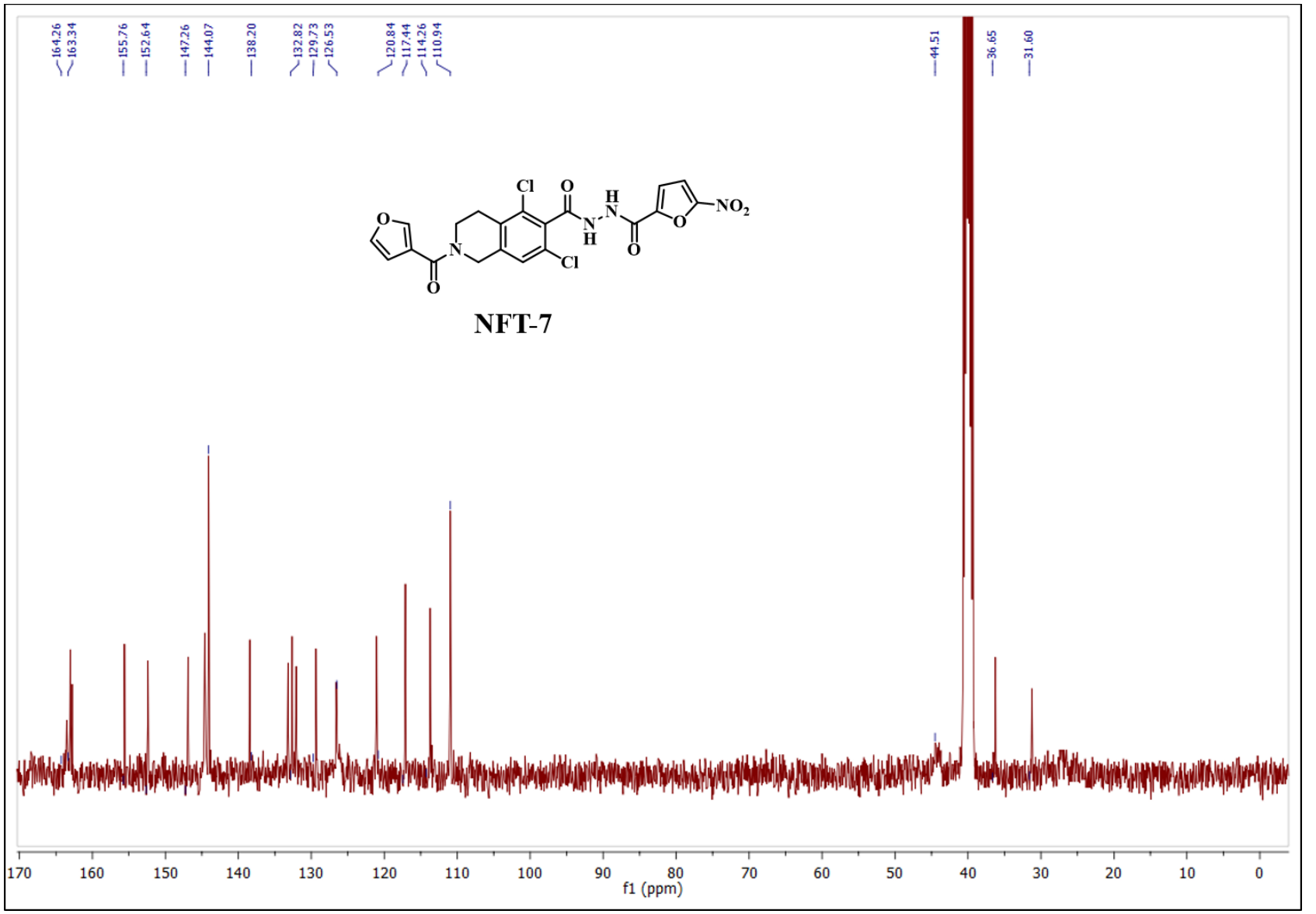

^{13}C NMR (101 MHz, DMSO-d_6) spectrum of compound NFT-7

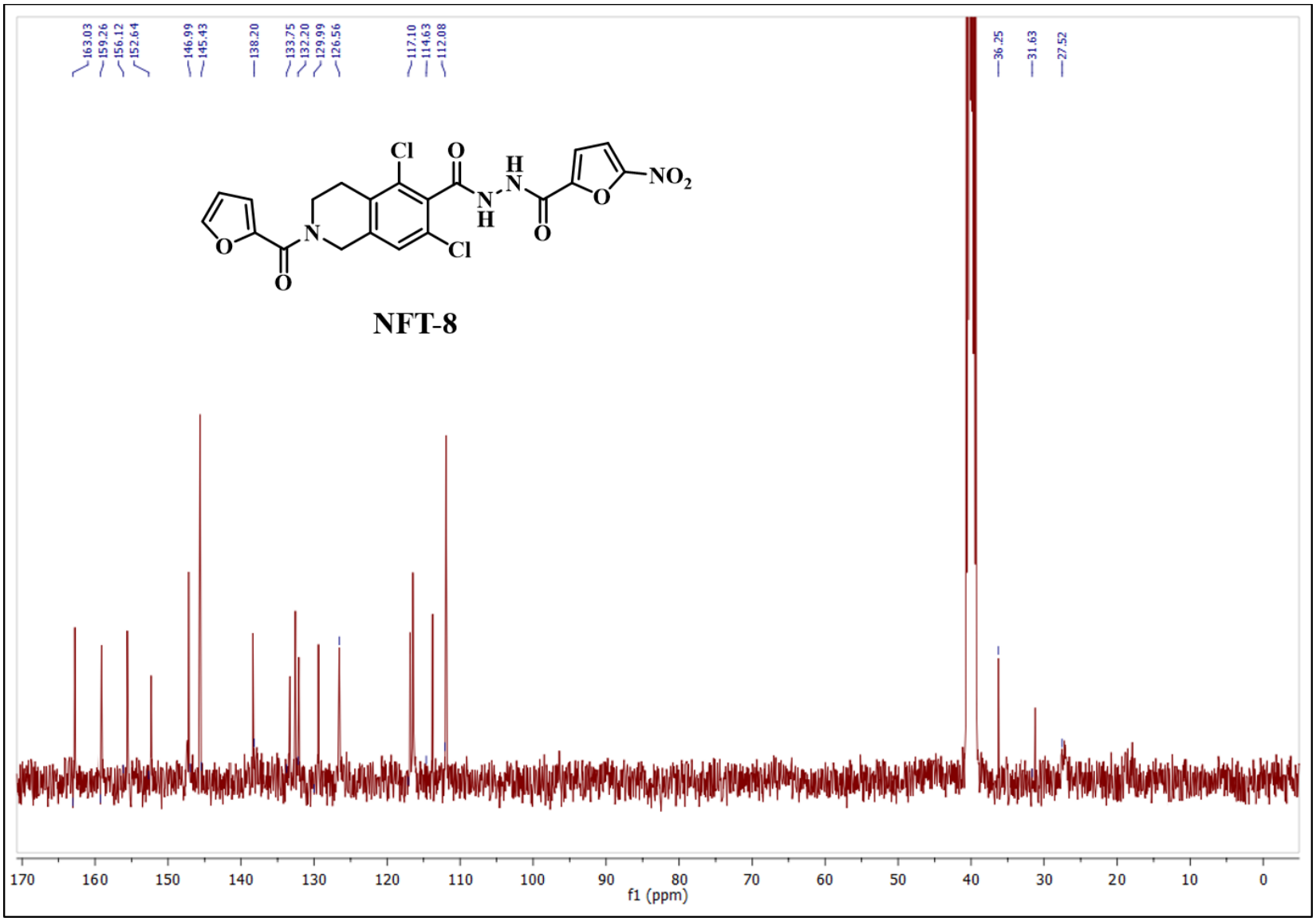

^{13}C NMR (101 MHz, DMSO-d_6) spectrum of compound NFT-8

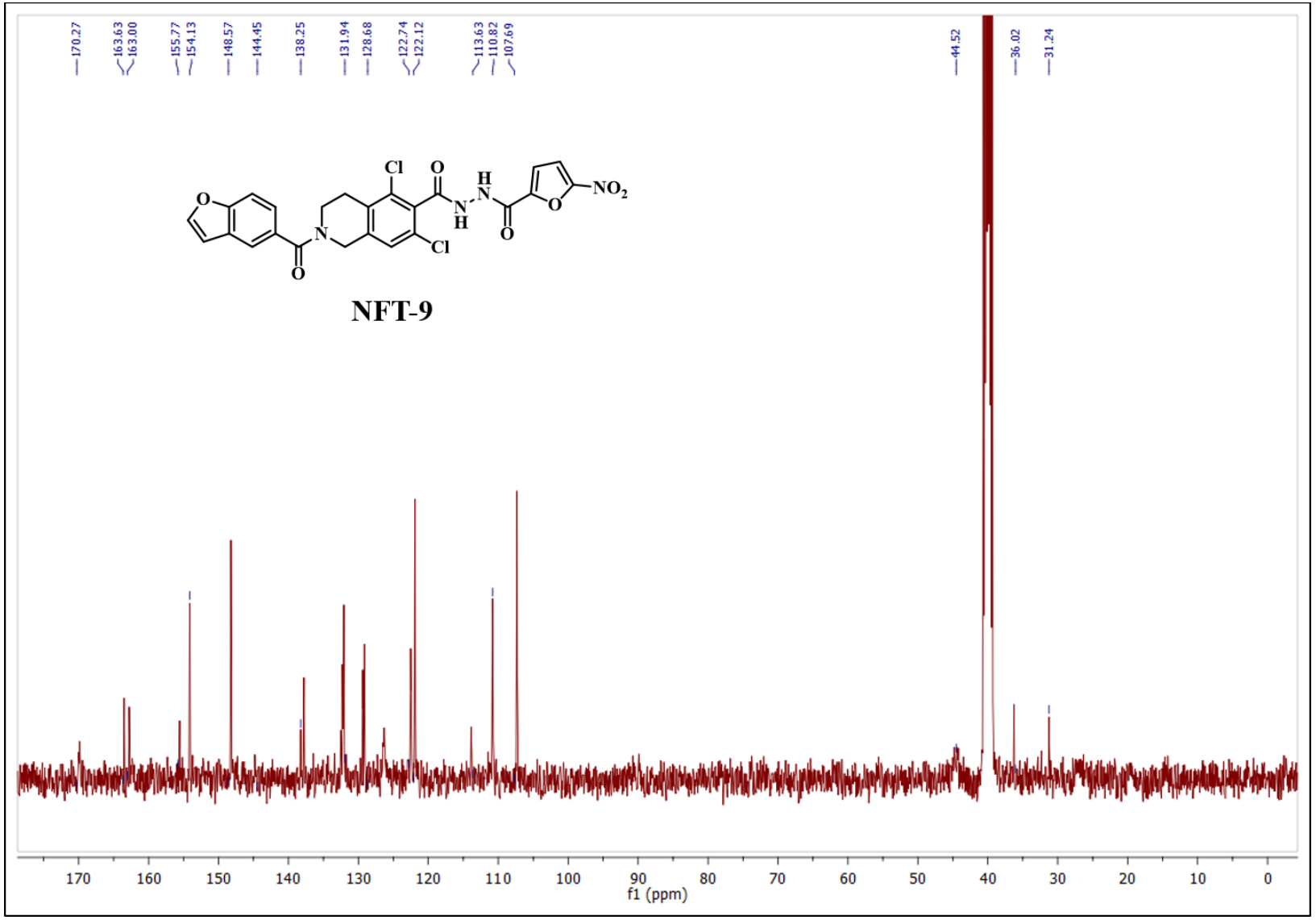

^{13}C NMR (101 MHz, DMSO-d_6) spectrum of compound NFT-9

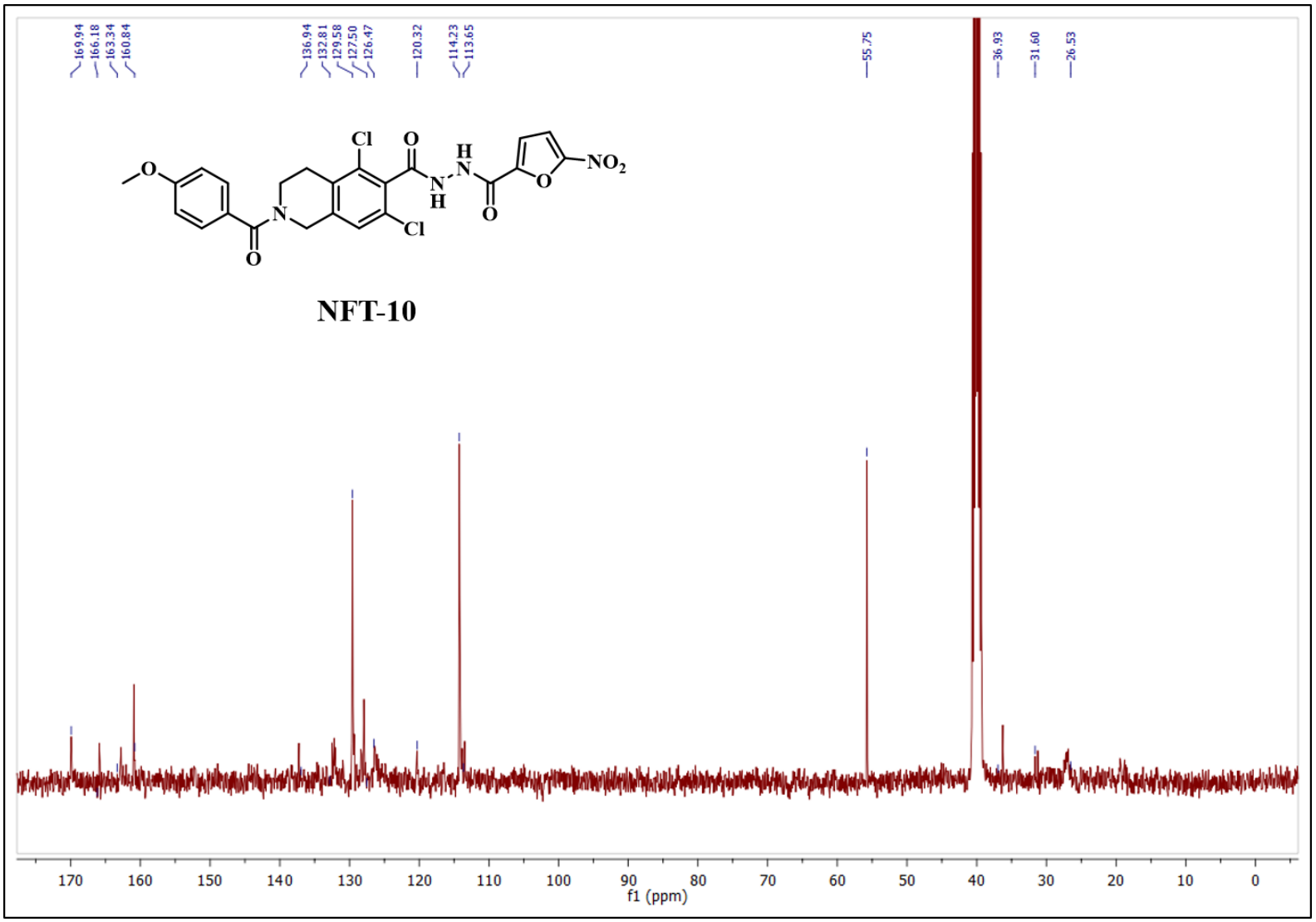

^{13}C NMR (101 MHz, DMSO-d_6) spectrum of compound NFT-10

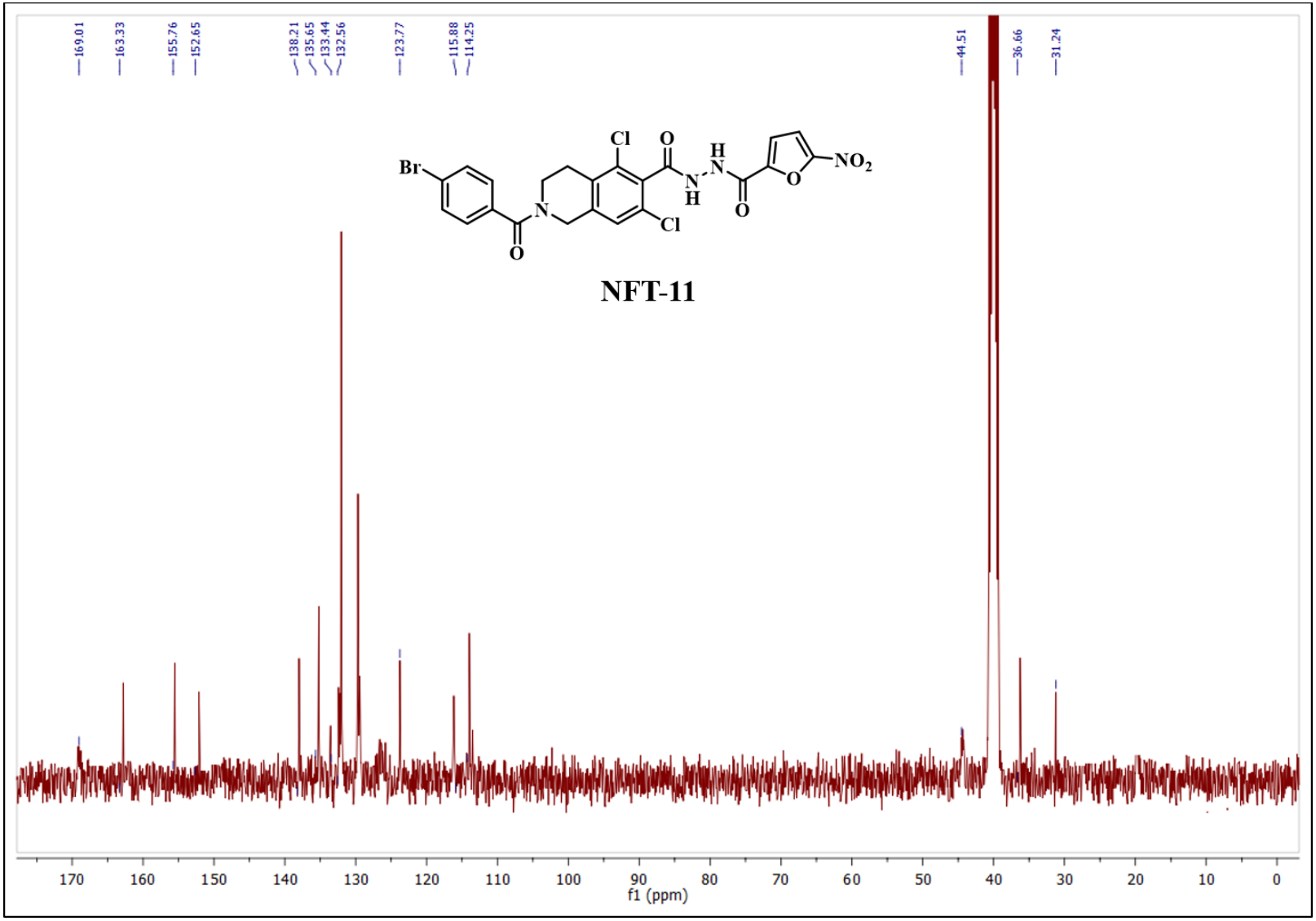

^{13}C NMR (101 MHz, DMSO-d_6) spectrum of compound NFT-11

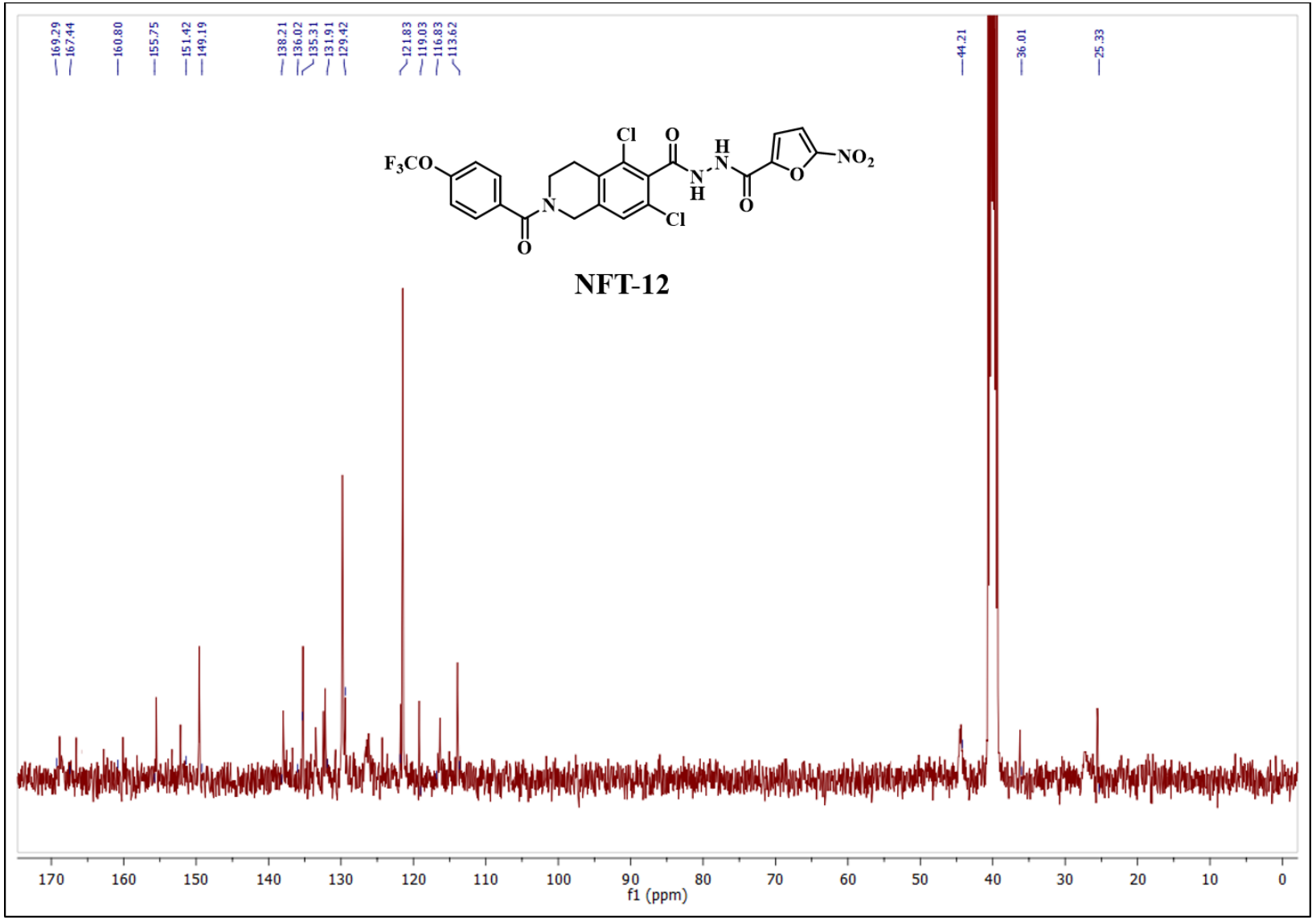

^{13}C NMR (101 MHz, DMSO-d_6) spectrum of compound NFT-12

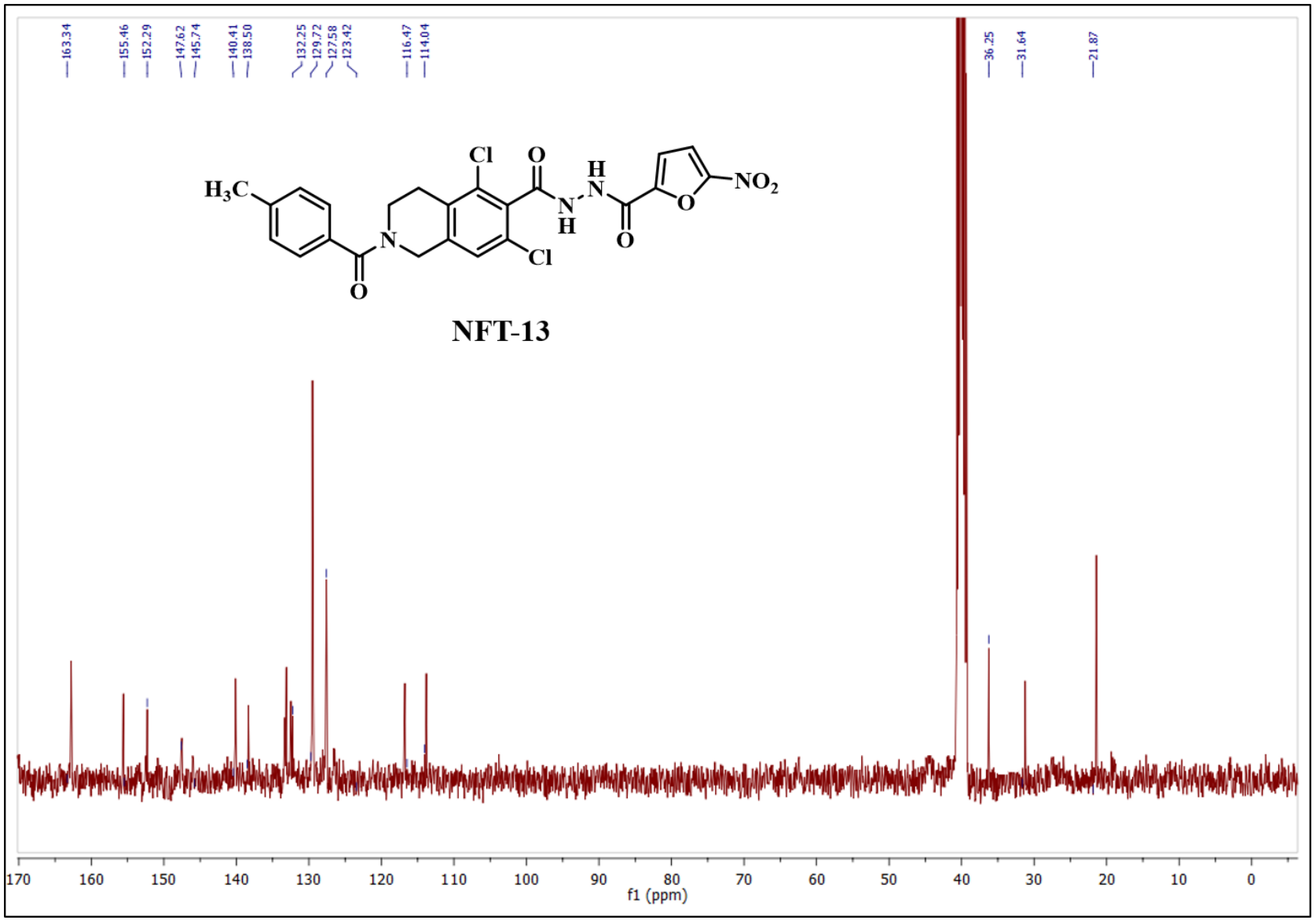

^{13}C NMR (101 MHz, DMSO-d_6) spectrum of compound NFT-13

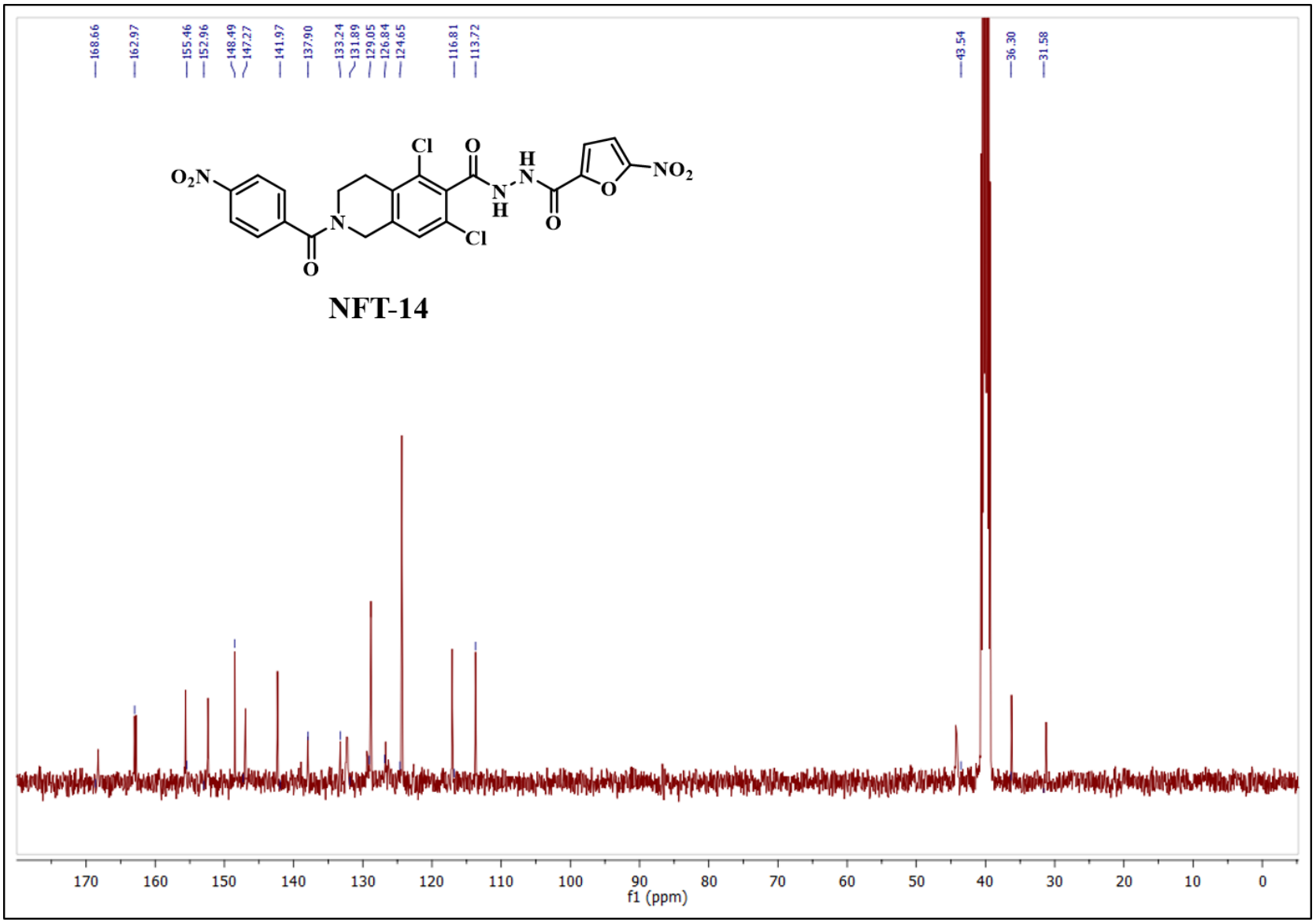

^{13}C NMR (101 MHz, DMSO-d_6) spectrum of compound NFT-14

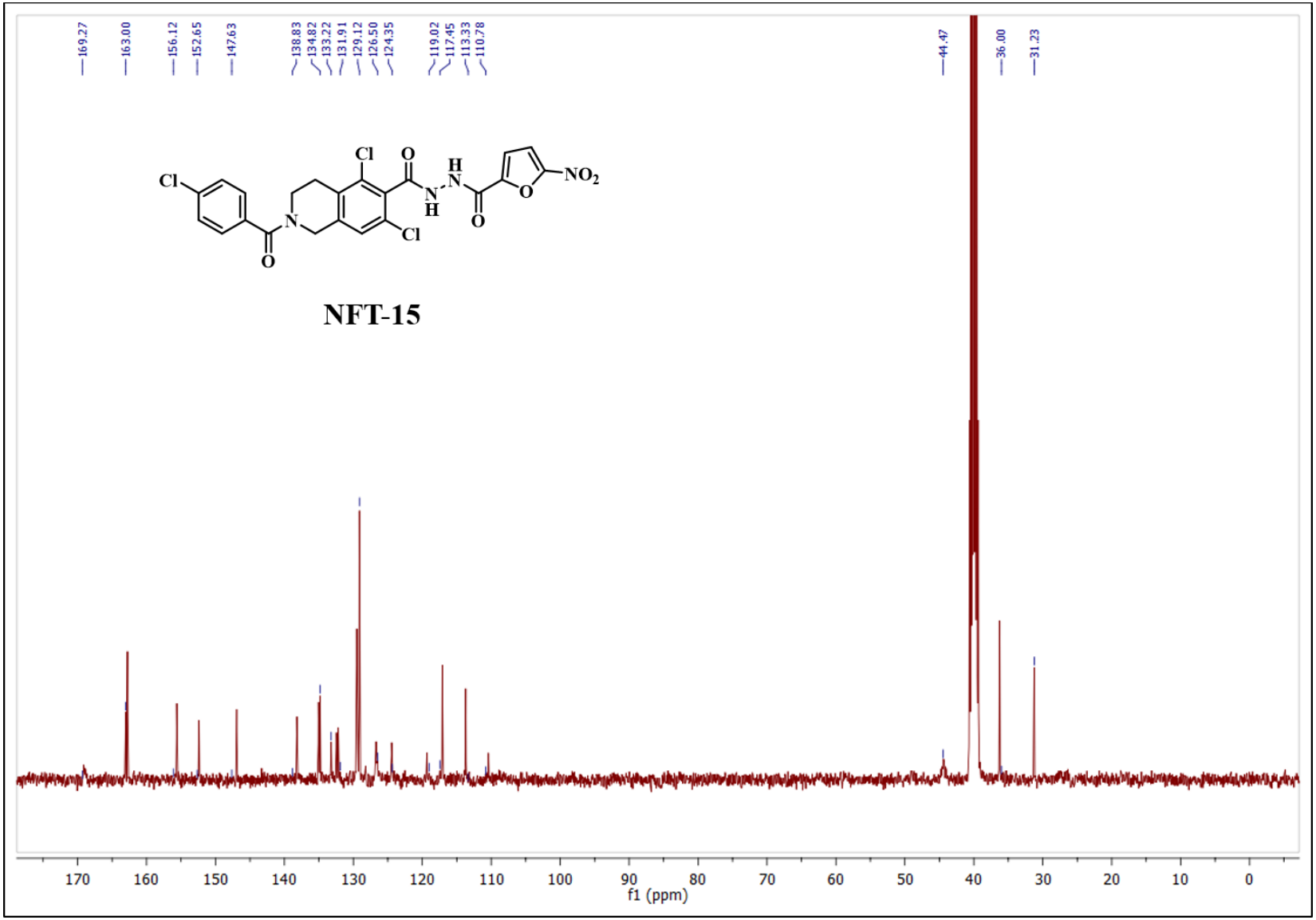

^{13}C NMR (101 MHz, DMSO-d_6) spectrum of compound NFT-15

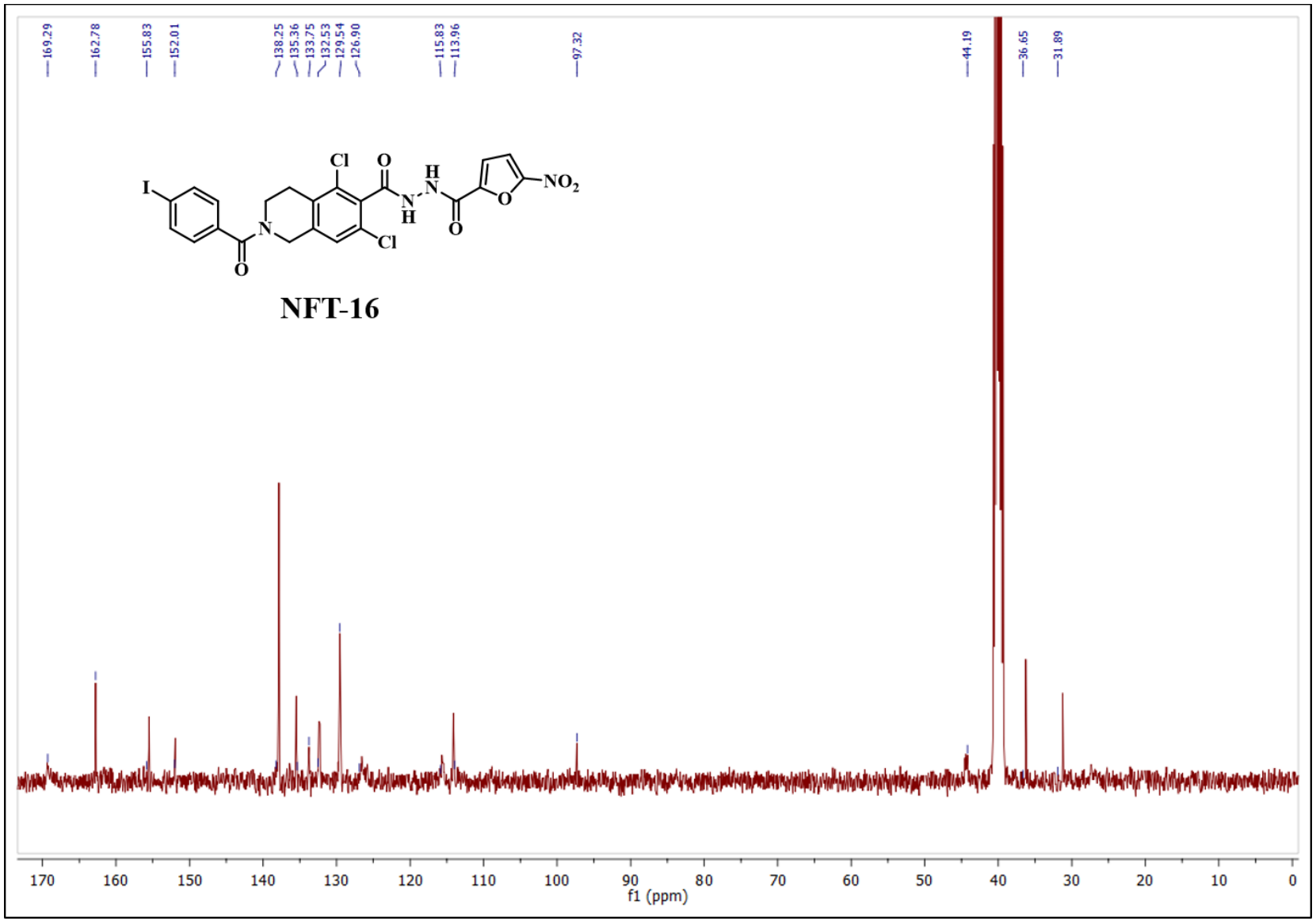

^{13}C NMR (101 MHz, DMSO-d_6) spectrum of compound NFT-16

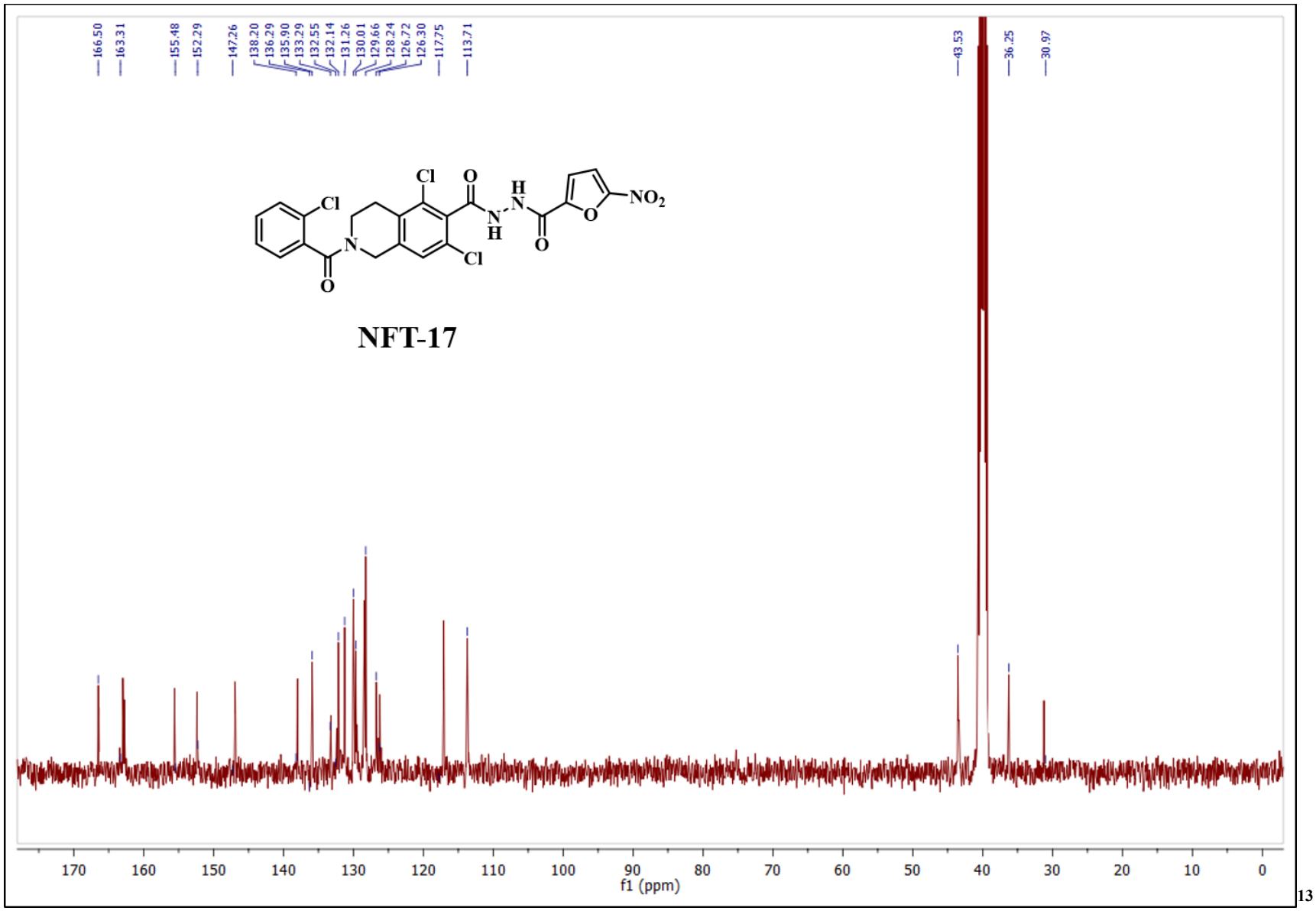

13

C NMR (101 MHz, DMSO-d_6) spectrum of compound NFT-17

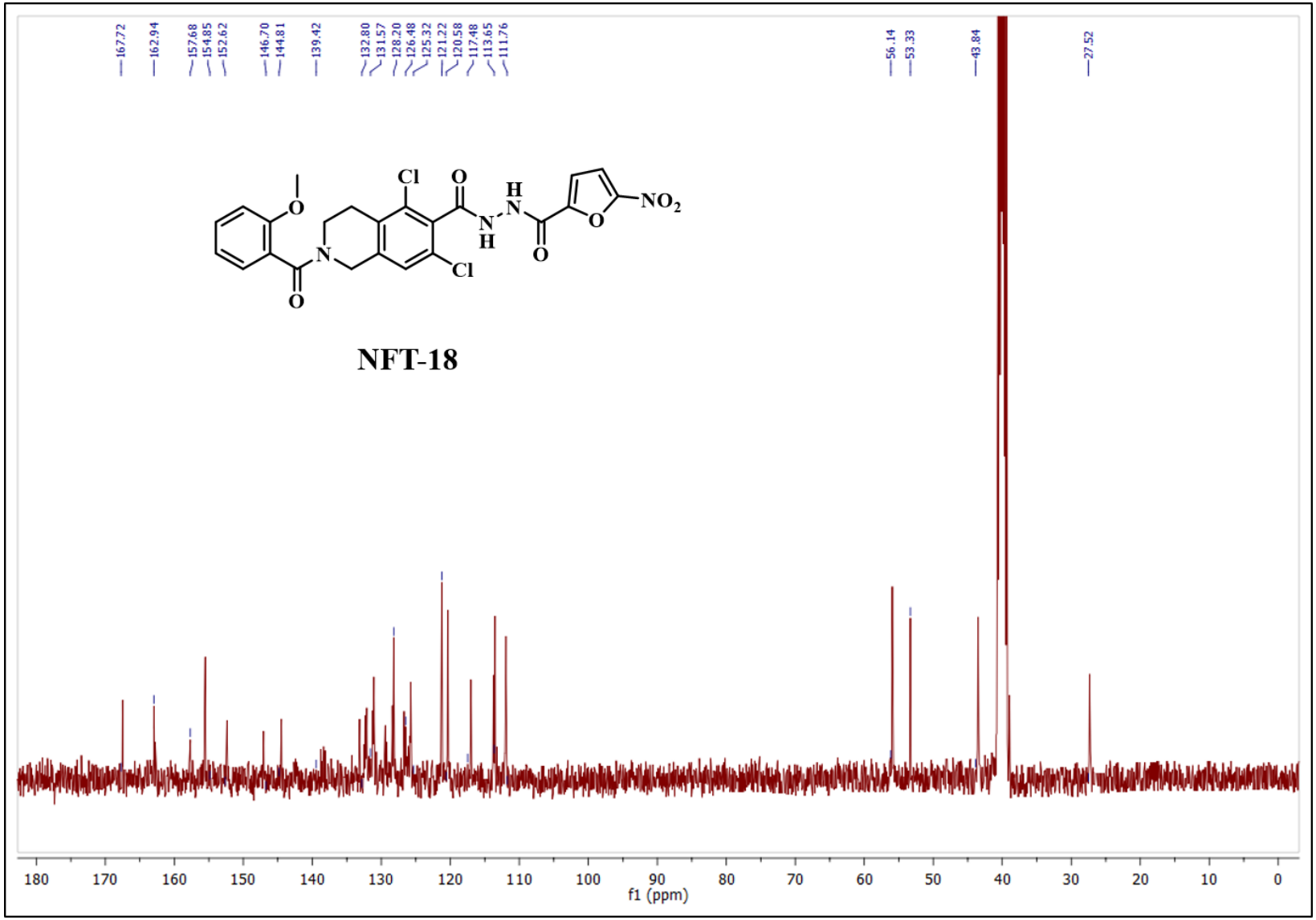

^{13}C NMR (101 MHz, DMSO-d_6) spectrum of compound NFT-18

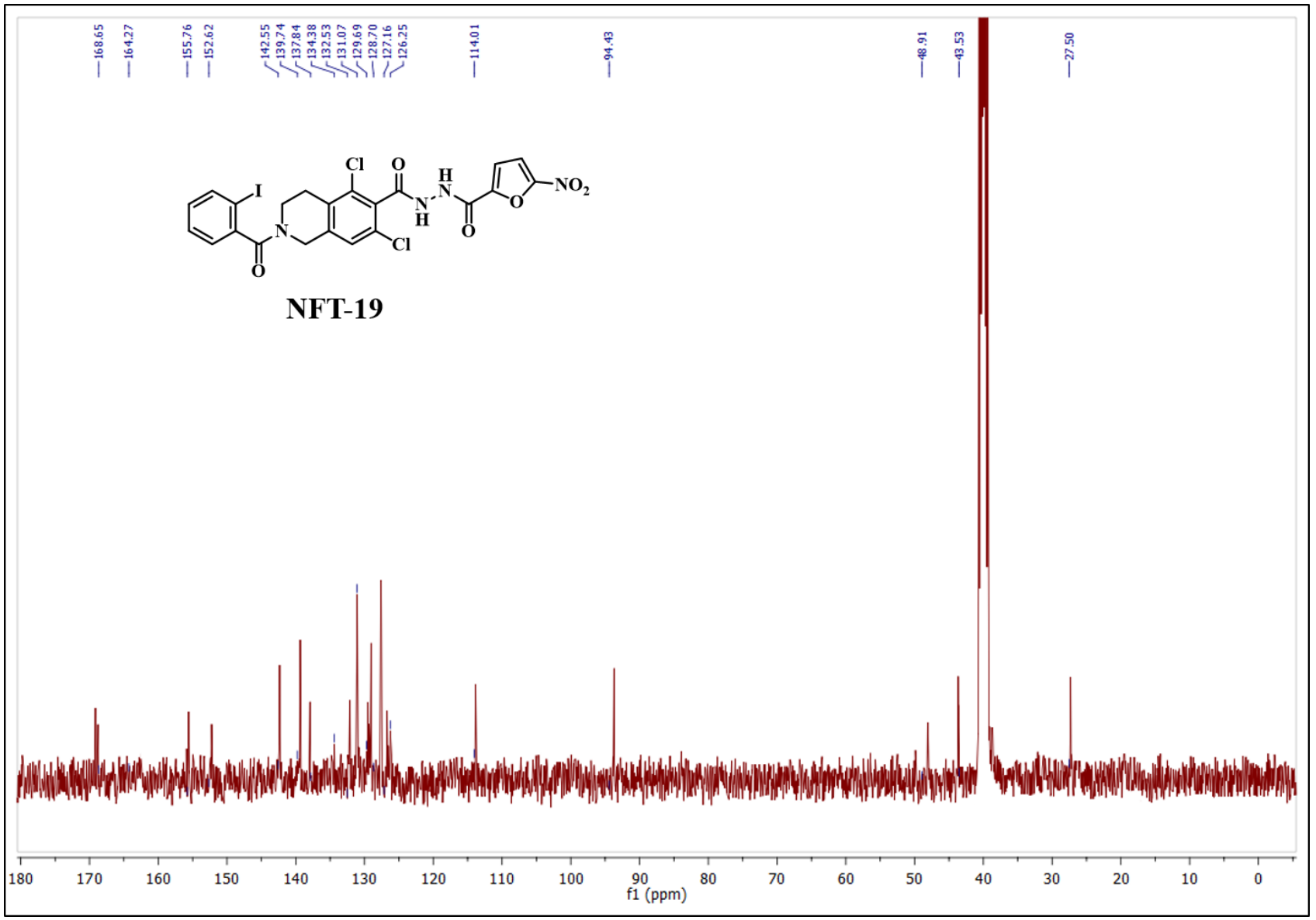

^{13}C NMR (101 MHz, DMSO-d_6) spectrum of compound NFT-19

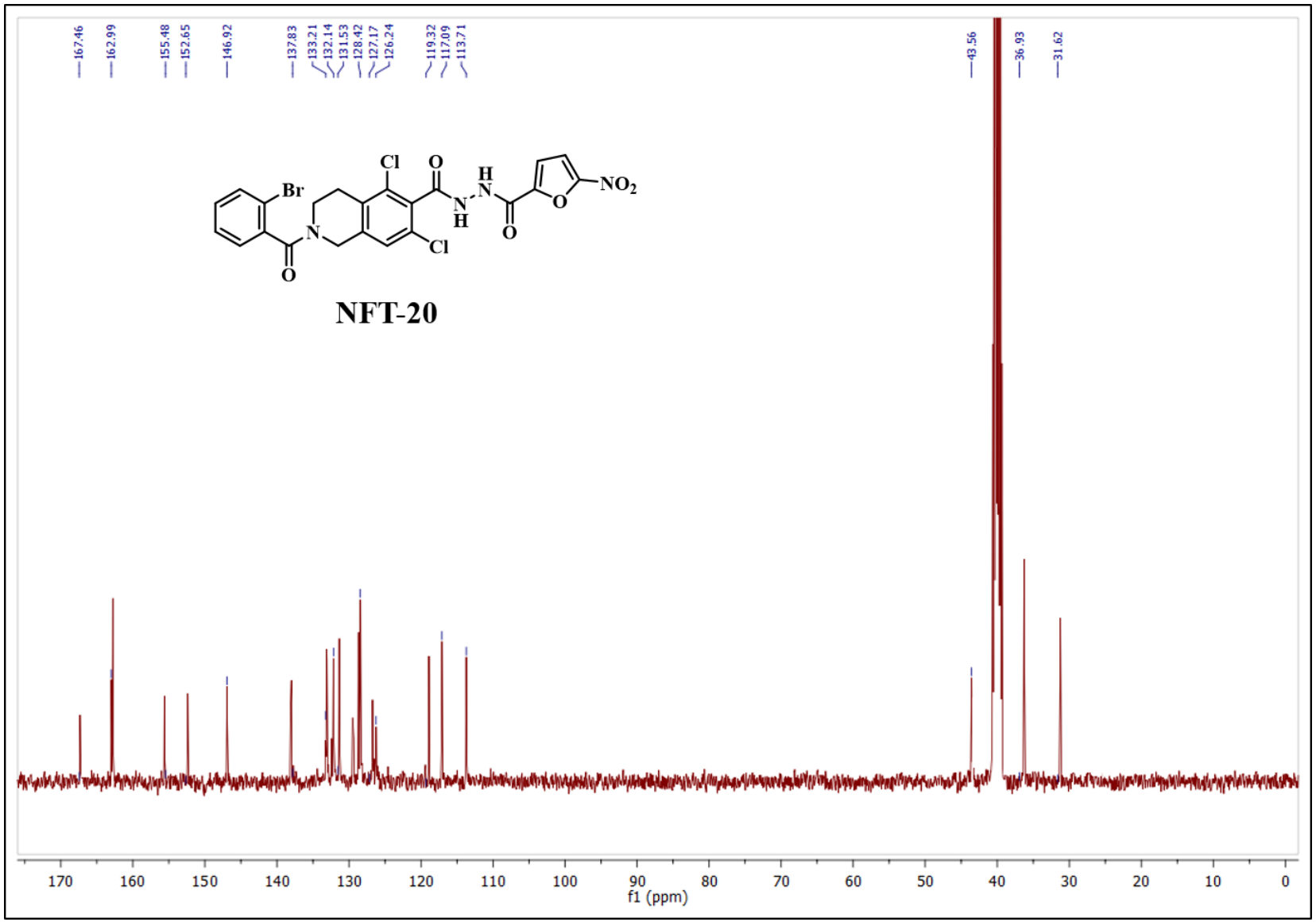

^{13}C NMR (101 MHz, DMSO-d_6) spectrum of compound NFT-20

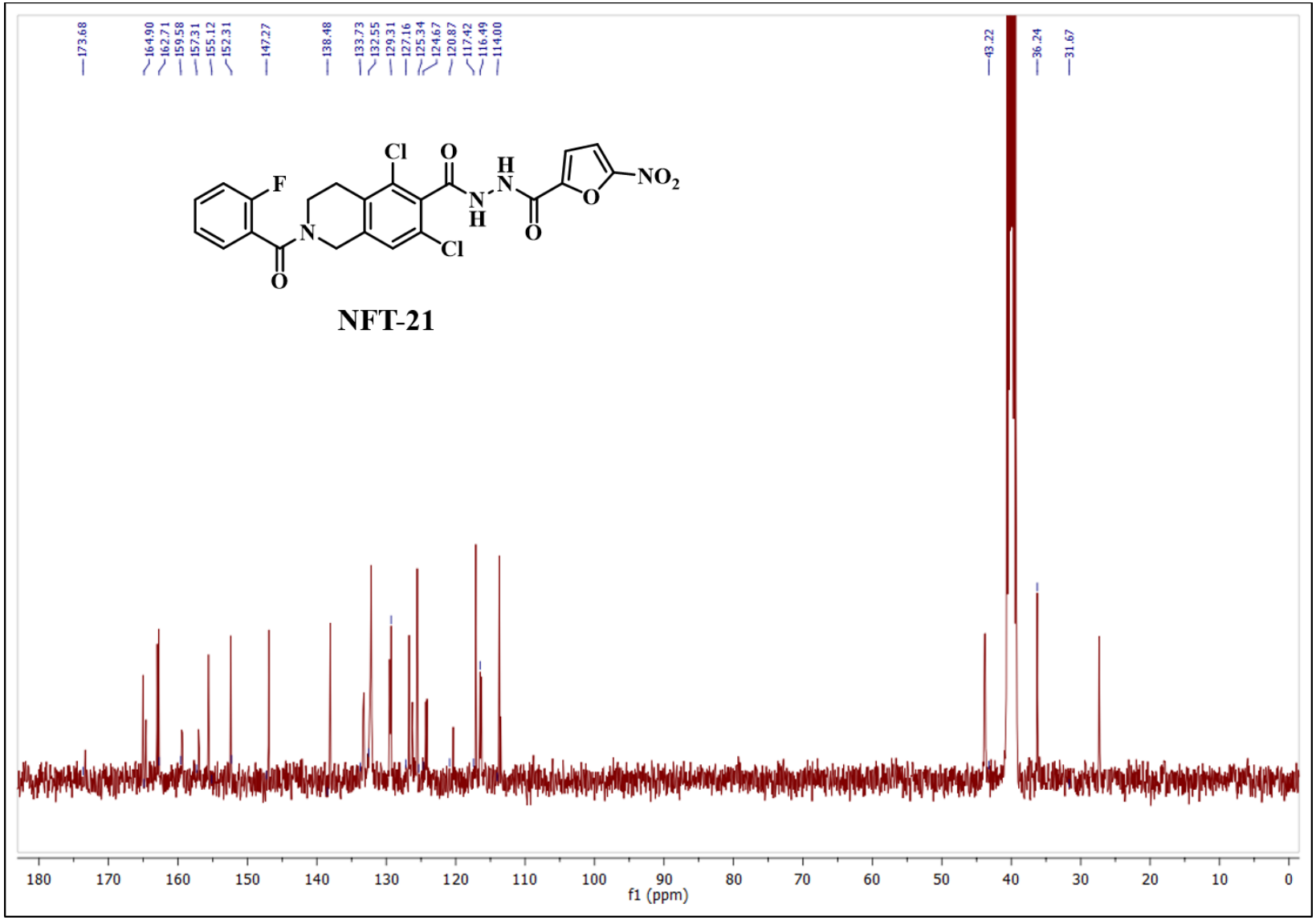

^{13}C NMR (101 MHz, DMSO-d_6) spectrum of compound NFT-21

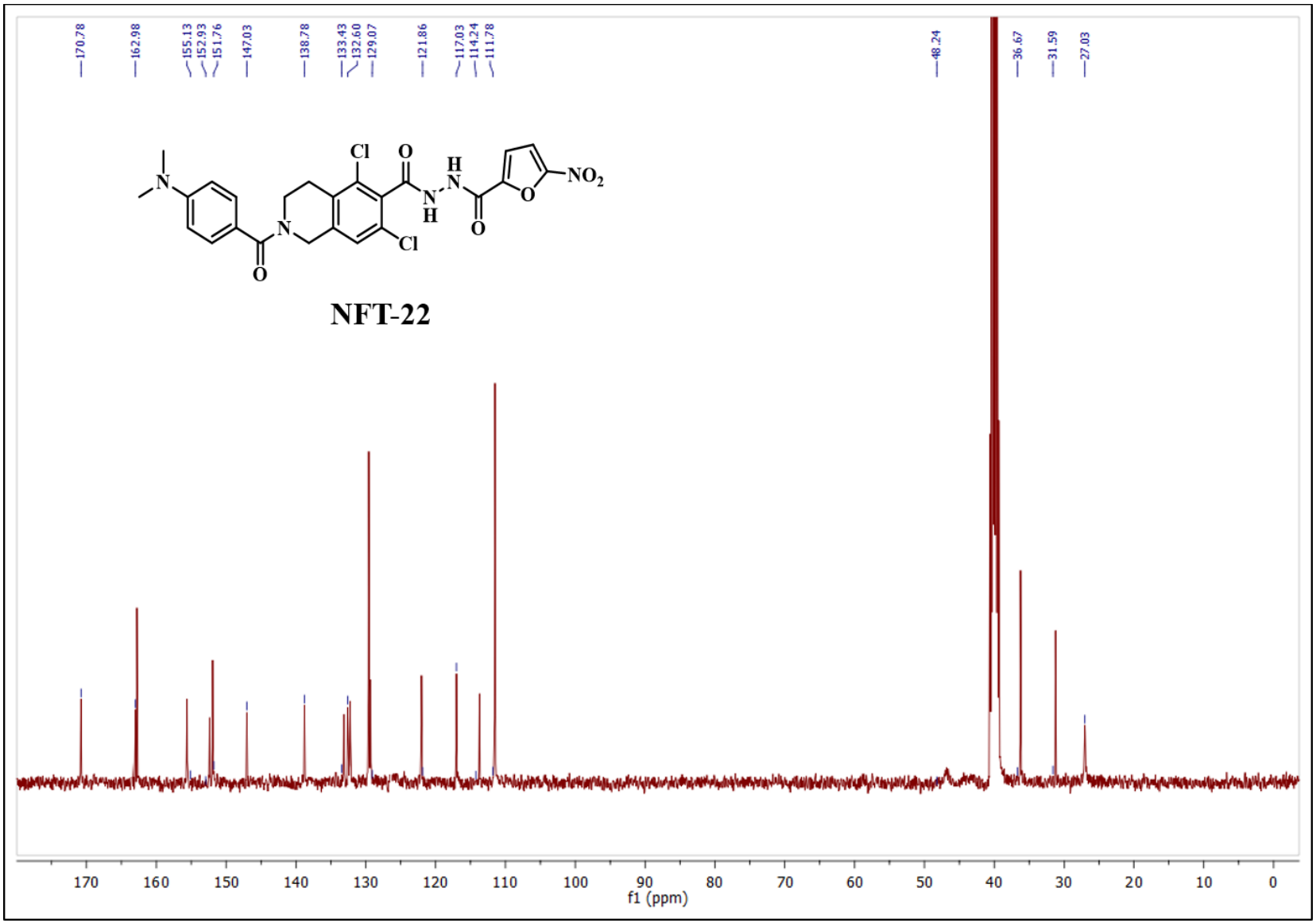

^{13}C NMR (101 MHz, DMSO-d_6) spectrum of compound NFT-22

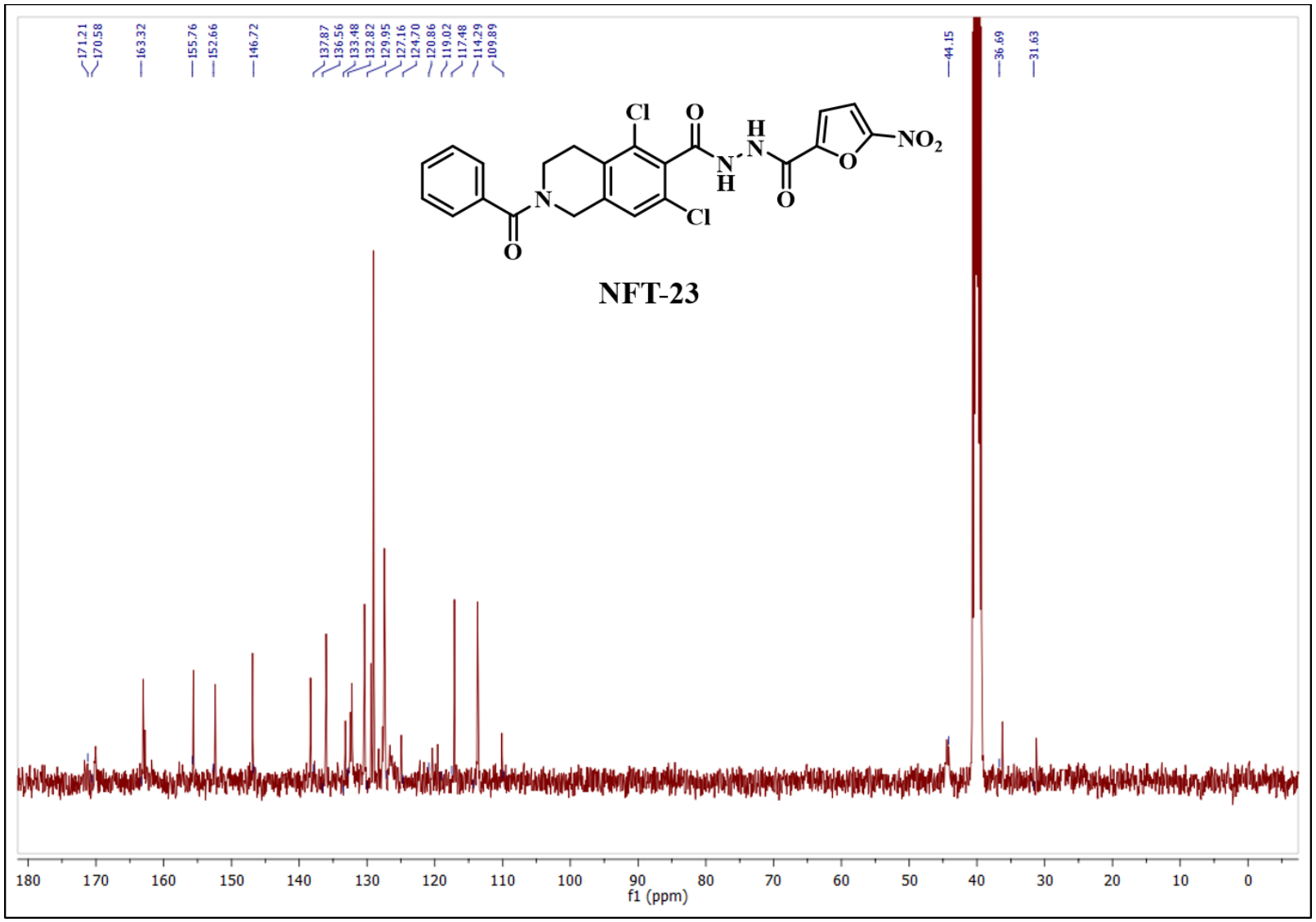

^{13}C NMR (101 MHz, DMSO-d_6) spectrum of compound NFT-23

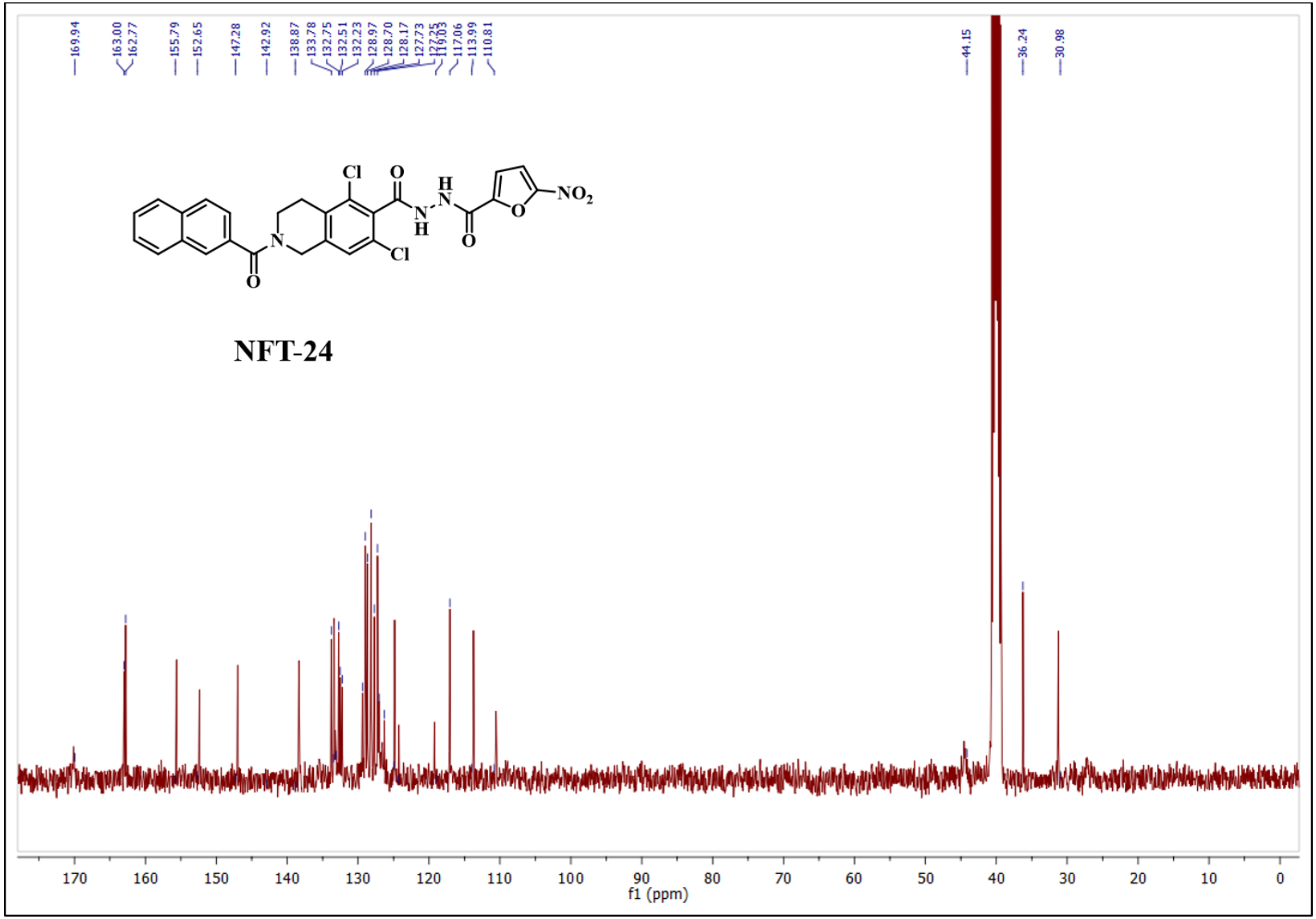

^{13}C NMR (101 MHz, DMSO-d_6) spectrum of compound NFT-24

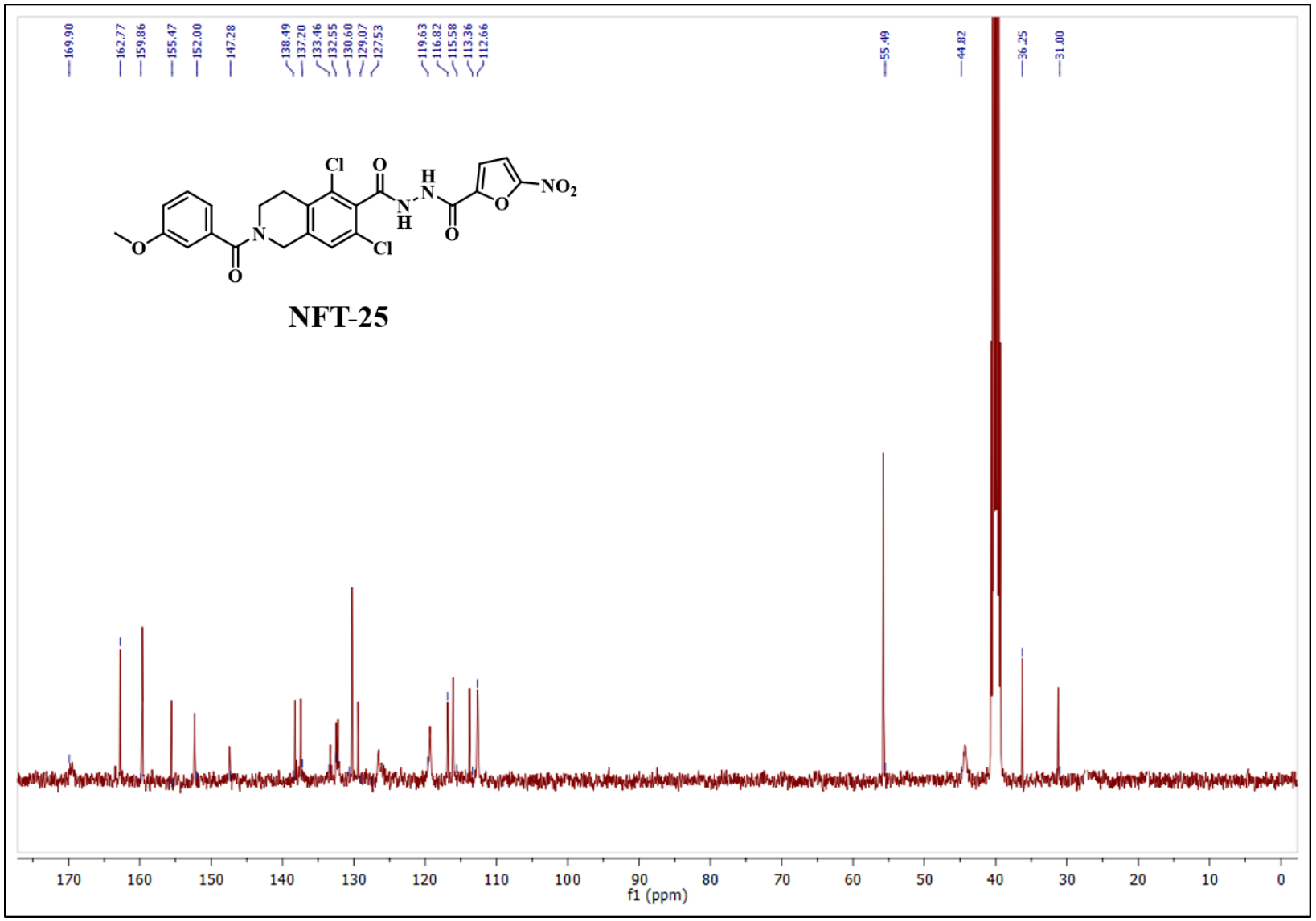

^{13}C NMR (101 MHz, DMSO-d_6) spectrum of compound NFT-25

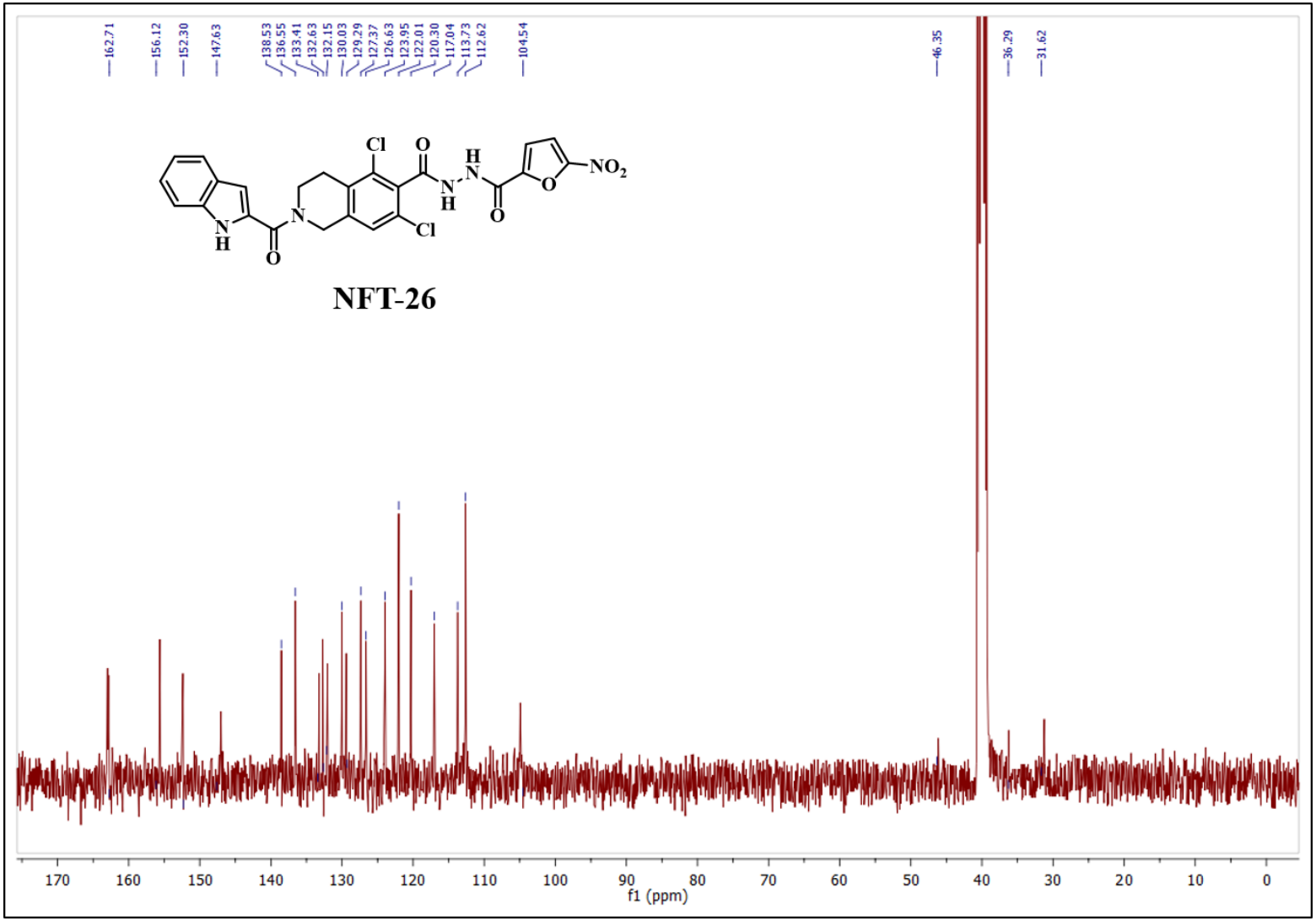

^{13}C NMR (101 MHz, DMSO-d_6) spectrum of compound NFT-26

8. Mass spectras of final compounds (NFT-1 to NFT-26):

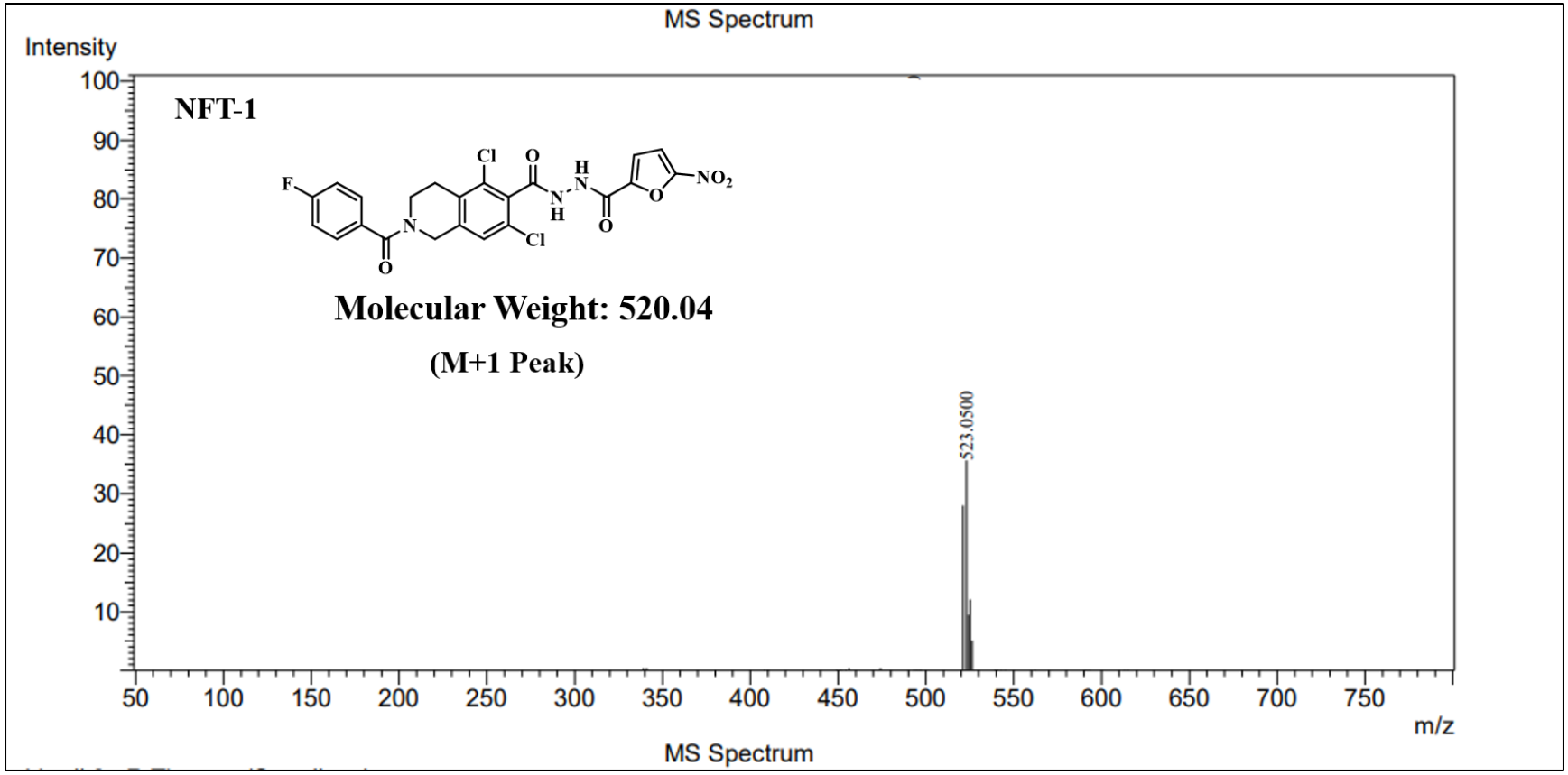

Mass spectra of compound NFT-1

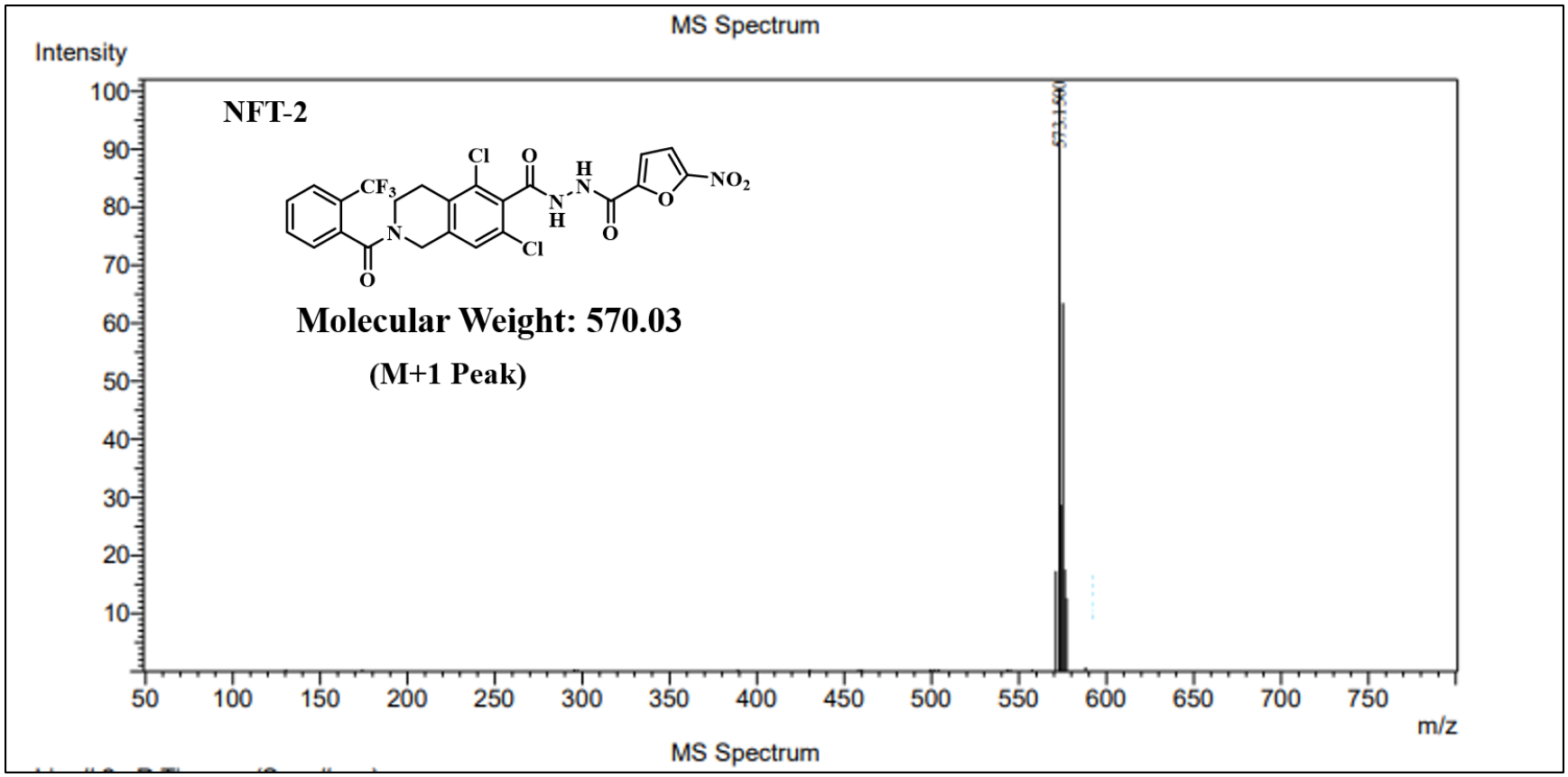

Mass spectra of compound NFT-2

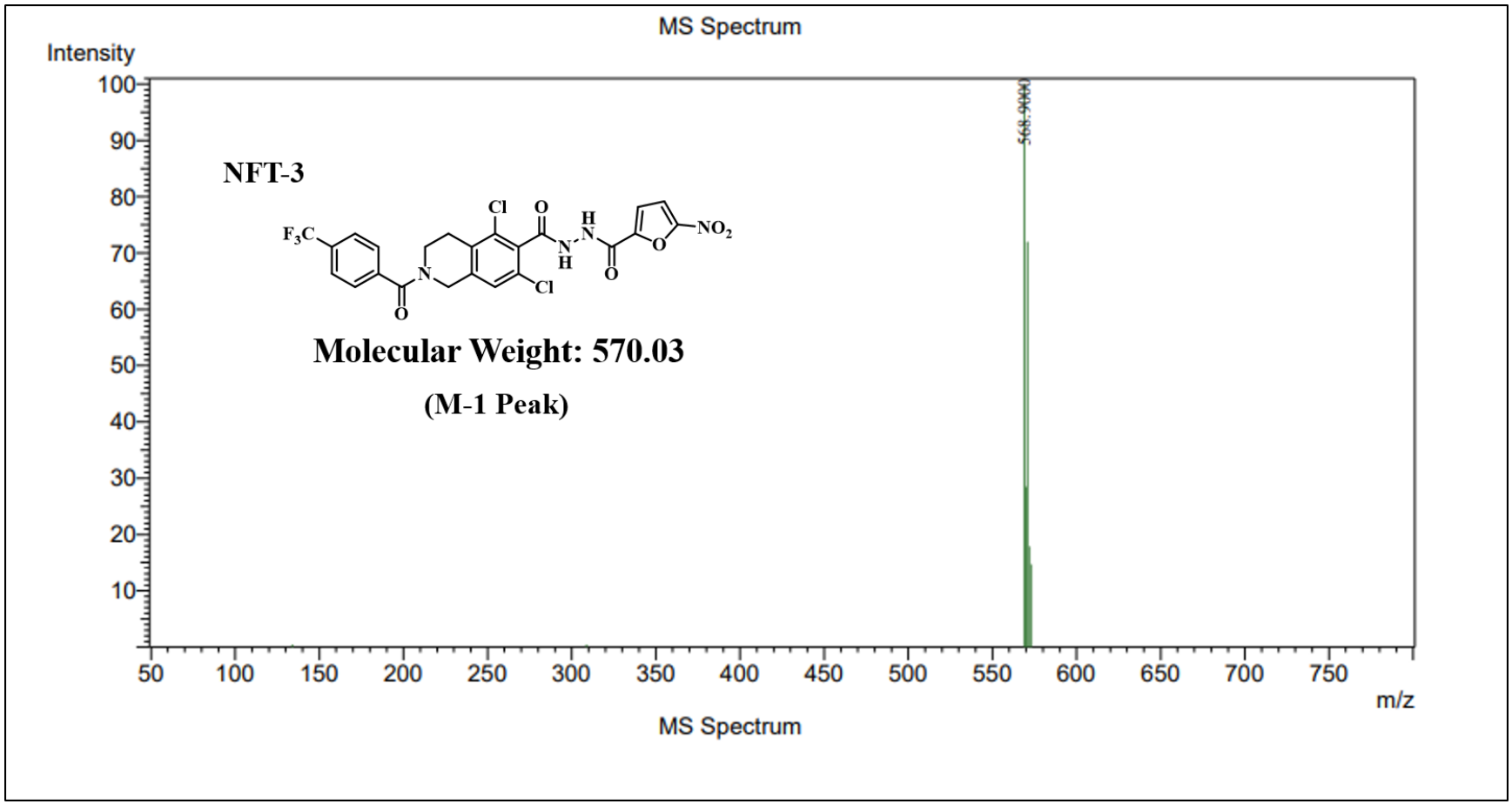

Mass spectra of compound NFT-3

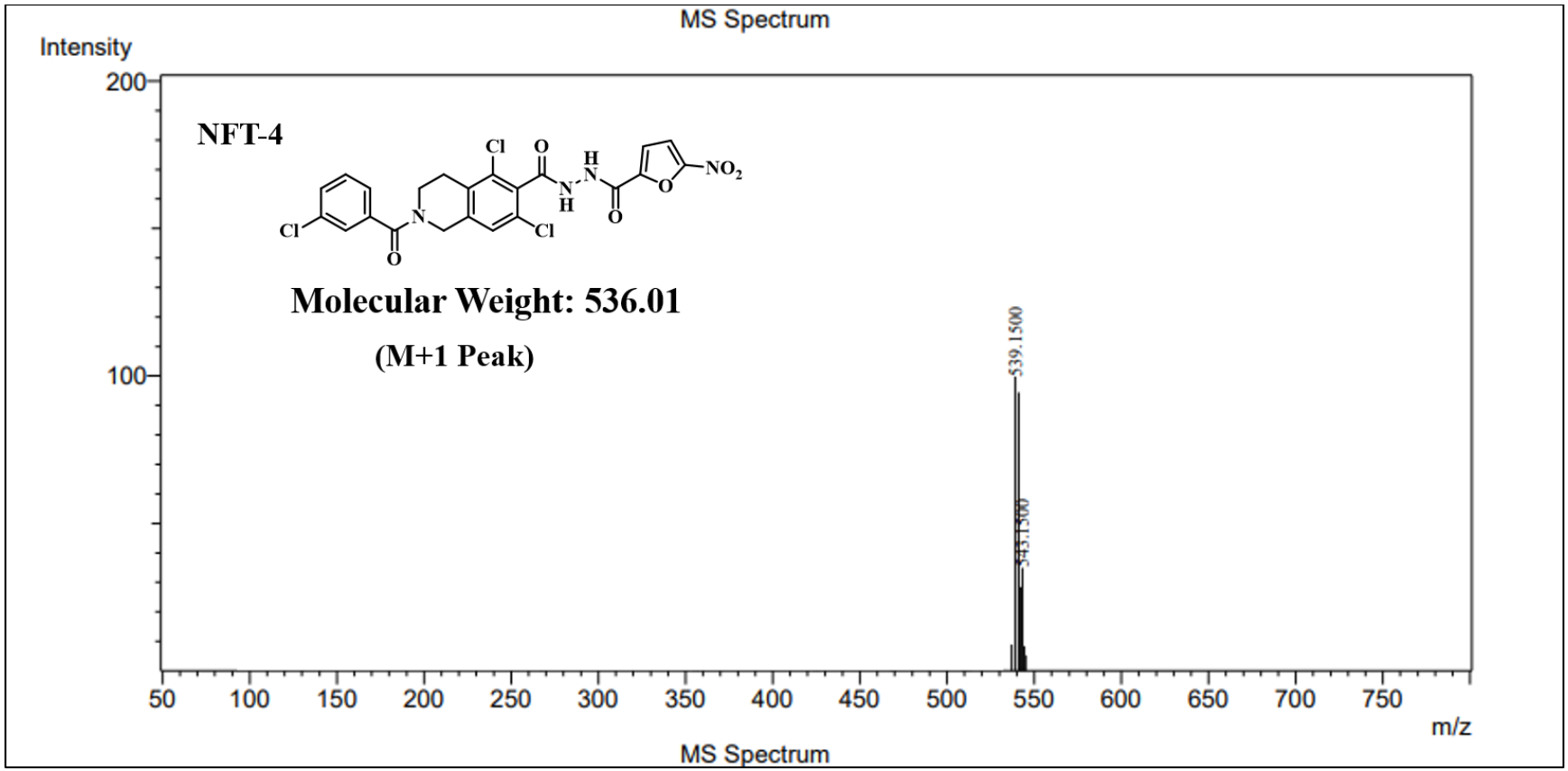

Mass spectra of compound NFT-4

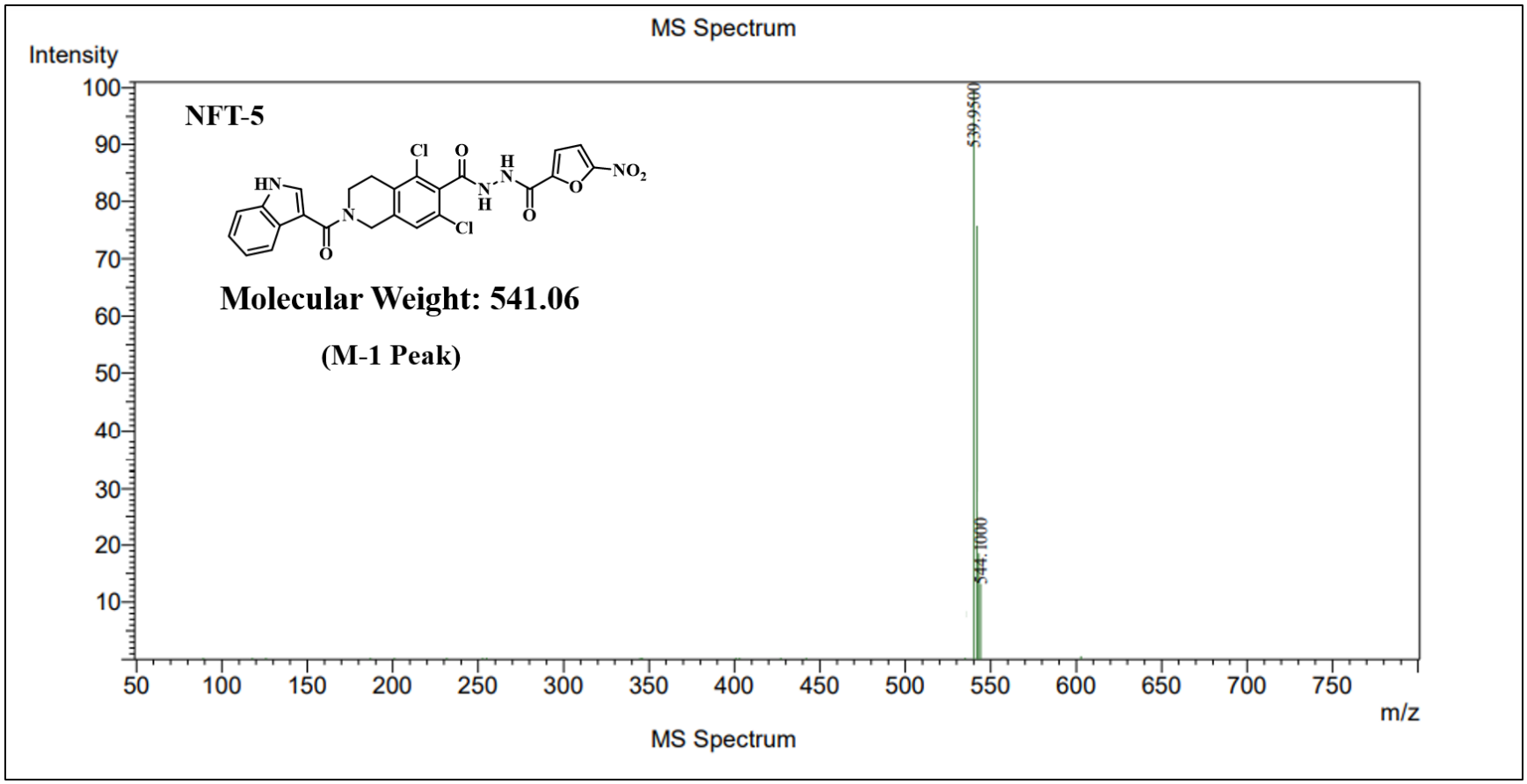

Mass spectra of compound NFT-5

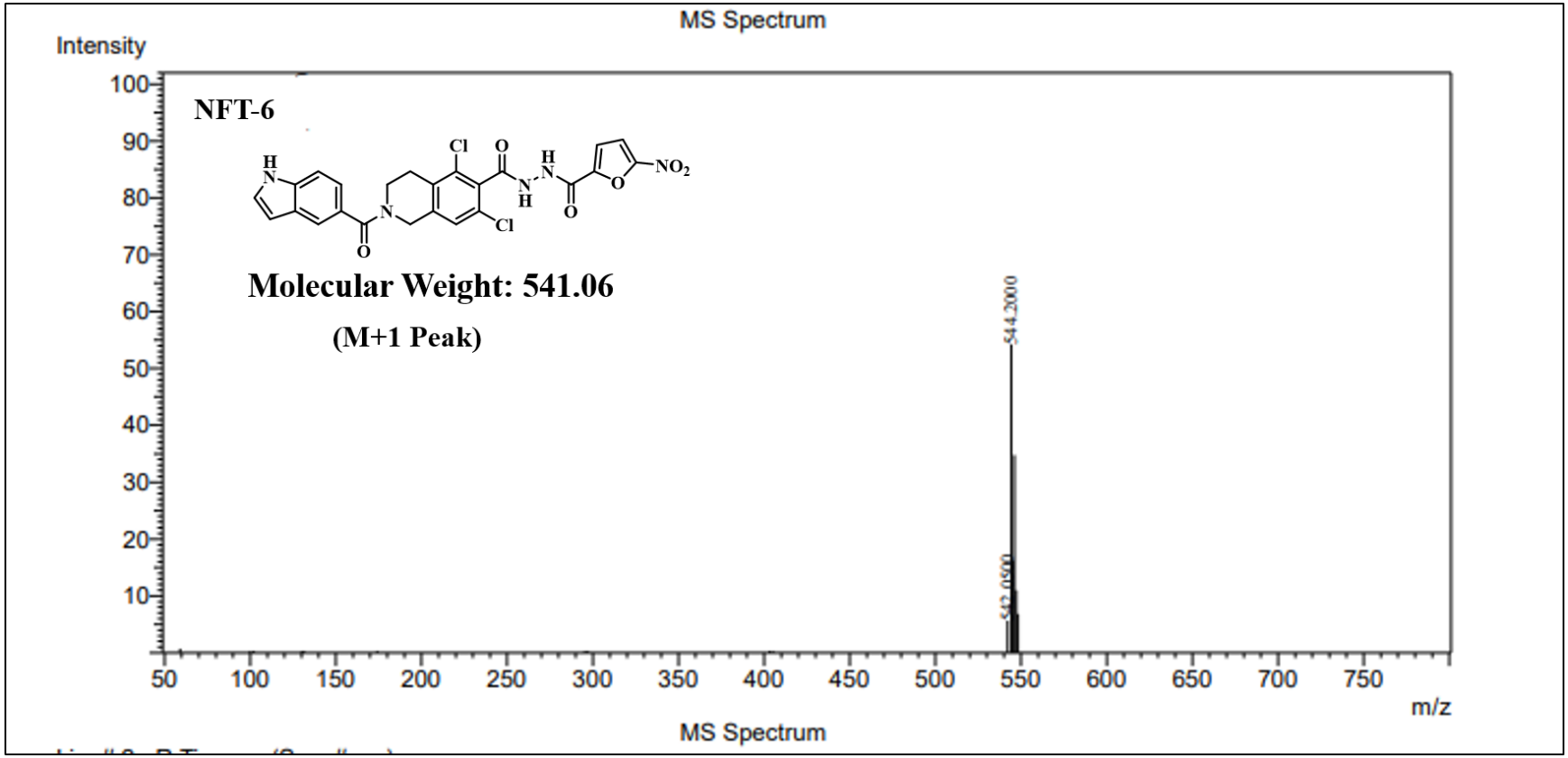

Mass spectra of compound NFT-6

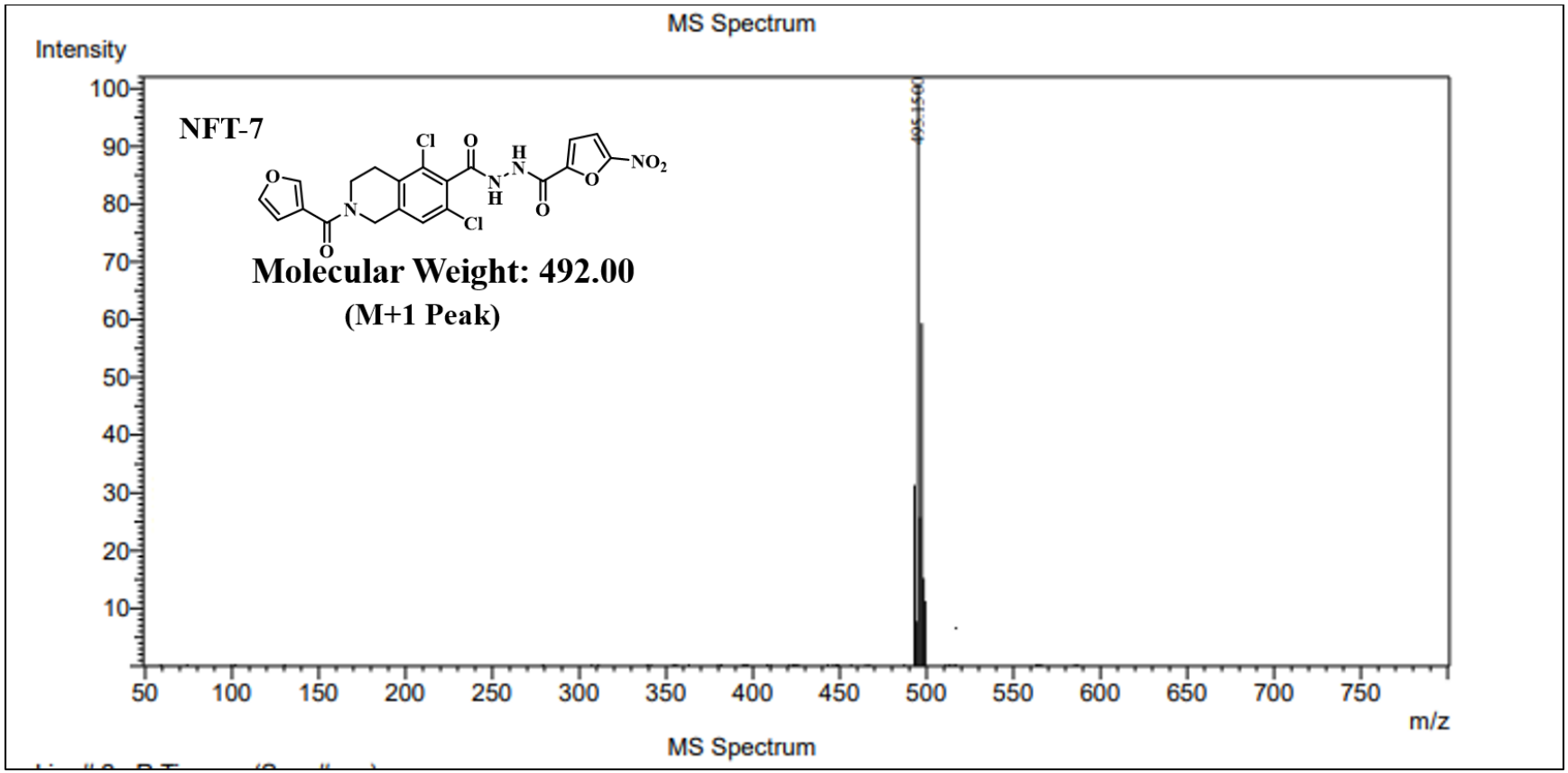

Mass spectra of compound NFT-7

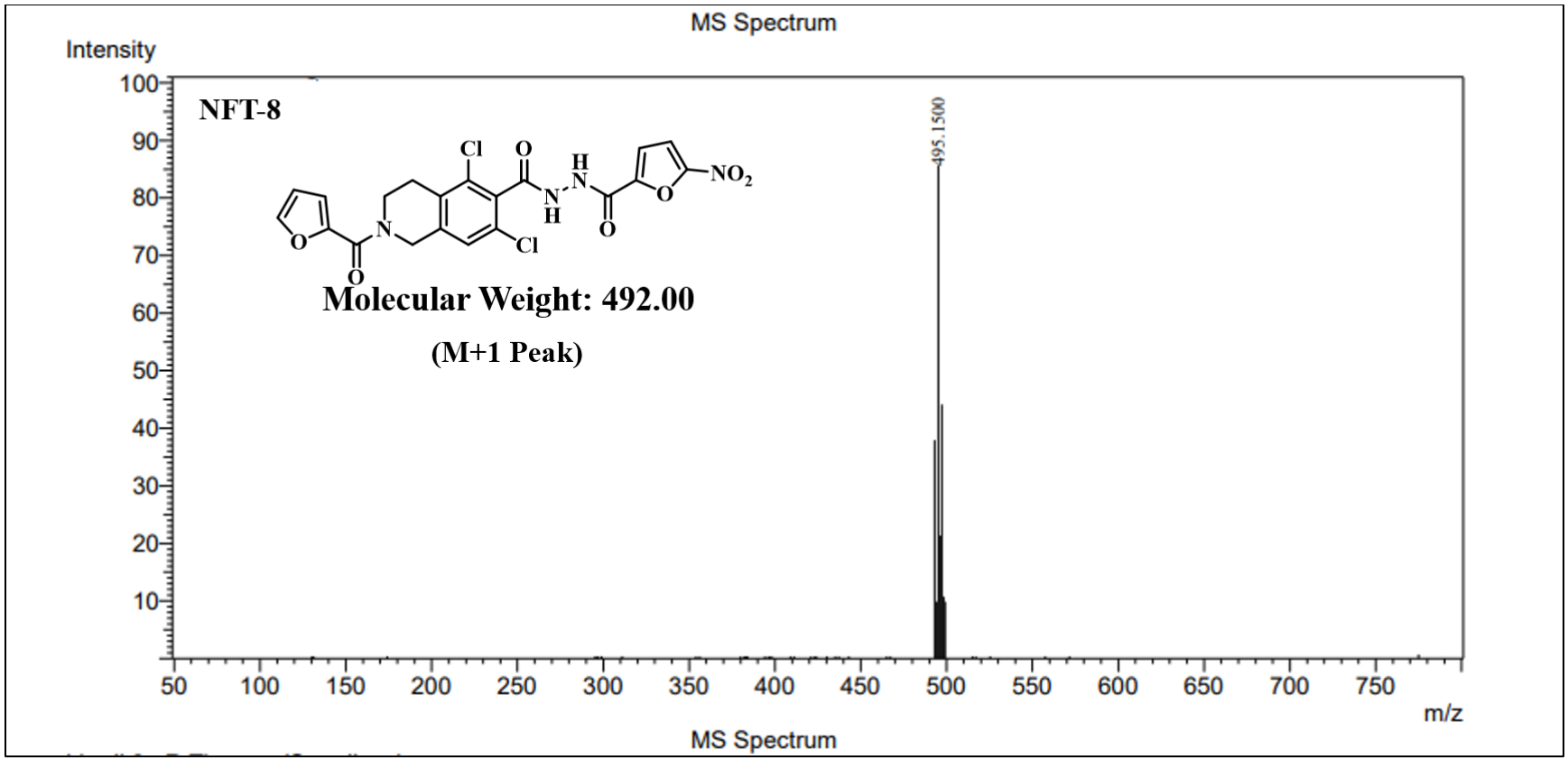

Mass spectra of compound NFT-8

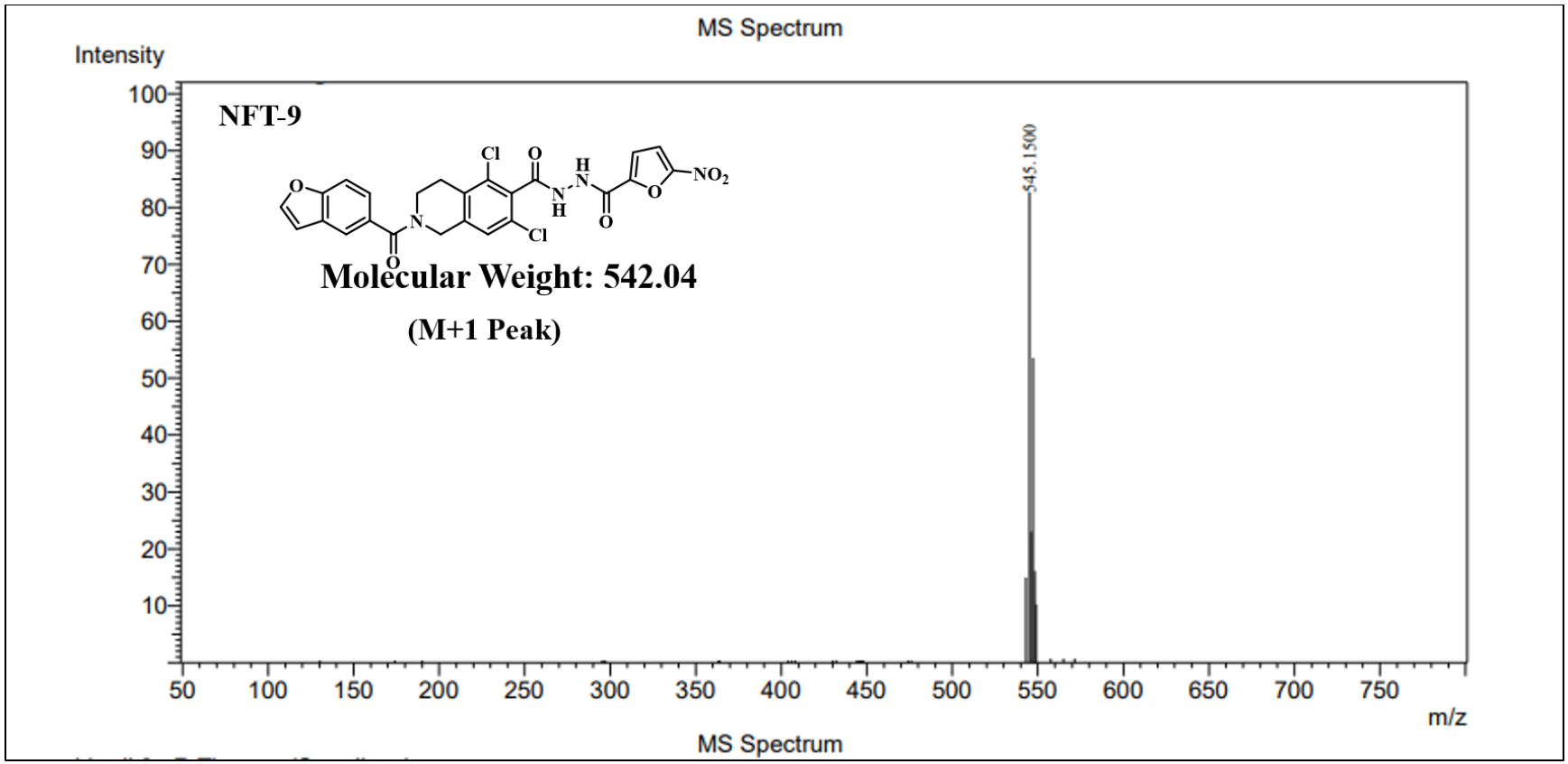

Mass spectra of compound NFT-9

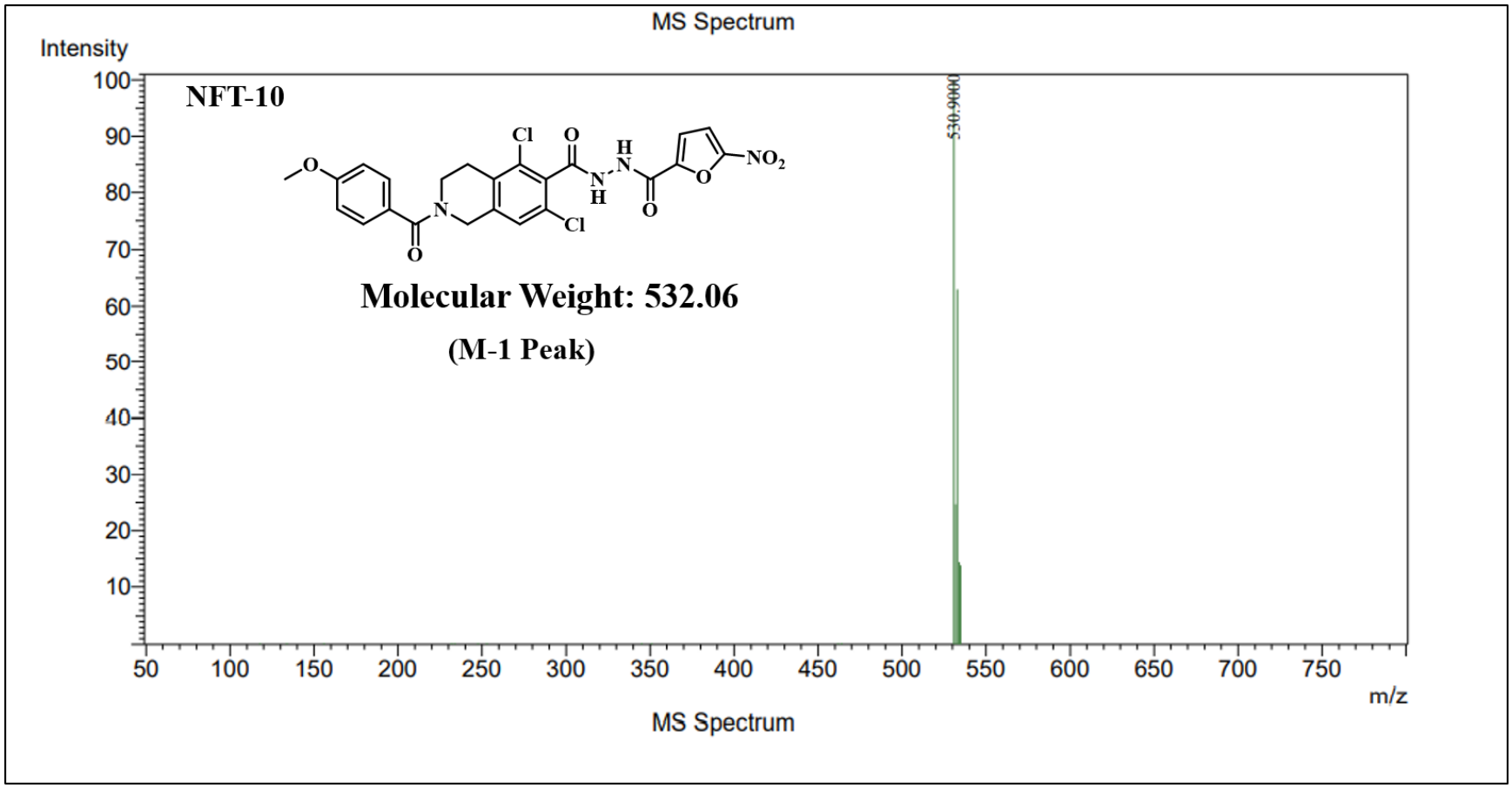

Mass spectra of compound NFT-10

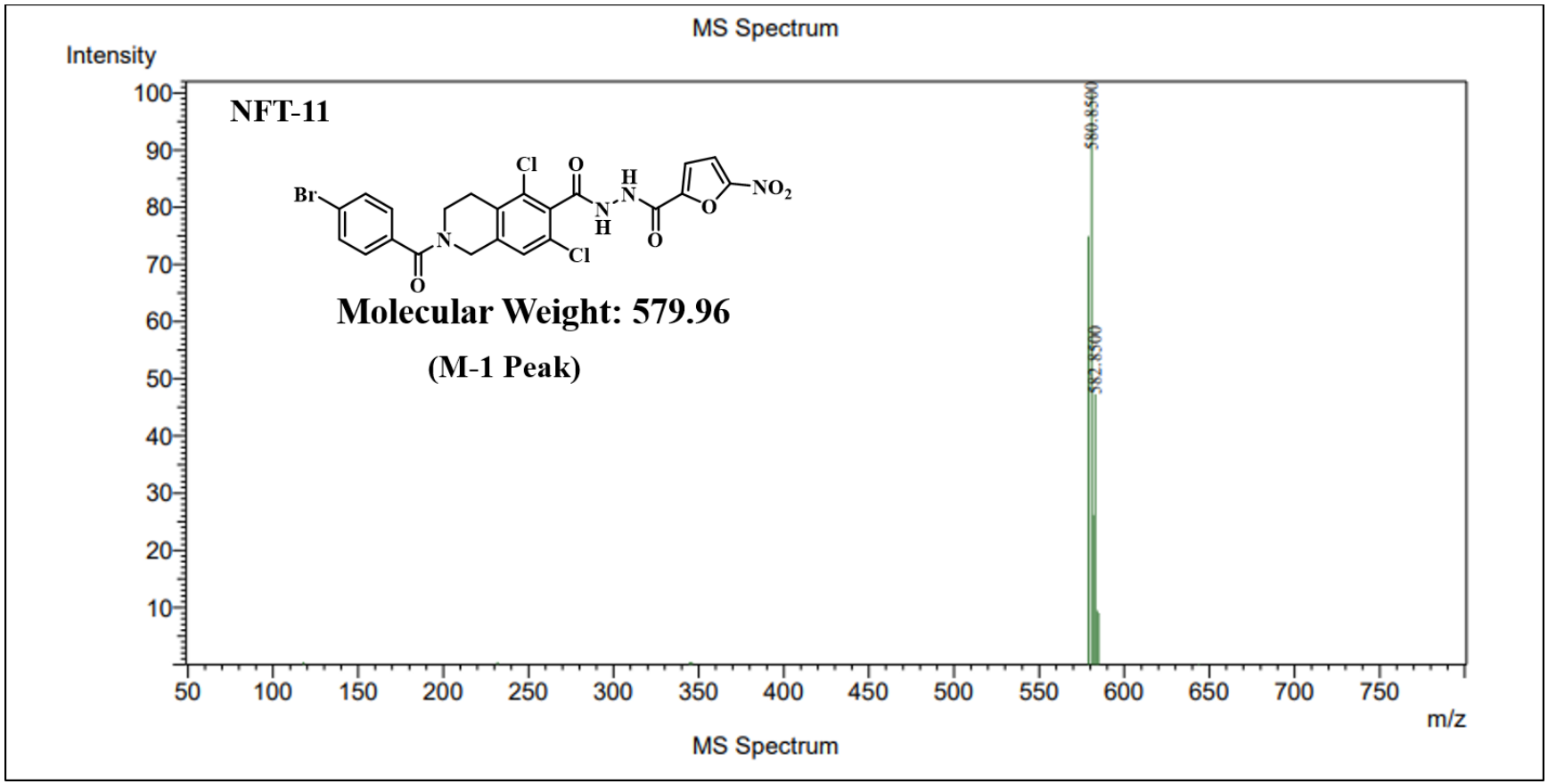

Mass spectra of compound NFT-11

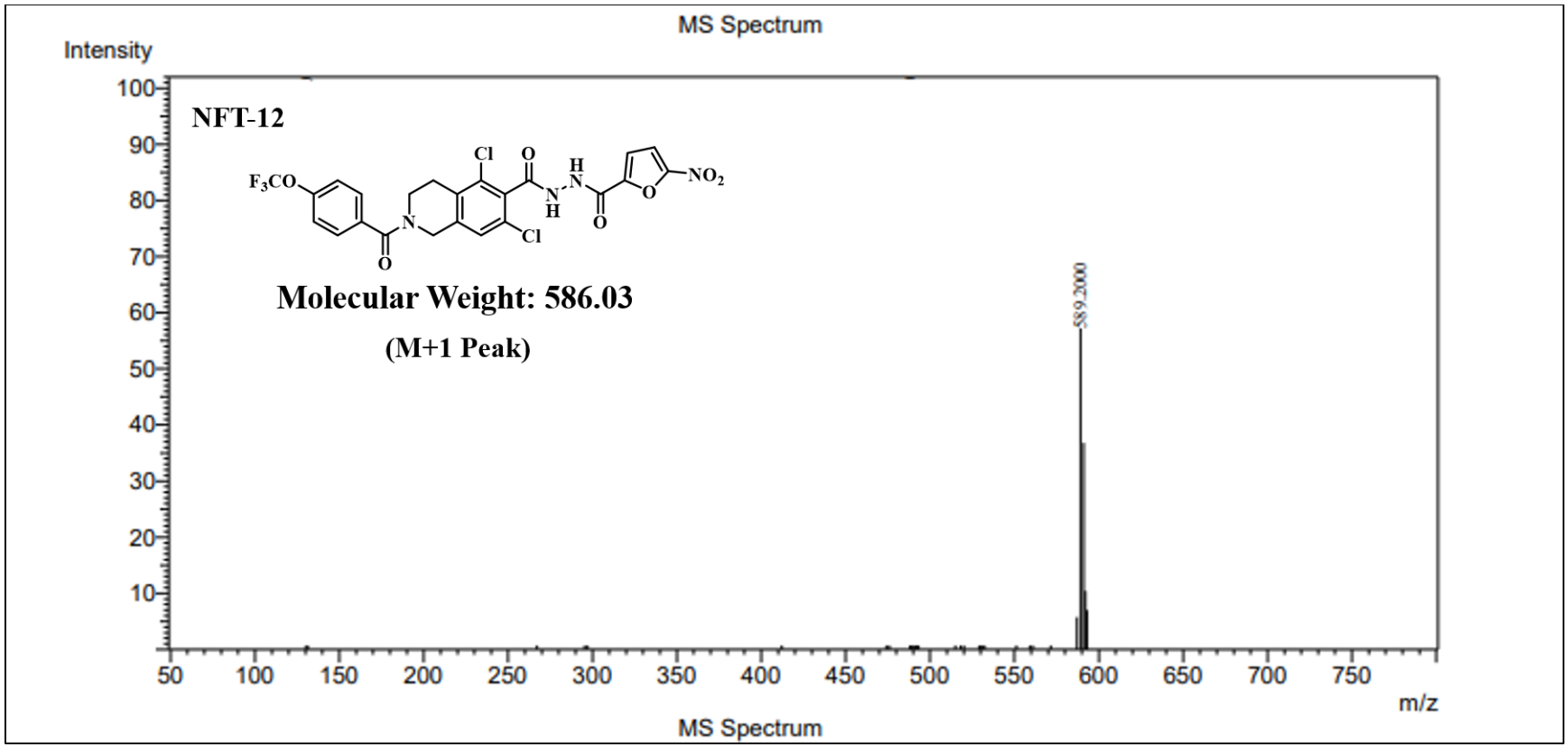

Mass spectra of compound NFT-12

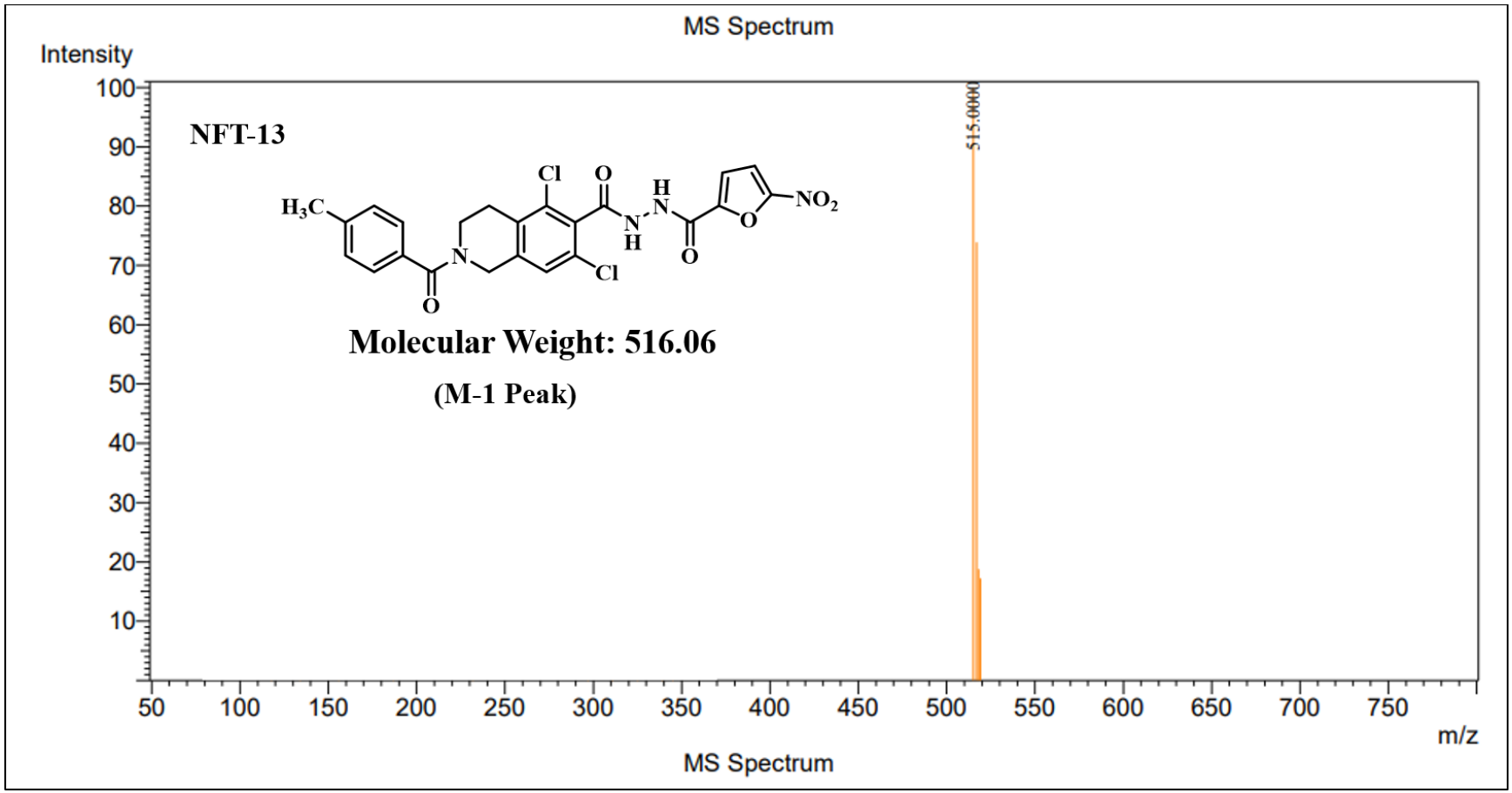

Mass spectra of compound NFT-13

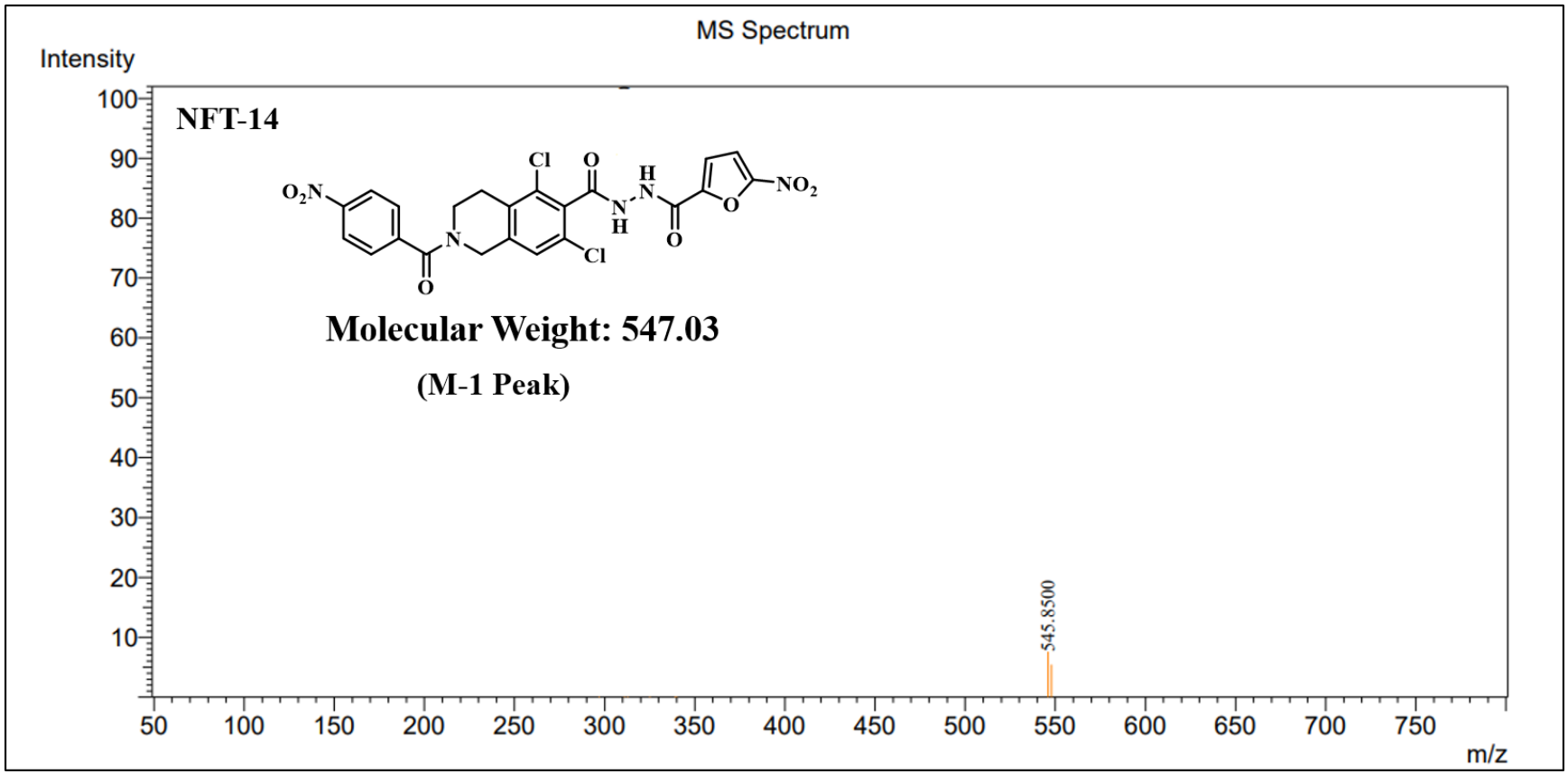

Mass spectra of compound NFT-14

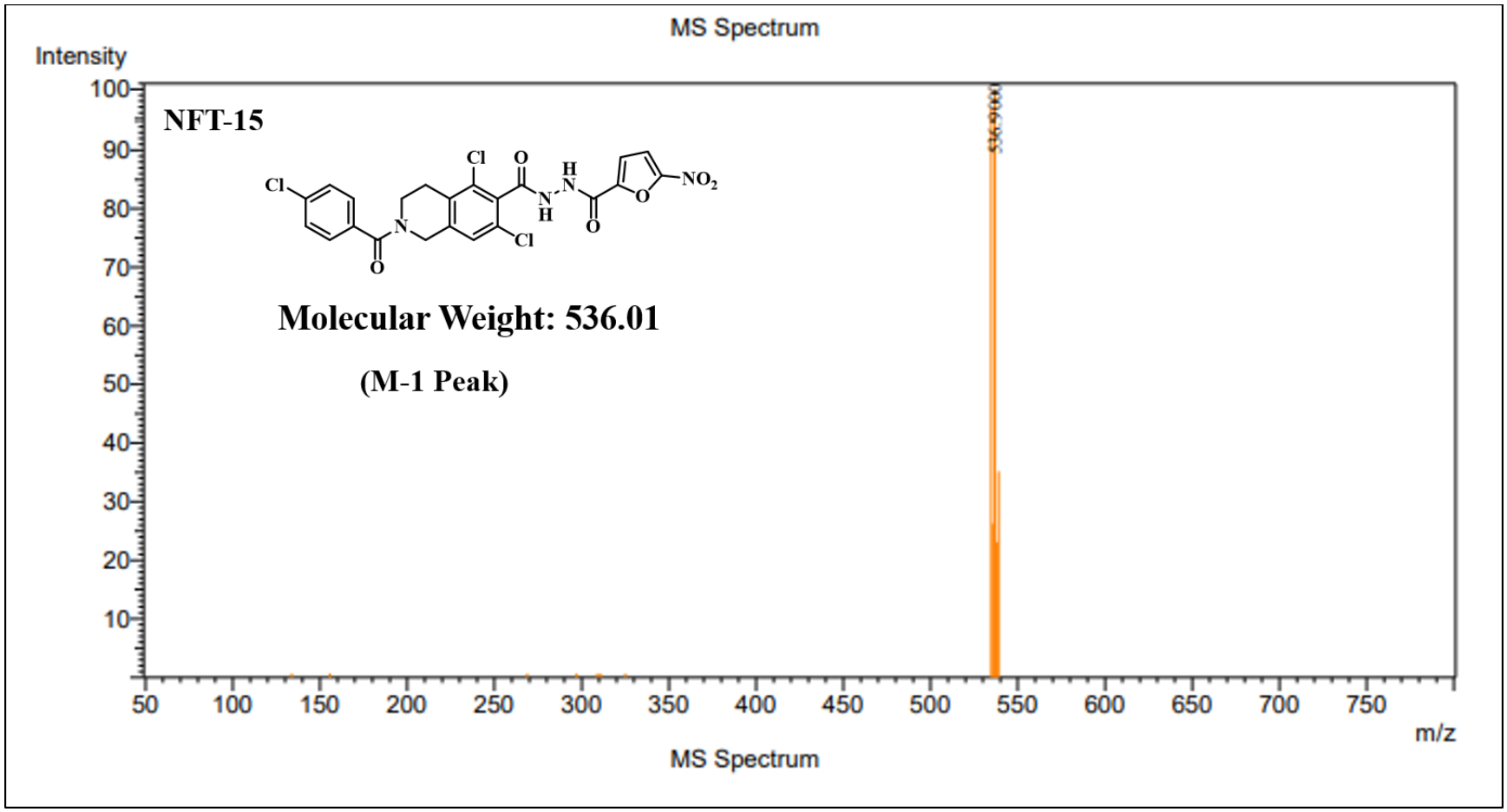

Mass spectra of compound NFT-15

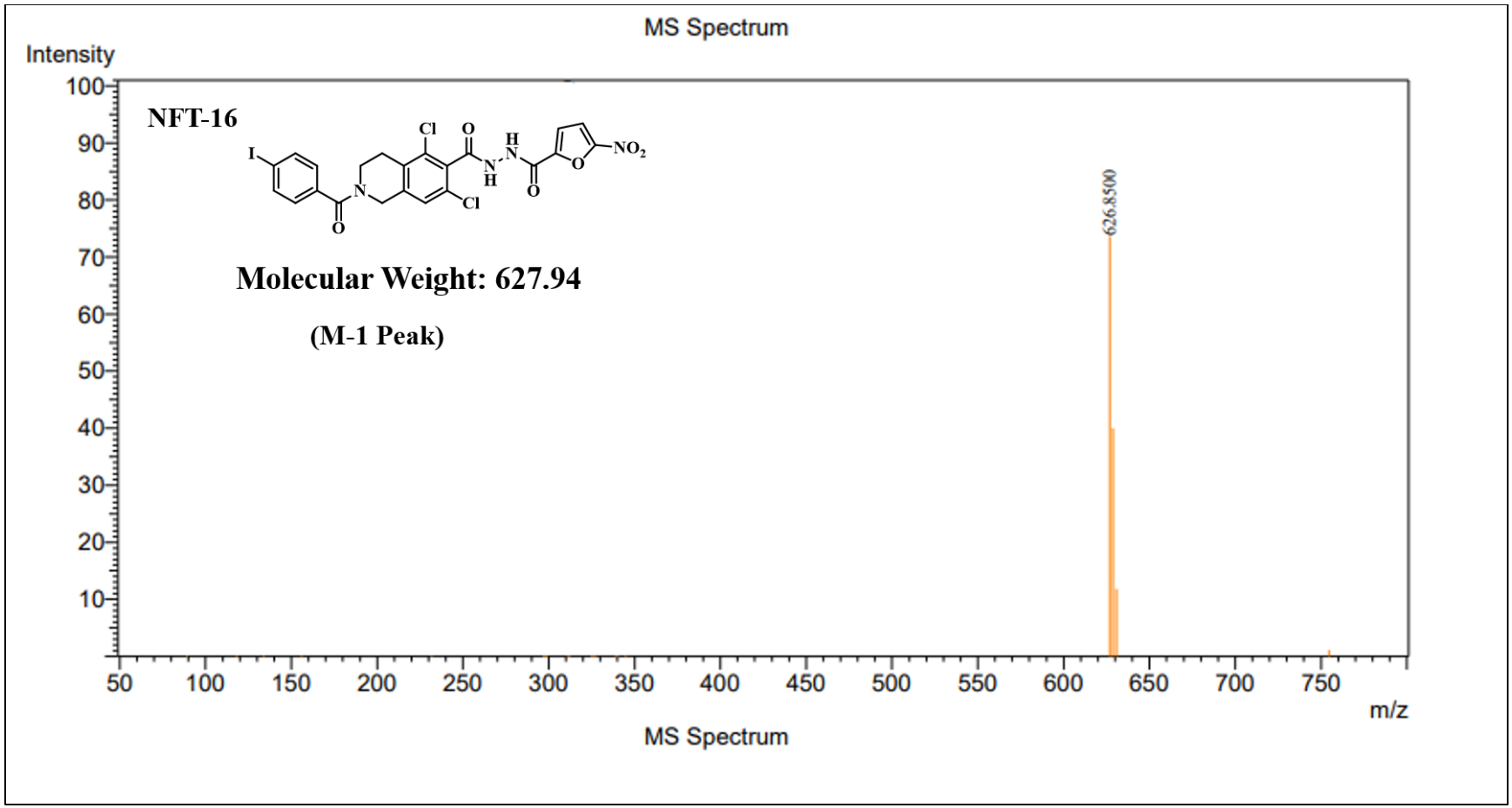

Mass spectra of compound NFT-16

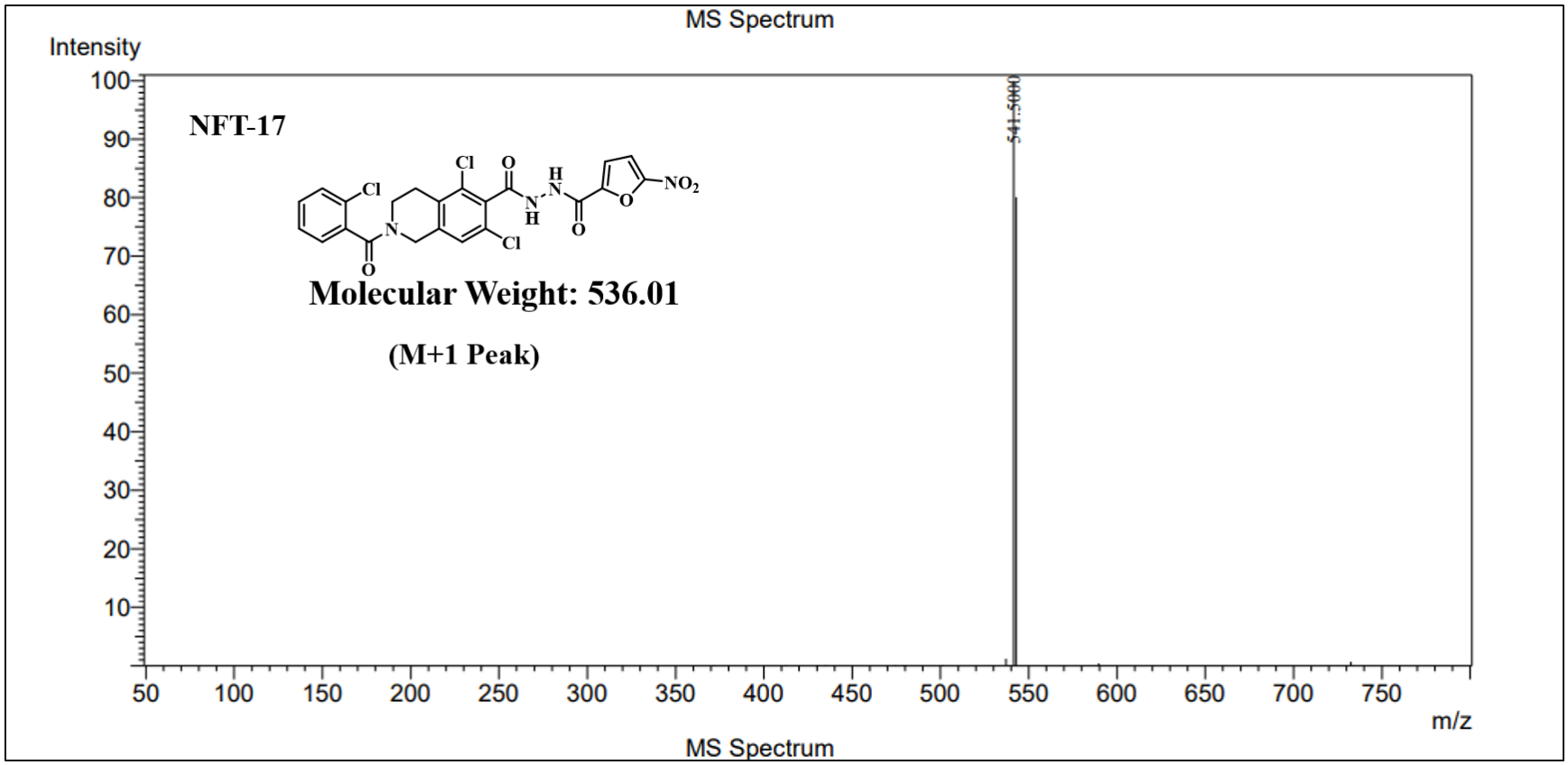

Mass spectra of compound NFT-17

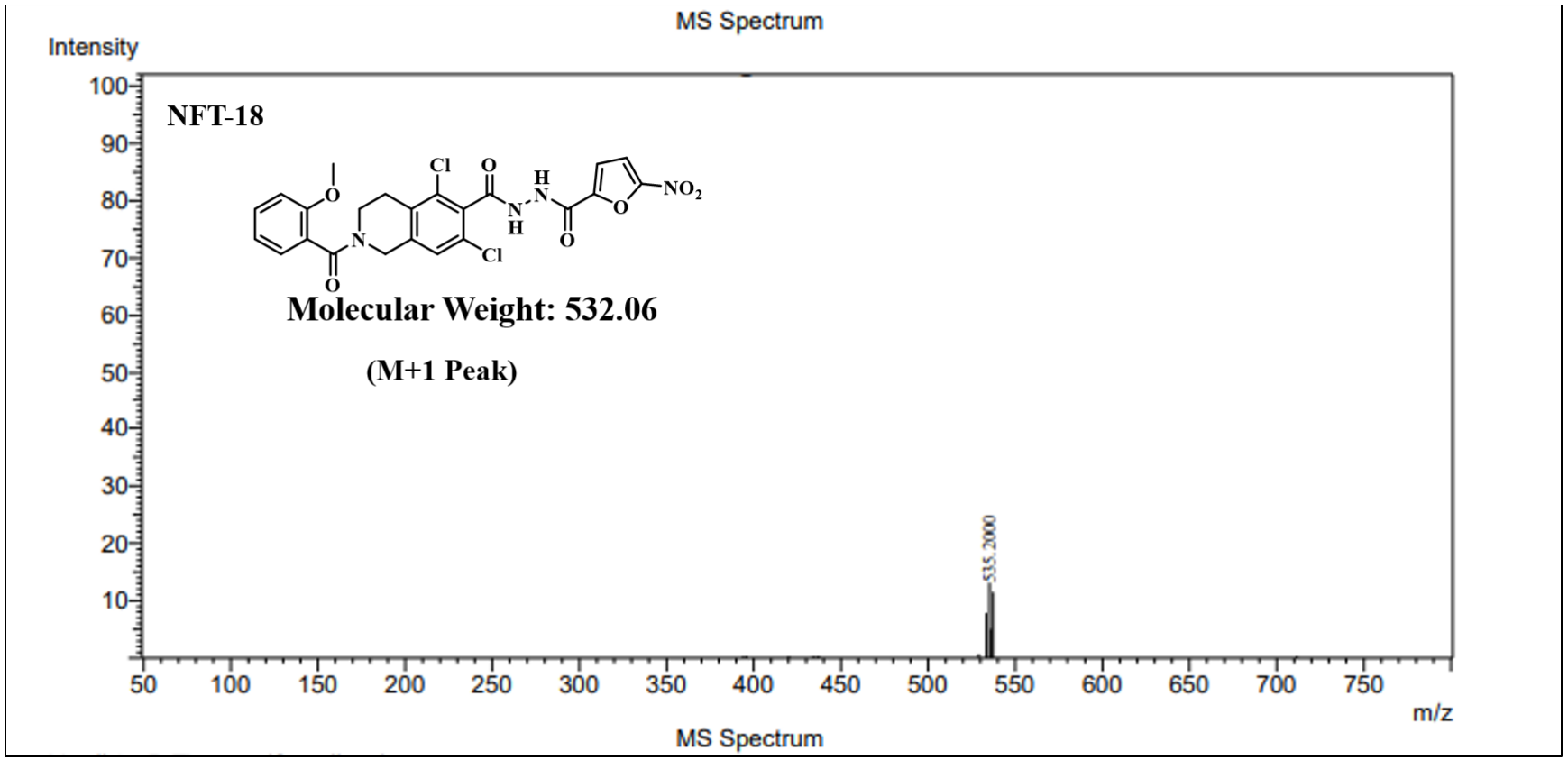

Mass spectra of compound NFT-18

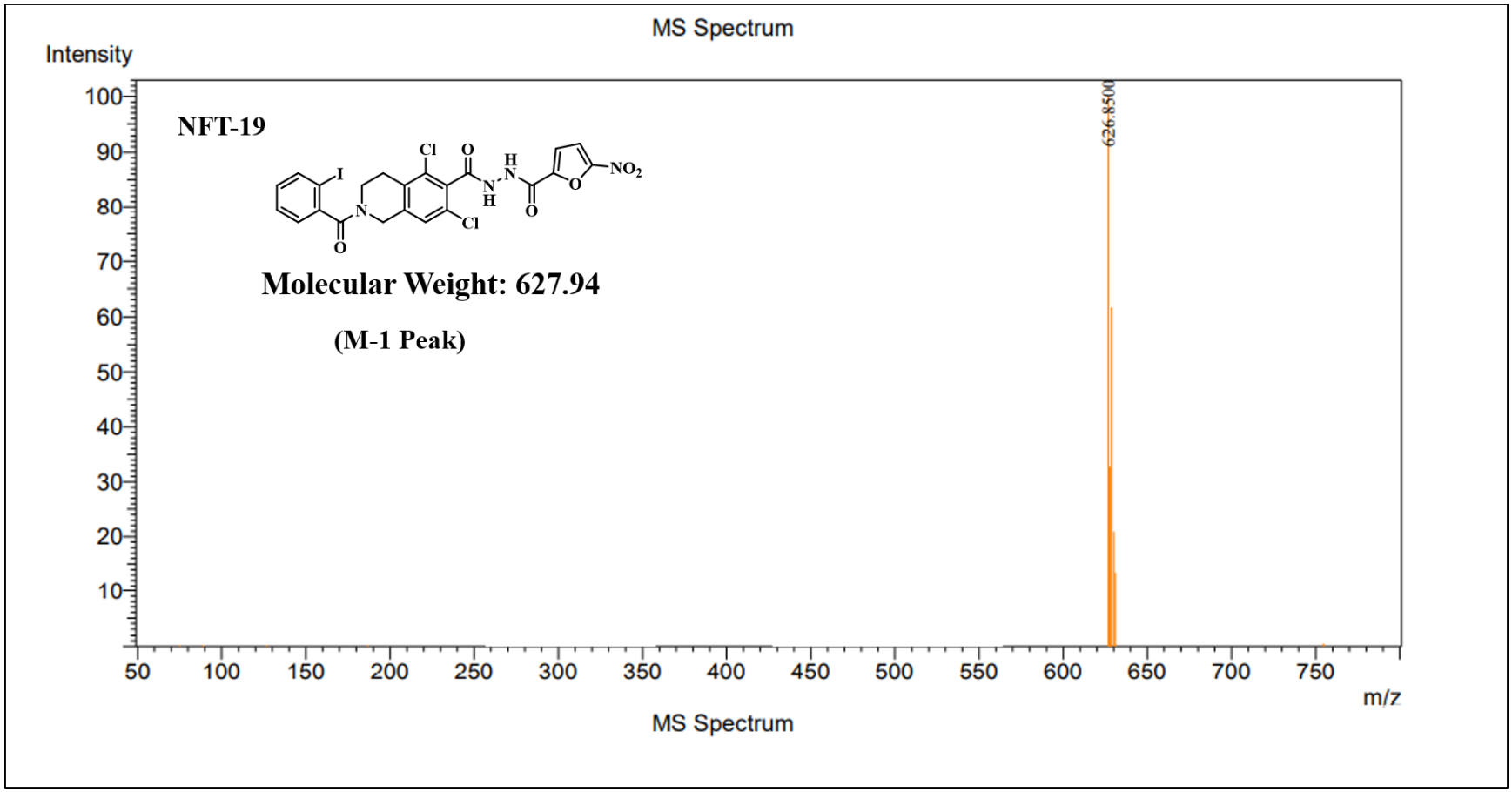

Mass spectra of compound NFT-19

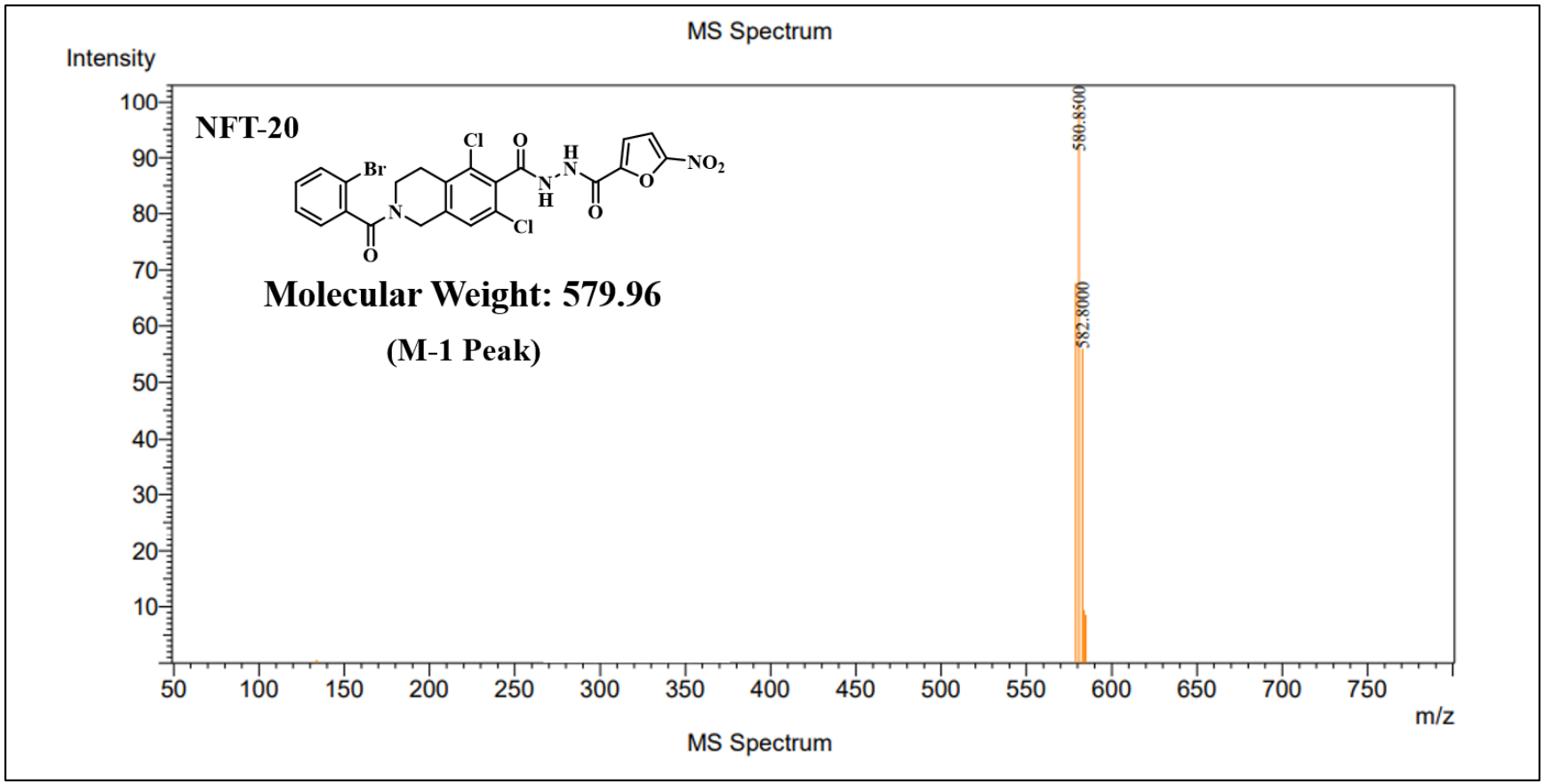

Mass spectra of compound NFT-20

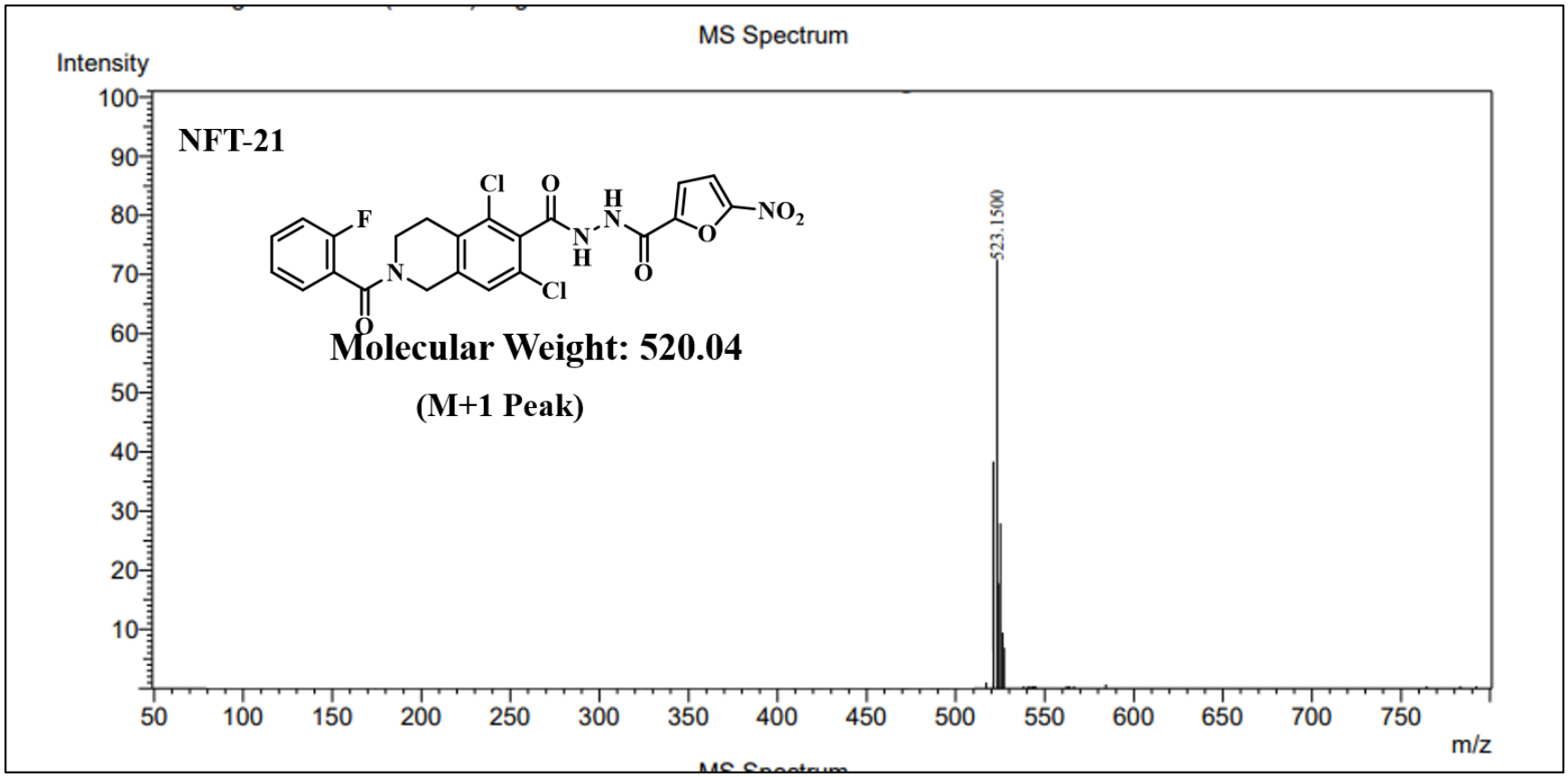

Mass spectra of compound NFT-21

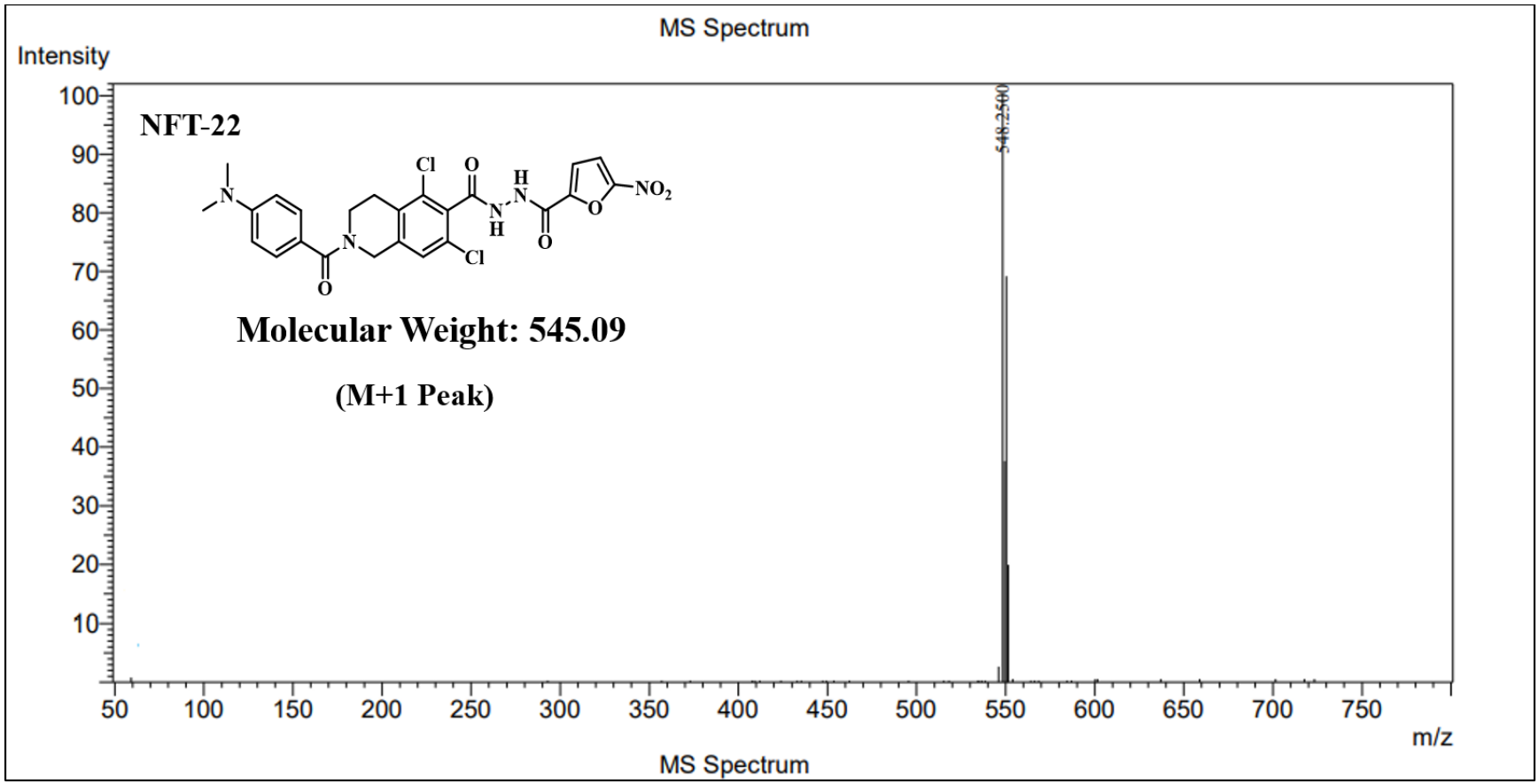

Mass spectra of compound NFT-22

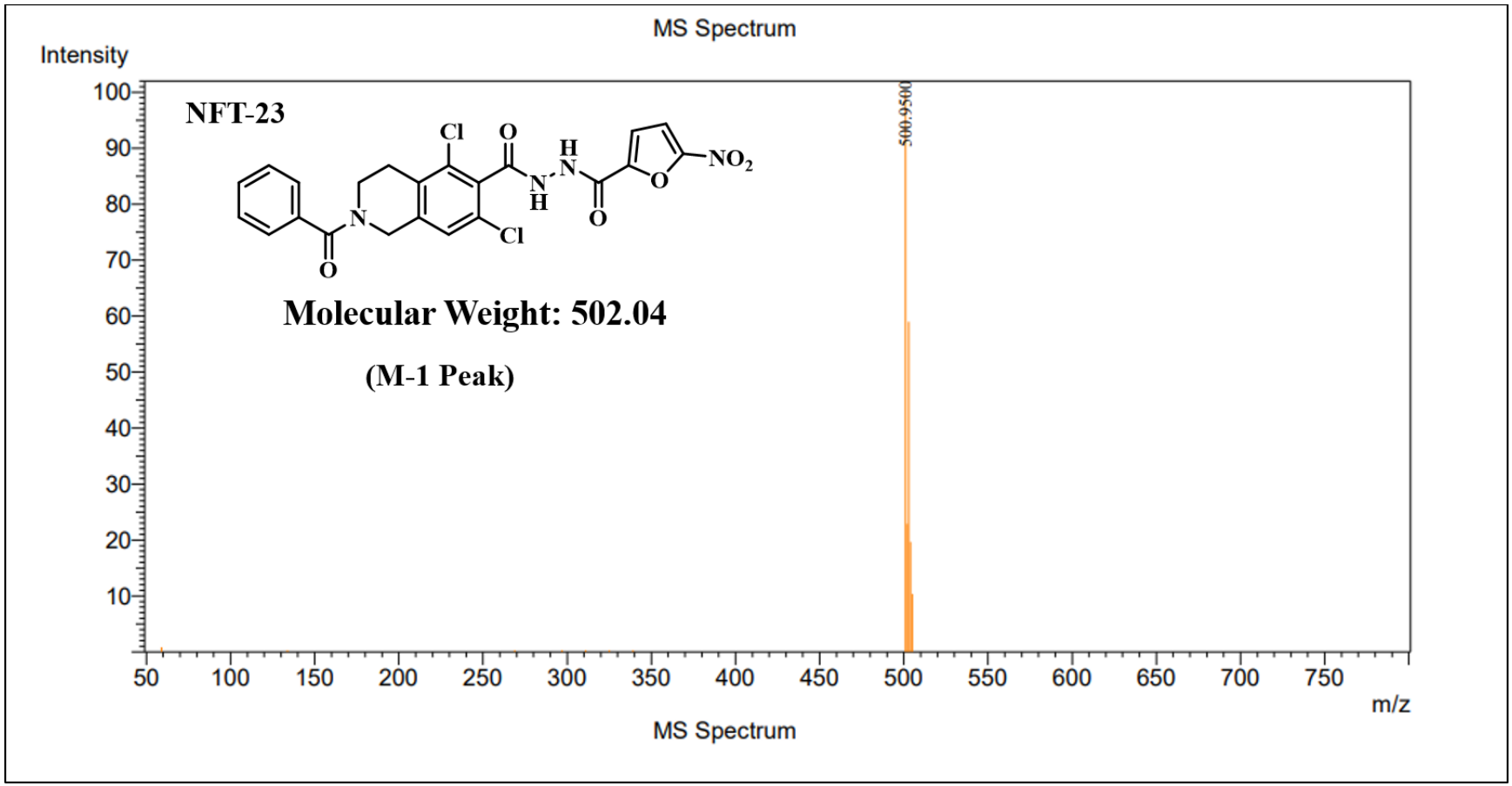

Mass spectra of compound NFT-23

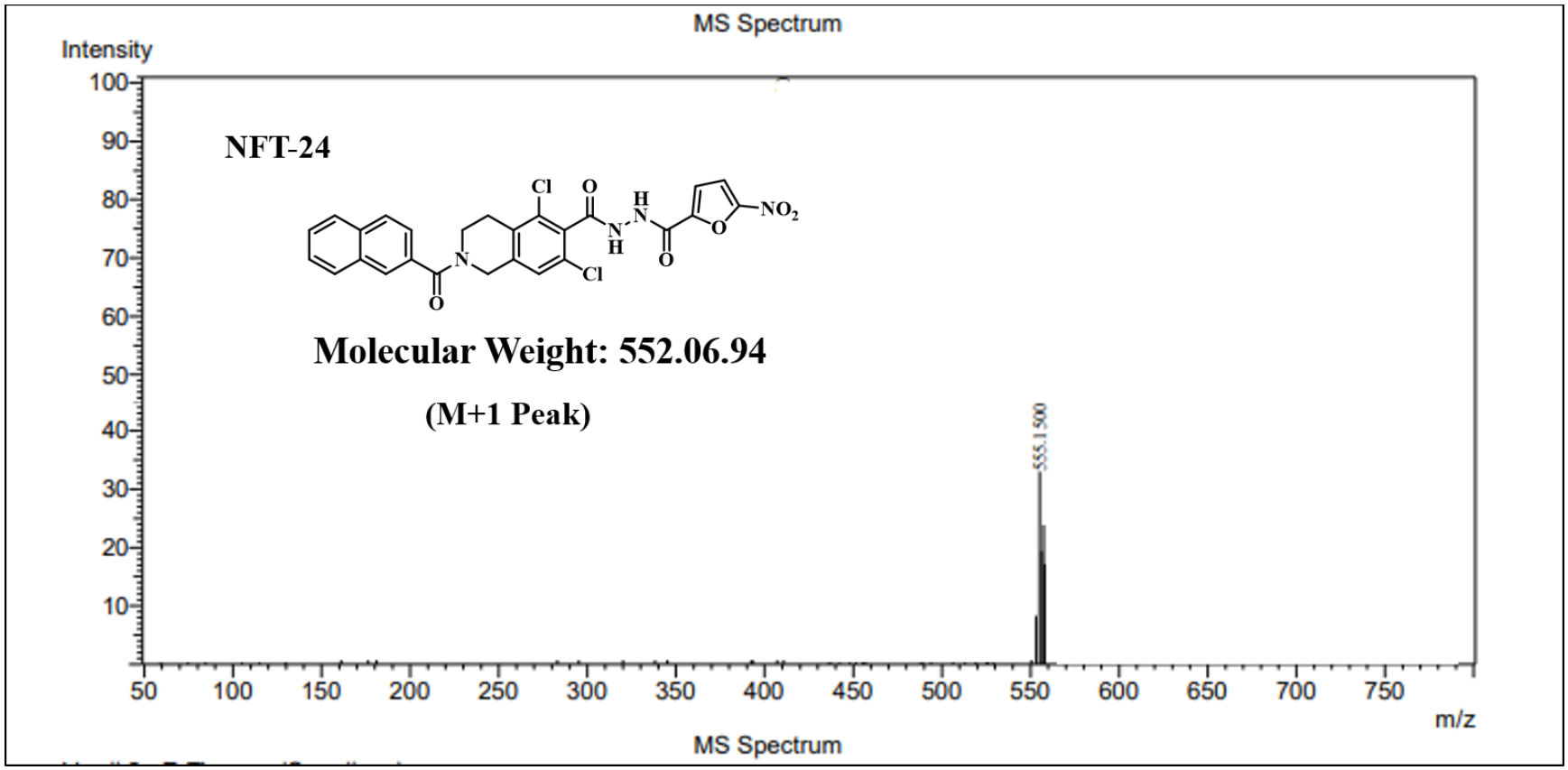

Mass spectra of compound NFT-24

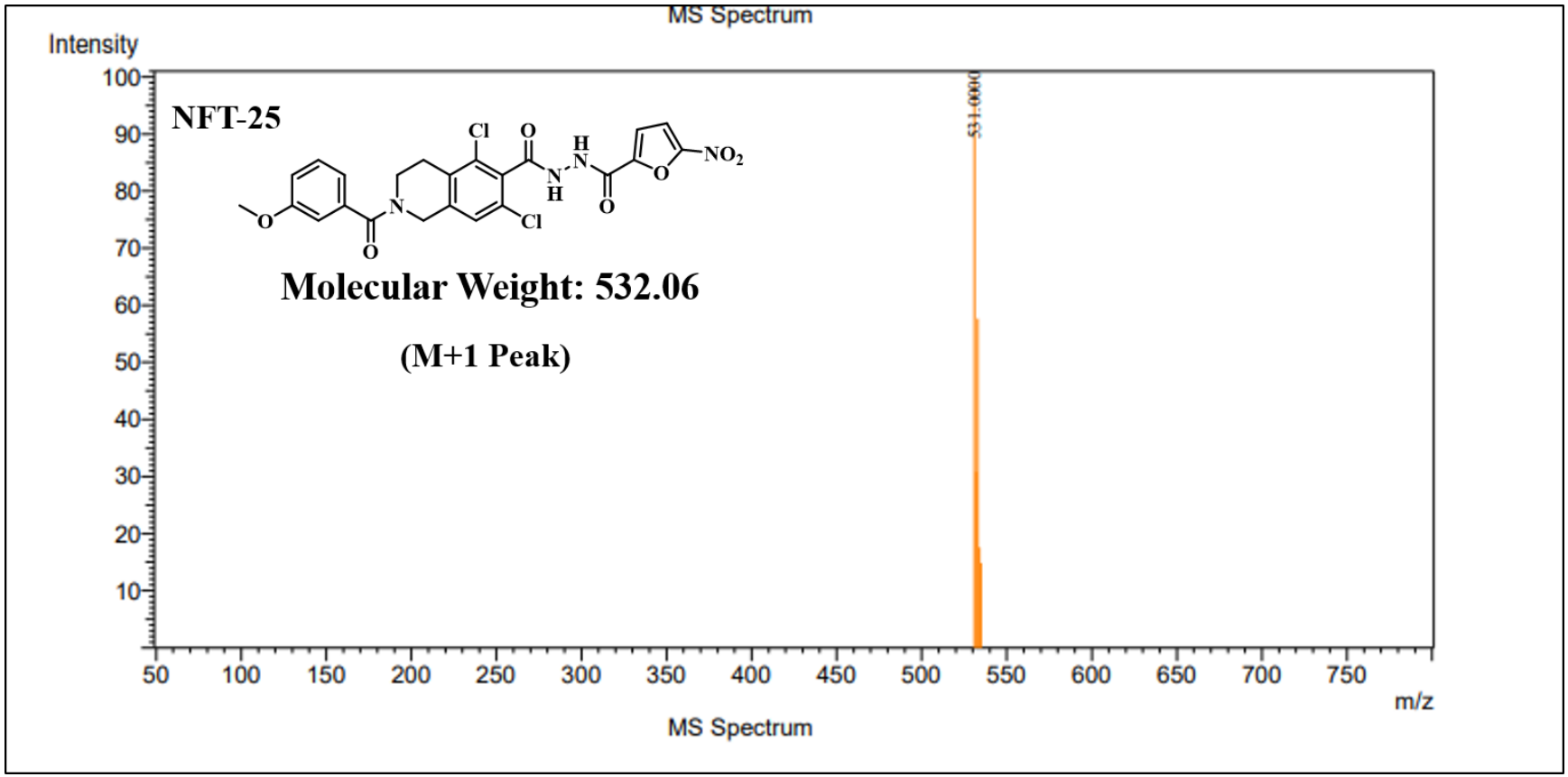

Mass spectra of compound NFT-25

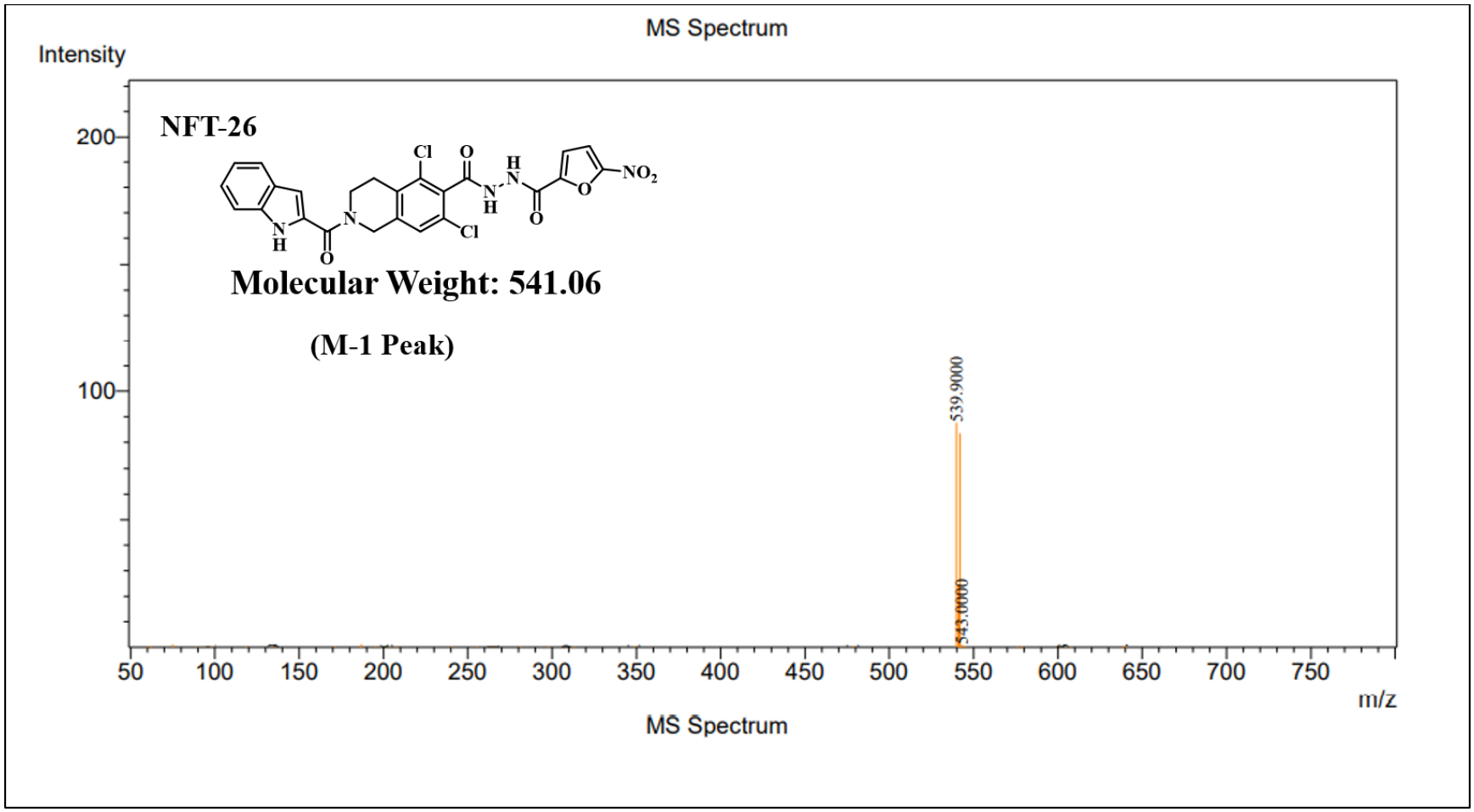

Mass spectra of compound NFT-26

9.References

[1] B.V.S. Kumar, Y.M. Khetmalis, A. Nandikolla, B.K. Kumar, K. Van Calster, S. Murugesan, D. Cappoen, K.V.G. Chandra Sekhar, Chem. Biodivers., 2023, e202200939.

[2] Rastogi, N., Goh, K.S., Wright, E.L. (1994). Potential drug targets for Mycobacterium avium defined by radiometric drug-inhibitor combination techniques. Antimicrobial Agents and Chemotherapy, 38(10), 2287-2295. https://doi:10.1128/AAC.38.10.2287.

[3] Shree B et al. Transforming Growth Factor-Beta-Regulated LncRNA-MUF Promotes Invasion by Modulating the miR-34a Snail1 Axis in Glioblastoma Multiforme. Front Onco. 2022 Feb 8;11:788755. doi: 10.3389/fonc.2021.788755. eCollection 2021.

[4] Khetmalis et al. Design, synthesis, and biological evaluation of tetrahydroisoquinoline based hydroxamate derivatives as HDAC 6 inhibitors for cancer therapy. Journal of Molecular structure 2023

[5] Schrödinger Release 2019-1: Maestro, Schrödinger, LLC, New York, NY, 2019. (n.d.).

[6] Li, H.J., Lai, C.T., Pan, P., Yu, W., Liu, N., Bommineni, G.R., Garcia-Diaz, M., Simmerling, C., Tonge, P.J. (2014) ACS Chem Biol 9: 986-993.

[7] Schrödinger Release 2020-4: Desmond Molecular Dynamics System, D. E. Shaw Research, New York, NY, 2020. Maestro-Desmond Interoperability Tools, Schrödinger, New York, NY, 2020. (n.d.).

[8] Schrodinger, 2019-1. (n.d.). Schrödinger Release 2019-1: LigPrep, Schrödinger, LLC, New York, NY, 2019.

[9] Schrödinger Release 2019-1: Schrödinger Suite 2019-1 Protein Preparation Wizard; Epik, Schrödinger, LLC, New York, NY, 2019. (n.d.).

[10] Mark, P., & Nilsson, L. (2001). Structure and dynamics of the TIP3P, SPC, and SPC/E water models at 298 K. Journal of Physical Chemistry A, 105(43), 9954–9960. https://doi.org/10.1021/jp003020w

[11] Berne, M. T. and B. J. G. J. M. (1993). Reversible multiple time scale molecular dynamics. The Journal of Physical Chemistry, 97(51), 13429–13434. https://doi.org/10.1021/j100153a002

[12] Jorgensen, W. L., Maxwell, D. S., & Tirado-Rives, J. (1996). Development and Testing of the OPLS All-Atom Force Field on Conformational Energetics and Properties of Organic Liquids. Journal of the American Chemical Society, 118(45), 11225–11236. https://doi.org/10.1021/ja9621760

[13] Cheng, A., & Merz, K. M. (1996). Application of the Nosé−Hoover Chain Algorithm to the Study of Protein Dynamics. The Journal of Physical Chemistry, 100(5), 1927–1937. https://doi.org/10.1021/jp951968y

[14] Kalibaeva, G., Ferrario, M., & Ciccotti, G. (2003). Constant pressure-constant temperature molecular dynamics: A correct constrained NPT ensemble using the molecular virial. Molecular Physics, 101(6), 765–778. https://doi.org/10.1080/0026897021000044025

[15] Karan Kumar, B., Faheem, Balana Fouce, R., Melcon-Fernandez, E., Perez-Pertejo Yolanda, Y., Reguera, R. M., Adinarayana, N., Chandra Sekhar, K. V. G., Vanaparthi, S., & Murugesan, S. (2021). Design, synthesis and evaluation of novel β-carboline ester analogues as potential anti-leishmanial agents. Journal of Biomolecular Structure and Dynamics, 0(0), 1–16. https://doi.org/10.1080/07391102.2021.1973564

[16] Kumar, B. K., Faheem, Sekhar, K. V. G. C., Ojha, R., Prajapati, V. K., Pai, A., & Murugesan, S. (2020). Pharmacophore based virtual screening, molecular docking, molecular dynamics and MM-GBSA approach for identification of prospective SARS-CoV-2 inhibitor from natural product databases. Journal of Biomolecular Structure and Dynamics, 0(0), 1–24. https://doi.org/10.1080/07391102.2020.1824814